



EMG Pattern Prediction for Upper Limb Movements Based on Wavelet and Hilbert-Huang Transform

Alvaro Altamirano Altamirano

► To cite this version:

Alvaro Altamirano Altamirano. EMG Pattern Prediction for Upper Limb Movements Based on Wavelet and Hilbert-Huang Transform. Automatic. Université de Lorraine; Instituto politécnico nacional (México), 2017. English. NNT : 2017LORR0261 . tel-01698393v2

HAL Id: tel-01698393

<https://tel.archives-ouvertes.fr/tel-01698393v2>

Submitted on 1 Feb 2018

HAL is a multi-disciplinary open access archive for the deposit and dissemination of scientific research documents, whether they are published or not. The documents may come from teaching and research institutions in France or abroad, or from public or private research centers.

L'archive ouverte pluridisciplinaire **HAL**, est destinée au dépôt et à la diffusion de documents scientifiques de niveau recherche, publiés ou non, émanant des établissements d'enseignement et de recherche français ou étrangers, des laboratoires publics ou privés.



AVERTISSEMENT

Ce document est le fruit d'un long travail approuvé par le jury de soutenance et mis à disposition de l'ensemble de la communauté universitaire élargie.

Il est soumis à la propriété intellectuelle de l'auteur. Ceci implique une obligation de citation et de référencement lors de l'utilisation de ce document.

D'autre part, toute contrefaçon, plagiat, reproduction illicite encourt une poursuite pénale.

Contact : ddoc-theses-contact@univ-lorraine.fr

LIENS

Code de la Propriété Intellectuelle. articles L 122. 4

Code de la Propriété Intellectuelle. articles L 335.2- L 335.10

http://www.cfcopies.com/V2/leg/leg_droi.php

<http://www.culture.gouv.fr/culture/infos-pratiques/droits/protection.htm>



UNIVERSITÉ
DE LORRAINE

École Doctorale IAEM Lorraine



EMG Pattern Prediction for Upper Limb Movements Based on Wavelet and Hilbert-Huang Transform

THESIS

Doctorat de l'Université de Lorraine
PhD in Electrical Engineering

Mention: Automatique, Traitement du Signal et des Images, Génie Informatique
Thèse en cotutelle avec le CINVESTAV-IPN

Préparé au:

**Centre de Recherche en Automatique de Nancy, UMR 7039 CNRS/UL
et Bioelectronics LAREMUS Laboratory, CINVESTAV-IPN**

Presentée et soutenue publiquement
le 30 novembre 2017
par:

Alvaro ALTAMIRANO ALTAMIRANO

Composition du jury:

<i>Rapporteurs:</i>	Abdel-Kader BOULANOUAR	Ingénieur de Recherche, ToNIC INSERM UMR 1214, Université de Toulouse, France.
	Jesús Enrique CHONG QUERO	PhD, ITESM <i>Campus Estado de México</i> , Mexique.
<i>Examinateurs:</i>	Christian DAUL	PU, Université de Lorraine, CRAN, Nancy.
	Josefina GUTIERREZ MARTINEZ	PhD, <i>Instituto Nacional de Rehabilitación</i> , Mexique.
<i>Directeurs</i>	Didier WOLF	PU, Université de Lorraine, CRAN, Nancy.
	Lorenzo LEIJA SALAS	PhD, CINVESTAV-IPN, Mexique.
<i>Invités</i>	Roberto MUÑOZ GUERRERO	PhD, CINVESTAV-IPN, Mexique.
	Arturo VERA HERNÁNDEZ	PhD, CINVESTAV-IPN, Mexique.

Acknowledgements

For their contribution and support for this research I would like to acknowledge the following institutions and persons:

To the Mexican and French community.

To the National Council of Science and Technology of Mexico.

To the Evaluation-orientation de la Coopération Scientifique NORD of France.

To the National Polytechnique Institute and its National Center of Research and Advance Studies of Mexico.

To the Université de Lorraine of France.

To the Electrical Engineering Department, the Bioelectronics section and LAREMUS Laboratory.

To the *Centre de Recherche en Automatique de Nancy* CNRS UMR 7039 of France.

To my advisors: Dr. Lorenzo LEIJA SALAS & Pf. Didier WOLF.

To my lovemate, my wife, Claudia Violeta Cervantes Martínez, MSc. for the support and successful feedback.

Dedicatory

Con el más grande amor, cariño y dedicación por ser parte de Mí.

A ti Violeta por tu incondicional apoyo, paciencia y amor que me has brindado en todo momento, tuyo es este logro.

A mi mami, Alejandra López Ayala (t), quien vive en mí y en todos de los que te llevamos en nuestro memoria.

A mi madre, la Profra. María Flor Altamirano López, mi maestra, mi Madre.

Al mi padre, el Ing. Isaac Altamirano Méndez, por ser mi ejemplo y darme incondicionalmente tu total apoyo, tus enseñanzas de vida.

A mi hermano Arturo Altamirano, por ser parte de mí.

A la Profra. Cristina Cervantes Martínez, a Ninel Roselina Cervantes Martínez y a Luis Alonso Cervantes Martínez, por ser parte de nosotros.

A mi bisabuelo, tíos, primos, amigos y familiares que han sido parte de mí.

A mi gran amigo y hermano M. en C. Héctor Maldonado Loyo, por su incondicional apoyo.

A toda la sección de Bioelectrónica, y muy en especial, para Patricia Peña, Ma. Luisa Lorán y Georgina Olmos.

A mis amigos y compañeros.

All human wisdom is summed up in two words:

Wait and Hope.

Alexandre DUMAS

Table of contents

GLOSSARY	X
LIST OF FIGURES.....	XI
<i>Resumen</i>	<i>xv</i>
<i>Résumé</i>	<i>xvi</i>
Abstract.....	xvii
GENERAL INTRODUCTION	XIX
STATE OF THE ART	XXIII
Previous Related Works	xxiv
GOALS	3
General Goal.....	3
Specific Goals	3
Acquisition stage	3
Stationary Signal Analysis	3
Nonstationary Signal Analysis	3
General Block Diagram about Prediction System.....	4
CHAPTER 1 MUSCLES AND BIOPOTENTIALS.....	5
1.1 Muscle Anatomy and Physiology	5
1.1.1 Anatomy.....	5
1.1.2 Physiology	5
1.2 Biopotential Recording.....	9
1.2.1 The Ag/AgCl Electrode	10
1.3 sEMG signals	10
1.3.1 EMG Features	12
1.3.2 On MUAP shape and its properties.....	12
1.3.3 EMG description over voltage dimension.....	12
1.3.4 EMG description on time dimension	15
1.3.4.1 Frequency Spectrum.....	15
1.3.5 Electrical noise and factors affecting EMG signal.....	15
1.4 sEMG signal detection and acquisition.....	16
1.4.1 sEMG Normalization	16
1.4.2 EMG Filtering.....	17
1.4.3 EMG De-noising using Wavelets.....	17
1.4.4 EMG De-noising using Hilbert-Huang Transform	18
1.4.5 EMG signal decomposition.....	18
1.4.5.1 Challenges of sEMG decomposition	19

CHAPTER 2 MATHEMATICAL FRAMEWORK	21
2.1 Signals	21
2.1.1 Classification of signals.....	21
2.1.1.1 Deterministic Signal.....	21
2.1.1.2 Nondeterministic Signal.....	21
2.2 Wavelet and Hilbert-Huang Transforms	22
2.2.1 Wavelet Transform	22
2.2.1.1 Meyer Wavelet.....	23
2.2.1.2 Daubechies Wavelet.....	24
2.2.2 Hilbert-Huang Transform	24
2.2.2.1 Empirical Mode Decomposition (The sifting process)	25
2.2.2.2 Hilbert Transform	30
2.3 The Goertzel Algorithm.....	31
2.3.1 Summary.....	31
2.3.2 First-order Filters.....	31
2.3.3 Comparing FFT vs Goertzel algorithm.....	32
2.4 Kalman Filter	32
2.4.1 The Model	33
CHAPTER 3 METHODOLOGY	35
3.1 Acquisition	36
3.1.1 Electrodes array	37
3.1.2 Recording protocol	37
3.1.3 Normalization	38
3.2 Stationary Analysis	41
3.2.1 Wavelet Analysis	41
3.2.1.1 Histograms	44
3.2.2 Statistics: ANOVA, Levene & post hoc tests.....	47
3.2.3 Hilbert-Huang Analysis.....	48
3.2.3.1 Empirical Mode Decomposition	48
3.2.3.2 Hilbert Spectral Analysis	52
3.2.3.3 Instantaneous Frequency Estimation.....	53
3.3 Nonstationary Analysis	54
3.3.1 Dynamical Reconstruction using Hybrid Kalman filter	54
3.3.1.1 Prediction equations	55
3.3.1.2 Update equations.....	55
3.3.2 Single tone detection with Goertzel algorithm	56
CHAPTER 4 RESULTS & DISCUSSION.....	57
4.1 Muscular activity by movement.....	57
4.2 Wavelet Transform Analysis.....	58
4.3 Hilbert-Huang Analysis	62
4.4 Reconstruction.....	69
4.5 Curve fitting.....	74
4.6 Kalman filter, estimation and prediction	76
4.6.1 State-Space Representation of Nonlinear Model	76

4.7 Goertzel Filter, frequency detection	79
4.8 Contributions	82
4.8.1 Scientific contributions	82
4.8.2 Perspectives	83
CONCLUSIONS	84
PUBLICATIONS AND STAGES	86
International Journal JCR	86
International Conferences	86
Stages	86
REFERENCES	87
APPENDIX: MATLAB CODES OF THE ALGORITHMS	92
Hilbert-Huang transform	92
Empirical Mode Decomposition basis	92
Empirical Mode Decomposition for 4 Channels	98
Hilbert Transform and Instantaneous frequency	102
Wavelet Transform Algorithm	103
Kalman Filter Algorithm	106
Goertzel Algorithm	107

GLOSSARY

EMG	Electromyography	MU	Motor Unit
MUAP	Motor Unit Action Potential	DRG	Dorsal Root Ganglion
sEMG	Surface Electromyography	NMJ	Neuro Muscular Junction
AI	Artificial Intelligence	DFT	Direct Fourier Transform
WT	Wavelet Transform	CWT	Continuous Wavelet Transform
FT	Fourier Transform	IF	Instantaneous Frequency
WVD	Wigner-Ville Distribution	KF	Kalman Filter
HHT	Hilbert Huang Transform	GA	Goertzel Algorithm
ANN	Artificial Neural Networks		
DRNN	Dynamic Recurrent Neural Networks		
FLS	Fuzzy Logic System		
GA	Genetic Algorithm		
HOS	Higher-order statistical		
O&P	Orthesis and Prosthesis		
CWC	Continuous Wavelet Coefficients		
CWT	Continuous Wavelet Transform		
IMF	intrinsic mode functions		
EMD	Empirical Mode Decomposition		
iEMG	Indwelling Electromyography		
CMRR	Common Mode Rejection Ratio		
HT	Hilbert Transform		
HS	Hilbert Spectrum		
Ag	Silver		
AgCl	Silver Chloride		
NI	National Instruments		
DAQ	Data Acquisition		
A/D	Analog / Digital		
RMS	Root Medium Square		

LIST OF FIGURES

Figure 1. EMG prediction system block diagram.....	4
Figure 2. Elements of the peripheral nervous system. The peripheral nervous system includes the peripheral motor and sensory nerves their primary neurons, the anterior horn cells, and dorsal root ganglia; the neuromuscular junctions (NMJs); and muscle. The dorsal root ganglion, a bipolar cell located distal to the sensory root, is anatomically different from the anterior horn cell. Consequently, lesions of the nerve roots result in abnormalities of motor nerve conduction studies but do not affect sensory conduction studies, as the dorsal root ganglion and its peripheral nerve remain intact (Preston, 2013).	6
Figure 3. Resting membrane potential. At rest, the axonal membrane is negatively polarized, inside compared to outside. This resting potential results from the combination of a membrane that is semipermeable to charged particles and an active Na^+/K^+ pump. At rest, the concentration of Na^+ and large anions A^- greater inside the axon (Preston, 2013).	6
Figure 4. Voltage-gated sodium channel. The axonal membrane is lined with voltage-gated sodium channels. These channels are molecular pores with gates that open and close; when open, gates are selective for sodium A^+ (Preston, 2013).	6
Figure 5. Motor unit is defined as one axon, its anterior horn cell, and all connected muscle fibers and neuromuscular junctions. A nerve fiber action potential normally always results in depolarization of all the muscle fibers of the motor unit creating an electrical potential known as the motor unit action potential (MUAP) (Preston, 2013).	8
Figure 6. Neuromuscular junction. The neuromuscular junction is a specialized junction between the terminal axon and muscle fiber (Preston, 2013).	8
Figure 7. Volume conduction and waveform morphology. In upper image, an advancing action potential recorded by volume conduction will result in a triphasic potential that initially is positive, then is negative, and finally is positive again. In lower image, the depolarization occurs directly beneath the recording electrode, the initial positive phase is absent, and a biphasic, initially negative potential is seen. By convention, negative is up and positive is down in all nerve conduction and electromyographic traces (Preston, 2013).	9
Figure 8. Arrangement of a Ag/AgCl microelectrode (Rettinger, et al., 2016).....	10
Figure 9. General block diagram of the acquisition procedure of a digital signal.....	11
Figure 10. EMG signal and decomposition of MUAPs. (De Luca, et al., 2006).....	12
Figure 11 Histograms built from two different EMG signals (A, C) showing that statistical trend is maintained,.....	13
Figure 12 Increased electrical activity of muscle is expressed by a higher standard deviation, average didn't change.	14
Figure 13 Normal Distribution or Gauss Model. Symmetry axis over Average value and inflection points separated by a distance equal to RMS value.	14
Figure 14 EMG spectrum contains significant frequency components, from 10 Hz to 450 Hz.....	15
Figure 15. Stylized examples of the various challenges presented by the realistic behavior of EMG signals detected with indwelling sensors with small detection volume and susceptible to movement (De Luca, et al., 2006).....	19
Figure 16. Representation of Wavelet transform (Gao & Yan, 2011)	23
Figure 17. Wavelet Meyer (left) and its magnitude spectrum (right)	23
Figure 18. Daubechies wavelet (left) and its magnitude spectrum (right). a) Daubechies 2 base wavelet and b) Daubechies 4 base wavelet.....	24
Figure 19. Test data $x(t)$ (Huang, 2005)	26
Figure 20. The data (blue), upper and lower envelopes (green) defined by the local maxima and minima, respectively, and the mean value of the upper and lower envelopes given in red. (Huang, 2005).....	26
Figure 21. The data (pink) and h_1 (blue). (Huang, 2005)	27
Figure 22. (A, top) Repeated sifting steps with h_1 and m_2	28
Figure 23. The first IMF component c_1 after 12 steps. (Huang, 2005)	28
Figure 24. The original data (blue) and the residue r_1 (red). (Huang, 2005)	29

Figure 25. Kalman filter predict, measure, correct cycle iteratively and estimates the state at each time step.....	34
Figure 26. Block diagram of the Stationary Analysis. For Stationary Analysis is necessary the acquisition stage that comprises the electrode placing, 4-channels array acquisition system, recording data base, normalization and windowing of the signals. After acquisition, the analysis stage is based on Wavelet and Hilbert-Huang transforms used to identify the features, characteristics and patterns into the myoelectric signals. Result of these processes are databases and mathematical models that describes myoelectric signals in time and frequency.....	35
Figure 27. Block diagram of the Nonstationary Analysis. For Nonstationary Analysis is necessary the acquisition stage, that comprises the electrode placing, 4-channels array acquisition system, sampling, normalization and windowing to buffer the signals in a small-time slot. After acquisition, the filtering stage is a Kalman and Goertzel filters algorithms matching the input signals to predict, correct and identify the feature, characteristic or pattern of the de the myoelectric signals, these filters use the databases and mathematical models obtained in the Stationary Analysis.....	35
Figure 28. Block Diagram of Acquisition Stage. Acquisition of the signals consists in placing the electrodes over five forearm muscles of each subject using the 4-channels electrode array, signals from the muscles were sampled and recorded, and finally recorded signals were normalized and windowed previous to analyzing.....	36
Figure 29. Finger movements. 1) Finger II flexion, 2) Finger III flexion, 3) Fingers IV-V flexion, 4) Finger I flexion, 5) All fingers flexion, and 6) All fingers extension.....	36
Figure 30. Electrode configuration diagram with Vertex-focal distribution. Differential electrodes (V+ & V-) and Reference electrode placed between the muscles to reduce to 1-reference. Other reference electrode position could be in the other extrema between the differential electrodes. These are distributed over larger surface of the muscle.	37
Figure 31. Channel electrode array with focal-vertex basis configuration.....	38
Figure 32. Normalization processes. A) and C) are original signals of four channels system. B) are the amplified signals by the αi factors. D) shows the four channels in a 150 ms square window, as shown in figure C, amplified β times.....	39
Figure 33. Record normalized -1V to 1V, filtered between 20 Hz -500 Hz and windowed between 3.5s to 4.5s concerning to its 8s record number 3 of the user 1 for closing hand (CBA4_153).....	40
Figure 34. Block Diagram of the Stationary Analysis Stage. Stationary Analysis consist in the methods and processes used to analyze the recorded data using Wavelet and Hilbert-Huang Transforms. Features, characteristics and patterns were found, using these techniques are described, resulting in databases and mathematical models in time and frequency.....	41
Figure 35. Wavelet Daubechies. High order wavelets. Db44 (highlighted) was used in this work. (Rafiee, et al., 2011)	42
Figure 36. Wavelet Meyer.....	42
Figure 37. Wavelet logarithmic scale vs frequency for spectrogram description.....	43
Figure 38. sEMG signal from channel 3 in 1 second timeslot (upper) with the logarithmic scalogram for meyer wavelet coefficients (lower).....	44
Figure 39. Histogram of frequencies channel 4, obtained from the scalogram.....	45
Figure 40. Box plot of the frequencies for channel versus movement.....	46
Figure 41. Flow chart for the sifting algorithm, basis of EMD method.....	49
Figure 42. Intrinsic Mode Functions (IMFs) extracted from channel 1 for transitory stage of supination movement.50	50
Figure 43. Intrinsic Mode Functions (IMFs) extracted from channel 2 for transitory stage of supination movement.50	50
Figure 44. Intrinsic Mode Functions (IMFs) extracted from channel 3 for transitory stage of supination movement.51	51
Figure 45. Intrinsic Mode Functions (IMFs) extracted from channel 4 for transitory stage of supination movement.51	51
Figure 46. Block Diagram of the Nonstationary Analysis Stage. Nonstationary Analysis, propose the conditions, methods, techniques and processes to perform in short-time, under 100 ms, using Kalman Filter and Goertzel filter to identify the features, characteristics or patterns of myoelectric signals. Resulting data could be applied to a classifier system.....	54
Figure 47. Muscular contraction intensity of subject 1 for four channels versus six movements of the fingers. The map shows the intensity present in the four channels when a movement was performed: star represents 0.7 V to 1 V level, dot represents 0.35 V to 0.65 V level, and circle represents 0 V to 0.3 V. Each icon represents one of nine repetitions.....	57
Figure 48. Scalogram of CBA4_234 obtained with Daubechies 44 wavelet	58
Figure 49. Scalogram of CBA4_234 obtained with Meyer Wavelet.....	58
Figure 50. Scalograms for signal from channel 2 (Flexor digitorum superficialis). Meyer base (upper) and Daubechies base (bottom).....	59
Figure 51. 4-Channel Histogram of mean frequencies obtained from Wavelet Analysis.	60

Figure 52. 4-Channel Boxplot for ANOVA results of mean frequencies obtained from Wavelet analysis.....	61
Figure 53. sEMG signals and their IMFs of channel 3 related to the flexion and extension of all fingers. 6 decomposition levels are shown. IMF 2 shows two MUAPs in 50 ms and 100 ms approximately.....	62
Figure 54. Instantaneous frequency (upper) of the Intrinsic Mode Function 2 (lower) for signal of channel 3. Drastic frequency changes are present in the Instantaneous frequency related with the start and end of the contraction..	62
Figure 55. Time patterns associated to MUAP. Period of 24.5 ms average of MUAP.....	63
Figure 56. Hilbert transform (red lines envelops) of IMFs for Channel 1 during supination movement in transient segment.	64
Figure 57. Instantaneous frequencies for Channel 1 during supination movement in transient segment.	64
Figure 58. Hilbert transform of IMFs for Channel 2 during supination movement in transient segment.	65
Figure 59. Instantaneous frequencies for Channel 1 during supination movement in transient segment.	65
Figure 60. Hilbert transform of IMFs for Channel 3 during supination movement in transient segment.	66
Figure 61. Instantaneous frequencies for Channel 3 during supination movement in transient segment.	66
Figure 62. Hilbert transform of IMFs for Channel 3 during supination movement in transient segment.	67
Figure 63. Instantaneous frequencies for Channel 4 during supination movement in transient segment.	67
Figure 64. sEMG signal of Extensor Digitorum muscle (Channel 3) for All fingers extension (5th Movement). Upper figure shows 2 seconds of record with a 300 ms window between 450 ms -750 ms section. 3-Column section shows in the first column the IMFs, from 1 st to 6 th ; second column shows the Instantaneous Frequencies (IFs) of the previous IMF; third column shows the spectrogram of the previous IF.	68
Figure 65. Original signal from the record CBA_153_3 windowed between 250 ms and 450 ms.	69
Figure 66. Signal reconstruction using IMFs 1 to 6.	70
Figure 67. Signal reconstruction using IMFs 1 to 5.	70
Figure 68. Signal reconstruction using IMFs 1 to 4.	71
Figure 69. Signal reconstruction using IMFs 1 to 3.	71
Figure 70. IMF 2 from signal CBA4_153 channel 3 between 275ms to 425 ms.	72
Figure 71. Signal reconstruction using IMFs 2 and 3.....	72
Figure 72. Original signal vs reconstruction in different levels, from up to down: 1. Original signal, reconstruction 2. using IMFs 1 to 6, 3. IMFs 1 to 5, 4. IMFs 1 to 4, 5. IMFs 1 to 3, 6. IMFs 1 and 3, 7. IMFs 2 and 3, and IMF 2. The sequence shows a decrement in intensity directly dependent of the number of IMFs. IMF 2 is the most defined shape into all signals, the IMF 3 represents only a small significance in addition with IMF 2.	73
Figure 73. Frequency pattern plot with 83.3 Hz, 96.7 Hz and 113.3 Hz components.....	76
Figure 74. Kalman filter responses in simulated and real sEMG signals. a) Simulated sEMG signal (red line) is fitted with the math sEMG model established in the filtering parameters. b) Real sEMG signal (black line) is fitted with the math sEMG model settled in the parameters.	78
Figure 75. Periodogram of the PSD estimated with FFT for xpattern signal without noise.....	79
Figure 76. Periodogram of the PSD estimated with FFT for xpattern signal with white noise and power line noise.	80
Figure 77. Discrete Fourier Transform of the xpattern signal without noise obtained by Goertzel Algorithm.....	80
Figure 78. Discrete Fourier Transform of the xpattern signal with white and power line noises obtained by Goertzel Algorithm.	81

RESUMEN

En esta tesis se reportan los procesos para analizar las señales sEMG multicanal a través del uso de las transformaciones Wavelet y Hilbert-Huang, así como de otros métodos de análisis de señales, tales como filtros Kalman y Göertzel, como técnicas para detectar, medir, filtrar y descomponer esas señales sEMG para identificar los patrones en tiempo, frecuencia, espacio o su combinación, para movimientos de flexión y extensión de los dedos de la mano usando los músculos superficiales del antebrazo asociados a ellos para la predicción de sus movimientos y reducir el tiempo de cómputo de las características. El objetivo de la investigación es mejorar el tiempo de cálculo de las señales electromiográficas para el control de dispositivos protésicos usando sólo sensores superficiales. La hipótesis tiene como base que todos los movimientos de la mano son respuesta de la actividad mioeléctrica de músculos en específico del brazo y antebrazo, esta actividad eléctrica puede ser medida como una señal electromiográfica relacionada a una secuencia de movimientos de los elementos de la mano, los dedos. Cada dedo realiza una trayectoria desde la posición relajada hasta la última posición deseada, esta trayectoria no es un trazo instantáneo, por lo que, la señal mioeléctrica no es instantánea. La actividad eléctrica del músculo está presente en las señales registradas, entonces esta puede ser definida como un grupo de frecuencias o un trazo de energía. Esta actividad eléctrica puede ser reconocida por un algoritmo dentro de una base de datos de sus patrones, comparar la actividad eléctrica de los músculos en tiempo real contra estos datos para crear una tendencia del comportamiento de la mano y, posiblemente, predecirla para reducir el tiempo de cómputo para encontrar el movimiento específico antes o al mismo tiempo de su ejecución.

El objetivo general es la propuesta de un método y sus algoritmos para predecir y corregir los movimientos de la mano por medio de la identificación de los patrones y características de la señal mioeléctrica en músculos del antebrazo en un tiempo de procesamiento menor a los 100 ms. Los objetivos específicos se dividen en tres etapas : Adquisición, Análisis Estacionario de la Señal (SSA) y Análisis No-Estacionario de la Señal (NSA). La etapa de adquisición es común para las etapas SSA y NSA. Para la etapa de adquisición, las señales son adquiridas colocando electrodos superficiales Ag/AgCl sobre cinco músculos del antebrazo ligados a los dedos. Usando un arreglo configurado de 4 canales, las señales fueron muestreadas y registradas. Enseguida, las señales fueron normalizadas y recortadas dentro de una ventana cuadrada antes de ser analizada. Una base de datos de los seis movimientos de los dedos fue obtenida. El análisis estacionario consta de los métodos y procesos propuestos para analizar los datos registrados usando las transformadas Wavelet y Hilbert-Huang. Del uso de éstas, características particulares y específicas, así como patrones, fueron encontrados. Los escalogramas y las características estadísticas son reportadas. Los patrones de tiempo y frecuencia son descritos como modelos matemáticos. Una característica intrínseca de la actividad muscular que está asociada a la intensidad muscular de la señal mioeléctrica, también se muestra. Los resultados son de utilidad para la propuesta de procesos de filtrado e identificación de características en tiempo real. Por otro lado, en el análisis no estacionario de las señales, se proponen las condiciones, métodos, técnicas y procesos para realizar en un corto tiempo, un periodo de menos de 100 ms, la identificación de las características y patrones de las señales mioeléctricas. El filtro Kalman mejora la eliminación de ruido y la reconstrucción de la señal para predecir la señal de entrada, la señal mioeléctrica. La señal de salida del filtro Kalman entra al filtro Goertzel, que detecta señales específicas usando la transformada de Fourier discreta con base en los patrones y características modelados. Los resultantes de estos filtros pueden ser aplicados directamente a un sistema protésico como señal de control o introducidos a un sistema de clasificación, dependiendo de la complejidad del sistema de adquisición, los canales o movimientos.

El sistema de predicción propuesto se adapta a aplicaciones de tiempo real usando sólo las señales mioeléctricas como entrada. La naturaleza dinámica del filtro Kalman provee para la variación de tiempo una fusión óptima de la información mioeléctrica, intensidad muscular y estadística de los movimientos. Usando el filtro Kalman es posible reducir el ruido y reconstruir rápidamente la forma de onda deseada. El filtro Goertzel reconoce de forma simple las frecuencias deseadas en un periodo cercano a 5 ms. El patrón de tiempo establece una señal de activación de 24.5 ms, un periodo de 30 ms de reconstitución y otro de 24.5 ms de desactivación. Éstos periodos sugieren que la ventana óptima de análisis es de 30 ms para aplicar cualquier método utilizado en este trabajo. Con una ventana de 30 ms, en 15 ms se podría realizar la predicción y 5 ms para detectar el tono ; por tanto el tiempo para la identificación, detección, predicción y corrección de la señal mioeléctrica puede ser realizada en un tiempo menor a 100 ms.

RÉSUMÉ

Cette thèse rapporte les processus pour analyser l'signal sEMG multicanal à l'aide de la transformée en ondelettes, transformation de Hilbert-Huang et d'autres méthodes d'analyse des signaux, tels que les filtres de Kalman et Goertzel, comme techniques pour détecter, mesurer, filtrer et décomposent ceux les signaux sEMG pour identifier des tendances dans le temps, fréquence, espace ou combinaison des mouvements de flexion-extension des doigts de la main à l'aide de muscles superficiels lien-doigts afin de prédire le mouvement de la main et de minimiser le temps de calcul. Le but de notre recherche est d'améliorer le temps de calcul pour les caractéristiques des signaux myoélectrique pour contrôler des prothèses à l'aide de capteurs superficiels. L'hypothèse est fondée par l'idée que tous les mouvements de la main sont une réponse active à l'activité myoélectrique des muscles spécifiques, que l'activité électrique peut être mesure comme un signal associé à une séquence de mouvement des éléments de la main, doigts. Chaque doigt peut effectuer une trajectoire de la position de repos à la position finale, cette trajectoire n'est pas un chemin d'accès instantané, le signal myoélectrique n'est donc pas une activité instantanée. L'activité électrique du muscle est présente sur les signaux enregistrés, alors cela pourrait être définie comme un groupe de fréquences. Cette activité électrique pourrait être reconnu pour un algorithme à partir d'une base de données de ses modèles, comparer l'activité électrique des muscles en temps réel par rapport à ces données pour créer une tendance du comportement de la main et prévoir pour réduire les temps de calcul pour trouver le mouvement spécifique avant ou en même temps.

L'objectif général est de proposer une méthode et ses algorithmes pour prévoir et corriger les mouvements de la main par l'identification des caractéristiques des signaux myoélectriques et patterns dans les muscles de l'avant-bras en moins de 100 ms temps de traitement. Les objectifs spécifiques se compose de trois étapes : analyse de signal stationnaire (SSA), Acquisition et analyse de Signal stationnaire (NSA). La phase d'acquisition est commune pour SSA et NSA. Pour l'étape de l'acquisition, les signaux sont acquis en plaçant des électrodes de surface, Ag/AgCl, sur cinq muscles lien-doigt avant-bras des sujets. Utilisez une configuration de matrice 4 canaux électrode, ces signaux ont été échantillonnés et enregistré. Ensuite, les signaux ont été normalisés et fenêtré avant les étapes de l'analyses. Base de données pour six mouvements des doigts ont été obtenus. L'analyse stationnaire consiste dans les méthodes et procédés proposés pour analyser les données enregistrées en utilisant les ondelettes et transforme de Hilbert-Huang. Les caractéristiques et les modèles ont été trouvés à l'aide de ces techniques. Scalogrammes et caractéristiques statistiques sont rapportés. Les patrons temporels et fréquentiels sont décrits comme des modèles mathématiques. Une caractéristique intrinsèque de l'activité musculaire liée à l'intensité du signal sEMG est également montrée. Les résultats sont utiles à proposer un processus de filtrage en temps réel. L'analyse de signaux non stationnaires, est une proposition pour les conditions, les méthodes, les techniques et les procédés d'accomplir en temps réel ou courte durée, moins de 100 ms de fente de traitement, à l'aide de filtres de Kalman et Goertzel pour identifier les fonctions, les caractéristiques ou les patrons des signaux myoélectriques. Filtre Kalman améliore le débruitage et à la reconstruction pour prédire le signal d'entrée, le signal myoélectrique. Le signal de sortie du filtre de Kalman va au filtre Goertzel, qui détecte les signaux spécifiques à l'aide de la transformée de Fourier discrète basée sur les modèles modélisés. Les résultats de ces filtres peuvent être appliquées directement sur le système de prothèse comme un signal de commande ou être appliquées à un système de classification.

La méthode de prédiction proposé est adaptée aux applications en temps réel en utilisant uniquement les signaux myoélectrique comme entrée. La nature dynamique du filtre Kalman prévoit la fusion optimale de l'information de variable dans le temps et permet d'appréhender l'activité myoélectrique, caractéristiques de l'intensité musculaire et statistiques des mouvements. À l'aide de filtre Kalman est également possible réduire le bruit et fournir une reconstruction rapide de la forme de la forme désirée des modèles signalés. Le filtre Goertzel fournit une méthode simple d'identification des fréquences motif dans une période de presque 5 ms ou plus, juste pour repérer les fréquences souhaitées. Le patron de temps établit une période de 24,5 ms pour signal d'activation, une période de 30 ms de réversibilité et 24,5 ms du délai accordé pour signal de désactivation. Ces temps suggèrent que le fenêtrage durée minimale est de 30 ms pour appliquer la l'analyse utilisée pour ce travail. Avec une fenêtre de 30 ms, presque 15 ms à exécute prédiction et 5 ms pour effectuer la détection de tonalité ; puis le temps consommation pour l'identification, prédiction, la détection et la correction du signal myoélectrique pouvaient être pratiquées à moins de 100 ms.

ABSTRACT

This thesis reports the processes to analyze multichannel sEMG signals using Wavelet transform, Hilbert-Huang Transform, and other analysis methods, such like Kalman filter and Goertzel filter, as techniques to detect, measure, filter and decompose those sEMG signals to identify patterns in time, frequency, space or combination for flexion-extension movements of the fingers of the hand using link-fingers superficial muscles in order to predict the movement of the hand and minimize the time computing. The aim of our research is to improve time computing for EMG signals characteristics to control prosthetic devices using superficial sensors and not indwelling, last one has inherent limitations. The hypothesis is based by the idea that all hand movements are an active response to the myoelectric activity of specific muscles present in the arm and forearm, that electric activity can be measure as an EMG signal related to a sequence of movement of the elements of the hand, fingers. Each finger can perform a trajectory from doss position to last position, this trajectory is not an instantaneous path, therefore, the myoelectric signal is not an instantaneous activity. The electric activity of the muscle is present on the recorded signals, so then this could be defined as a group of frequencies or path of energy. This electric activity could be recognized for an algorithm from a database of its patterns, compare the electric activity of the muscles in real time versus this data to create a trend of the behavior of the hand and, possibly, predicting to reduce time computing to find the specific movement before or at the same time.

The general goal is to propose a method and its algorithms to predict and correct the movements of the hand by the identification of the myoelectric signal characteristics and patterns in the forearm muscles in under 100 ms time of processing. The Specific goals is composed by three stages: Acquisition, Stationary Signal Analysis (SSA) and Nonstationary Signal Analysis (NSA). The Acquisition stage is common for SSA and NSA. For the acquisition stage, the signals are acquired by placing Ag/AgCl surface electrodes over five forearm link-finger muscles of the subjects. Using a 4-channel electrode array configuration, these signals were sampled and recorded. Then, signals were normalized and windowed previous to the analyzing steps. Database for six movements of the fingers were obtained. The stationary analysis consists in the methods and processes proposed to analyze the recorded data using Wavelet and Hilbert-Huang Transforms. Features, characteristics and patterns were found using these techniques. Scalograms and Statistical features are reported. Time and frequency patterns are described as mathematical models. A intrinsic characteristic of the muscular activity related with the intensity of the sEMG signal is also showed. Results are useful to propose a real-time filtering processes. The nonstationary signal analysis, is a proposal for the conditions, methods, techniques and processes to perform in short-time, or real-time under 100 ms of processing slot, using Kalman and Goertzel filters to identify the features, characteristics or patterns of the myoelectric signals. Kalman filter improves the denoising and reconstruction to predict the input signal, myoelectric signal. The output signal from Kalman Filter goes to the Goertzel filter, that detects specific signals using the Discrete Fourier Transform based on the modeled patterns. Results from these filters could be applied directly to the prosthetic system as a control signal or be applied to a classifier system, depending on the complexity of the acquisition system, channels or movements.

Proposed prediction method is suitable for real-time applications using only the EMG signals as input. The dynamical nature of the Kalman filter provides for the time varying optimal fusion of the information and allows to consider myoelectric activity, muscular intensity features and statistical of the finger movements. Using Kalman filter is also possible to reduce the noise and provide a quick reconstruction of the desired shape form of the patterns reported. Goertzel filter provides a simple identification method of the pattern frequencies in a time of almost 5 ms or above, just to locate the desired frequencies. The time pattern establishes a period of 24.5 ms for activation signal, a period of 30 ms for reversibility and 24.5 ms of period for deactivation signal. This time slot suggest that the minimum time windowing is 30 ms to apply any of the analyzing method used for this work. With a window of 30 ms, almost 15 ms to performs prediction and 5 ms to perform tone detection; then time consumption for the identification, detection, prediction and correction of the myoelectric signal could be performed in under 100 ms.

GENERAL INTRODUCTION

The main function of the hand is grasp. The elements that are responsible of grasping are the fingers, which coordinated can do more than 27 combinations. By the way, the main function of a prosthetic hand is to grasp an object (Altamirano-Altamirano, et al., 2013). Primary functions of the prosthetic hand are based on electromechanical devices that are activated by instructions, those came from a control system. Control system is operated and monitored by a program constructed over an algorithm that guide and execute tasks to perform each movement of the hand.

Human movement control system is in the central nervous system and downwards over the peripheral nervous system, a complex communication web with its own language. Each action of the body is ruled by the central nervous instructions (Basmajian & De Luca, 1985). Also, human body signals of activation, control and monitoring have special codification that are very different from the programming languages such as C++, assembly language and others. The interpretation of the instructions that muscles receive from nervous system to perform movements are useful for the development of artificial elements like prostheses or orthoses.

Prosthetic hands are tools for user assistance, must be quick and precise in response. These devices should fit to daily life. Time computing improvement of the calculations of the signals and their characteristics could decrease the requirements of the prosthetic system in electronic, mechanic and energy devices.

Superficial myoelectric signals provide enough data about muscular activity in a non-invasive way, this information came in patterns that can be used as a very effective source of control (Boostani & Moradi, 2003) (Chu, et al., 2005) (Castellini & van der Smagt, 2009) (Rafiee, et al., 2010).

sEMG signals are motor unit action potentials (MUAPs) combination of muscle fibers that surround a superficial electrode placed over skin surface, then position of the electrode is very important to obtain MUAPs from one, two or more muscle at the same time. The shapes and firing rates of MUAPs are an important source of information (Adam, et al., 1998)(Adam & De Luca, 2003). sEMG signals are capable to provide enough information about muscular activity in a non-invasive way becoming an effective source for prosthetic control (Boostani & Moradi, 2003) (Chu, et al., 2005) (Castellini & van der Smagt, 2009)(Rafiee, et al., 2010).

sEMG signals are very noisy (Loren & Wilkins, 2011) (Nait-Ali, 2009), this noise could be produced by the electronic system, be inherent to the body or be interfered by EM sources (Pallás-Areny & Webster, 1999). Common noise is provided by tissues that surround muscles or the muscles themselves, as MUAPs by movements of the users, artifacts, and electric EMG interference (Chowdhury, et al., 2013) such as line power sources or wireless devices such as Bluetooth, Wi-Fi, IR, etcetera. It's important to clean the sEMG signals to take out the MUAP signal without noise and then analyze it to obtain information available into the sEMG signal as timing, firing rates, synchronization, intervals, and morphology of the MUAPs to known health and anatomy of muscle fibers (De Luca, et al., 2006).

Several algorithms have been proposed to clean, denoise or filter the sEMG signals , however, the latest methods in recent years, worked under the decomposition basis to extract all possible sinusoids and non-sinusoids components into a MUAP, these methods perform decomposition in order to detect differences in shapes, tack changes and, even, solve superposition (Lesser, et al., 1995) (Fang, et al., 1997) (Yamada, et al., 2003) (Zennaro, et al., 2003) (De Luca, et al., 2006)

For sEMG or iEMG signals it is not enough to identify the presence of a certain frequency in the signal, it is necessary to localize this frequency in time-space, thus to provide more information about

muscle's behavior related to specific movements, pattern contraction and pathological disorders (Pinzon-Morales, et al., 2011).

In recent years, methods like Wavelets and Hilbert-Huang transform have been proposed to denoise, filter, decompose, detect, analyze and predict non-stationary and non-linear signals to achieve their characteristics and patterns in time, frequency, energy and intensity (Flanders, 2002) (Meeson, 2005) (Tsolis & Xenos, 2011) (Chung & Dong-ling, 2004) (Phinyomark, et al., 2011) (Zhang & Zhou, 2014) (Yan & Lu, 2014). Works developed by Carlo De Luca and Hamid Nawab, are focused on sEMG and iEMG decomposition and improving methods to solve accuracy and consistency of the MUAPs achieved by using knowledge-based Artificial Intelligence framework (De Luca, et al., 2006) (Nawab, et al., 2002).

Raw sEMG signal is a source of information with many noise. This information could be useful if is well analyzed, quantified, classified (Basmajian & De Luca, 1985). Recent research support the hypothesis that EMG signals could be used to anticipate movements of the muscles (Hoffman & Herr, 2002) (Hou, et al., 2004) and then to take decisions in advance to control orthotic or prosthetic devices (Park, et al., 2012)(Hoozemans & van Dieën, 2005)(Altamirano-Altamirano, et al., 2014) (Altamirano-Altamirano, et al., 2013).

One of the primary goals of our research is to improve time computing for EMG signals characteristics to control prosthetic devices using superficial sensors and not indwelling, last one has inherent limitations (Munoz, et al., 1997) (De Luca, et al., 2006). A prosthetic user needs to use easy-built systems for day-life in good or worst conditions such as no skin preparation, fixed sensors, quick response systems, and etcetera.

This works reports the processes to analyze multichannel sEMG signals using Wavelet transform, Hilbert-Huang Transform, and other analysis methods as techniques to detect, measure, filter and decompose those sEMG signals to identify patterns in time, frequency, space or combination for flexion-extension movements of the fingers of the hand using link-fingers superficial muscles.

The EMG signals are biomedical signals that measures electrical activities in the muscles during a contraction or relaxation process, this represents the neuromuscular activity. EMG signal is a complex signal, this is a signal control from the neural system to the muscles, and this also depends of the anatomical and physiological properties of muscles.

The main reason for the interest in EMG signal analysis is in clinical diagnosis, biomedical applications and rehabilitation area. The shapes and firing rates of Motor Unit Action Potentials (MUAPs) in EMG signals provide an important source of information for the diagnosis of neuromuscular disorders. Once appropriate algorithms and methods for EMG signal analysis are readily available, the nature and characteristics of the signal can be understood and hardware implementations can be made for various EMG signal related applications.

There are limitations in detections and characterization of existing non-linearity in the surface electromyography (sEMG) signal, estimation of the phase, acquiring exact information due to derivation from normality (Sahid, 2004). Recent advances in technologies in signal processing and mathematical models have made in practical to develop advanced EMG detection and analysis techniques. Various mathematical techniques and Artificial Intelligence (AI) have received extensive attraction. Mathematical models include Wavelet Transform (WT), time-frequency approaches, Fourier Transform (FT), Wigner-Ville Distribution (WVD), statistical measures, higher order statistics and Hilbert-Huang Transform (HHT). Artificial Intelligence approaches toward signal recognition include Artificial Neural Networks (ANN), Dynamic Recurrent Neural Networks (DRNN), and Fuzzy Logic System (FLS). Genetic Algorithm (GA) has also been applied in evolvable chip for the mapping of EMG inputs to desired hand actions. In the other hand, methods like Mean Frequency (MF), Median Frequency (MF), Mean Peak Frequency (PKF), Mean Power (MNP), Spectral Moments or Central Frequency Variance are not good to classify EMG signals (Phinyomark, et al., 2011).

Wavelet transform is well suited to non-linear signals like EMG. Time-frequency approach using WVD in hardware could allow for some real-time instruments that biofeedback situations. Higher-order

statistical (HOS) methods may be used for analyzing the EMG signal due to the unique properties of HOS applied to random time series.

Hilbert-Huang transform was developed by Huang in 1999 for time-frequency analysis that simultaneously offers a good resolution. This analysis consists in two main processes: Empirical Mode Decomposition (EMD) and Hilbert transform (HT) (Huang, et al., 1998) (Huang, 2005). EMD is a method to decompose nonlinear signals into fundamental signals called Intrinsic Mode Functions (IMFs). Result of these processes are symmetric signals described in time and frequency also in energy.

Myoelectric signals are set of several signals from the muscle fibers in addition with intrinsic noise components. These signals have specific time slots and frequencies, patterns. Mathematical models could be proposed to describe myoelectric activity. These models can be used to identify the behavior of the muscle for specific movements, i.e. for finger flexion and extension.

Recent investigations (Hoffman & Herr, 2002) support the hypothesis that EMG peripheral neural signals can be used to anticipate human movements approximately 100 ms in advance. These results suggest that EMG sensory data could be used to foresee the future biomechanics of a human, thereby making it possible to anticipate the movement intent of the Orthosis & Prosthesis (O&P) user.

Predictive and filtering algorithms were applied as methods to improve the myoelectric signal analysis to obtain their patterns and characteristics. Kalman filter provides trajectory correction of an input signal to avoid noise and artifact interference, also an approximation of the desired signal. Then, a Goertzel filter, related to Discrete Fourier transform filter, is applied to the output of Kalman filter to identify the desired signal and result into a false or true unique signal.

Systems based on myoelectric signal control require specific features inputs according to the process. For prosthetic systems, it is necessary to define the kind of prosthesis and its capability just to select the activation mode, the controlling parameters and variables to consider. It seems, then, that the problem of control by the patient is going to be a major issue in the next years. As the prosthetic hand becomes more flexible; how is the patient supposed to precisely command the prosthesis what to do? Operating hand requires a fine and quick control, possibly down to the level of the single fingers:

1. Presented with a certain task such as turning a door handle or grabbing a car key, the patient must be able to enforce the correct grasping type; this involves the activation of some joint
2. Each person is different from each other. The EMG signals are not the same for all persons. We need a common signal, pattern or behavior for all.
3. Electronic devices always perform tasks in time. When you process an EMG signal there will be a delay in time to get the answer or the solution.
4. Acquisition systems always will have noise, inherent or induced, there is not ideal signals. We should improve denoising, mostly, from the first stage of acquisition: electrodes.

The characteristics of ideal upper limb myoelectric control system should satisfy following criteria:

1. The control should be intuitive for user, as natural movements.
2. The system should be robust to doffing and donning.
3. It should be able to adapt to physiological changes, such as sweating, fatigue or neurological disorders.
4. Easy and short training/calibration.
5. Quick response systems as possible embedded, not have big devices.
6. Quick response algorithms, under 300 ms.
7. Analysis and time computing versus complexity to perform real-time applications (Chu, et al., 2005) (Huang & Chen, 1999).

The hypothesis is because all hand movements are an active response to the myoelectric activity of specific muscles present in the arm and forearm, that electric activity can be measured as an EMG signal related to a sequence of movement of the elements of the hand, fingers. Each finger can perform a trajectory from a rest position to last position, this trajectory is not an instantaneous path, therefore, the myoelectric

signal is not an instantaneous activity, such as Dirac function, it has a trajectory too. The trajectory of the electric activity of the muscle is present on the EMG signal(s) recorded, so then this trajectory could be defined as a group of frequencies, a path of energy or have another shape. So, this trajectory could be recognized for an algorithm and, first, create a database of this patterns, and then, compare the electric activity of the muscles in real time versus this data to create a trend of the behavior of the hand and, possibly, take decisions in advance to reduce time computing to find the specific movement before or at the same time of performing by the muscle. This is to control a prosthetic hand prosthesis with five fingers.

STATE OF THE ART

In 2004, Hou, Zurada and Karwowski (Hou, *et al.*, 2004) proposed a novel structure of feed-forward neural network to obtain better accuracy of prediction. The task was to predict the magnitude of ten trunk muscles during manual lifting tasks. In this basic model, they predict EMG signals point by point. Each input vector consists of 12 kinematics variables of one sampling point of one subject, as well as the corresponding 15 subject variables. The timing variables the sampling point of the current input. The kinematics variables are time series, while the subject variables of each subject are constants. All sampling points of all subjects in a same motion were used to train the network one by one. By adding regional connections between the input and the output, this architecture of the neural network van has both global features and regional features extracted from the input. the global connections put more emphasis on the whole picture and determine the global trend of the predicted curve, while the regional connections concentrate on each point and modify the prediction locally. Back-propagation Algorithm is used in the modelling. A basic structure of neural network designed for this problem was discussed. Then overcome its dear backs, they propose a new structure.

In 2005, *Hoozemans and Van Dieën* (Hoozemans & van Dieën, 2005) presented a study to predict handgrip forces, their work consists on determine the validity of linear regression models using the surface electromyography (sEMG) of up to 6 forearm muscles. In the report, they used ideal conditions for isometric gripping tasks and normalized EMG to grip force calibrations. In the results, the predicted grip forces were close compared with the observed; they report that the EMG-hand force model appeared to be minimal affected by grip with, they also report that only 3 of 6 muscles should be assessed to arrive at sufficient level of validity.

In 2009, Castellini and van der Smagt (Castellini & van der Smagt, 2009) dealt with advanced robotic hand control via surface electromyography. They show that machine learning, together with a simple down-sampling algorithm, can be effectively used to control on-line, in real time, finger position as well as finger force a highly dexterous robotic hand. The system determines the type of grasp a human subject is willing to use, and the required amount of force involved, with a high degree of accuracy. This represents a remarkable improvement with respect to the state-of-the-art of feed-forward control of dexterous mechanical hands, and opens a scenario in which amputees will be able to control hand prostheses in a much finer way.

In 2010, Rafiee and his team (Rafiee, *et al.*, 2010) worked on a system based on CWC, they report that in classification, feature vector is defined as a compressed, meaningful vector/matrix possessing the significant information of different classes. In this research, CWC was used for the calculation of feature vectors for EMG signals. The CWC of the signal, itself, is not appropriate as a feature vector because it is computationally expensive.

In 2011, Pinzon-Morales and his team (Pinzon-Morales, *et al.*, 2011) proposed a method for hand movement pattern recognition from electrography (EMG) biological signals. The signals were recorded by a three-channel data acquisition system using surface electrodes placed over the forearm, and then processed to recognize five hand movements: opening, closing, supination, flexion and extension. Their proposal is based the combination of Hilbert-Huang Analysis with a fuzzy clustering classifier. A set of metrics, calculated from the time contour of the Hilbert Spectrum, was used to compute a discriminating three-dimensional feature space. Empirical analysis of the proposed method reveals an average accuracy rate of 96% in the recognition of surface EMG signals. This method introduces: 1) assumptions about linearity or stationary were not needed; 2) previous knowledge about the data in the feature extraction was not required to analyze the signal; and 3) high classification accuracy was achieved.

In 2013, Wang, Chen and Zhang (Wang, et al., 2013), presented a work of the prehensile hand gestures role in daily living for seizing of holding subjects stably. In order to realize the accurate recognition of eight prehensile hand gestures with a minimal number of electrodes, an off-line myoelectric control system with only two electrodes was developed. They used the mean absolute value, variance, the fourth-order autoregressive coefficient, zero crossings, mean frequency and middle frequency as original EMG feature set. The extent of dimension reduction was investigated and on the premise of it, the average accuracy can achieve 97.46% in the recognition of six hand gestures. An average method was proposed to improve the accuracy further, resulting in the average accuracy in eight gestures being 98.12% and the best individual accuracy of some hand gestures being 100%.

In 2014, Amsüss, Farina and their team (Amsuss, et al., 2014) proposed a self-correcting pattern recognition system of surface EMG signals for upper limb prosthesis control. This proposal is a postprocessing algorithm, aiming to detect and remove misclassifications of a pattern recognition system of forearm and hand motions. Various nonstationarities were included in the experimental protocol to account for challenges posed in real-life settings, such as different contraction levels, static and dynamic motion phases, and effects induced by day-to-day transfers, such as electrode shifts, impedance changes, and psychometric user variability. The system significantly reduced misclassifications to wrong active classes, this is a promising approach for improving the robustness of hand prosthesis controllability.

In 2014, Xing *et al* (Xing, et al., 2014), reported a real-time classifier system to recognize patterns to control a virtual myoelectric hand using a four-channel acquisition system with high-level classifiers to detect seven movements of the wrist.

In 2012, Park and his team (Park, *et al.*, 2012), developed a model to describe a real-time thumb-tip force prediction using sEMG signals. The Hill-based muscle model was used to predict the thumb-tip force under four different angle configurations. They used a mapping model from the literature to estimate the thumb-tip force from the muscle forces without considering complex thumb biomechanics. They compare the prediction performance using the linear regression and ANN methods. This method is feasible for the thumb-tip force prediction. The possible applications of this research include the control of finger-tip forces from noninvasive neuro-signals in robotic hand parts.

PREVIOUS RELATED WORKS

In 2016, J. Antonio Barraza Madrigal, PhD. presented the doctoral thesis named “Design and development of an ambulatory system for movement analysis: monitoring, reproduction and tracking of the shoulder movement.” CINVESTAV-IPN, Mexico.

In 2015, J. Antonio Ruvalcaba Granados, MSc. Presented the master thesis named “Design and development on an embedded electrode for superficial EMG signals acquisition.” CINVESTAV-IPN.

In 2012, Alvaro Altamirano Altamirano, MSc. Presented the master thesis named “Proposal of a anthropomorphic hand prototype to use as prosthesis.” CINVESTAV-IPN, Mexico.

In 2012, Moisés León Ponce, PhD. presented the doctoral thesis named “Classification of myoelectric patterns for the operation of anthropomorphic device.” CINVESTAV-IPN, Mexico

WORK & AUTHORS	CHARACTERISTICS			RESULTS
Self-correcting Pattern Recognition System of sEMG Signals for Upper Limb Prosthesis Control. Amsüs, Farina, et al. 2014	Self-correcting EMG pattern	Real-time movements of the hand.	Contraction levels, misclassification, motion phases	Algorithm that corrects the external parameters that affects the prediction conditions of the system
Prediction of EMG signals of trunks muscles in manual lifting using a Neural Network Model. Hou, et al., 2004	Cinematic variables	Artificial Neural Networks	Real-Time Analysis	Algorithm that predicts cinematic curves of the movements.
Prediction of handgrip forces using Surface EMG of forearm muscles. Hoozemans, et al. 2005	6 forearm channels with force feedback	Fuzzy Logic Systems	Stationary and Nonstationary analysis	Prediction of isometric grasping
Decomposition of Surface EMG Signals. De Luca, et al., 2006	4 channels over ocular muscles	Artificial Intelligence Decomposition	30 ms segmentation	Neuromotor signals and their firing rates
Mean frequency derived via Hilbert-Huang transform with application to fatigue EMG signal analysis. Xie & Wang, 2006	1 channel in arm muscle	Hilbert-Huang and Wavelet decomposition	500 ms segmentation	Hilbert-Huang analysis is optimal for short period analysis
Surface EMG in advanced hand prosthetics. Castellini, et al., 2009	6 channels	EMG characteristics	Real-Time analysis using Neuronal Networks	Direct EMG control in real-time
Pattern Recognition of Surface EMG Biological Signals by Means of Hilbert Spectrum and Fuzzy Clustering. Pinzon-Morales, et al., 2011	3 forearm channels	Empirical Mode Decomposition	Stationary signal analysis algorithms	EMG pattern classification for five movements of the hand
Real-time thumb-tip force predictions from noninvasive biosignals and biomechanical models. Park, et al., 2012	Prediction	Biomechanic feedback	Stationary analysis	Thumb force prediction
Emg Pattern Prediction For Upper Limb Movements Based On Wavelet And Hilbert-Huang Transform. Alvaro ALTAMIRANO ALTAMIRANO MSc. PhD Candidate	4, 8, 16 – Multichannel	Hilbert-Huang and Wavelet decomposition	30 ms segmentation Under 100 ms analysis	EMG characteristics for individual Time and Frequency patterns. Noise reduction Predictive basis of EMG model Real-time pattern identification Real-time prosthetic control
	EMG pattern prediction	Real-time filtering using mathematical models of comparison	Hand prosthetic prototype reconfigurable	

GOALS

GENERAL GOAL

Propose a method and its algorithms to predict and correct the movements of the hand by the identification of the myoelectric signal characteristics and patterns in the forearm muscles in under 100 ms time of processing.

SPECIFIC GOALS

The method is composed by three stages: Acquisition, Stationary Signal Analysis (Non-linear & Stationary Signals) and Nonstationary Signal Analysis (Non-linear and nonstationary Processes). The acquisition stage is common for SSA and NSA.

Acquisition stage

- Propose an acquisition protocol to obtain the myoelectric signals related to six movements of the fingers using the forearm muscles using superficial electrodes over the forearm muscles using a four channels acquisition system.
- Set a standard normalization and windowing settings to adapt input signals to the Stationary and Nonstationary analyses.

Stationary Signal Analysis

- Filter and decompose the acquired signals into Intrinsic Mode Functions (IMFs) of the signal using the Empirical Mode Decomposition (EMD) method.
- Obtain the spectrum data and the instantaneous frequencies of the IMFs using Hilbert transform.
- Obtain and model the characteristics and patterns of the myoelectric signals using mathematical methods.
- Analyze the myoelectric signal records using Wavelets and compare method with Hilbert-Huang Transform results.

Nonstationary Signal Analysis

- Propose the mathematical models of the patterns and the intrinsic characteristics as a basis.
- Propose a method using Kalman filter to predict and correct the input myoelectric signal using the mathematical model of the pattern.
- Propose a method using Goertzel filter to identify the predicted and corrected pattern as single tones.

GENERAL BLOCK DIAGRAM ABOUT PREDICTION SYSTEM

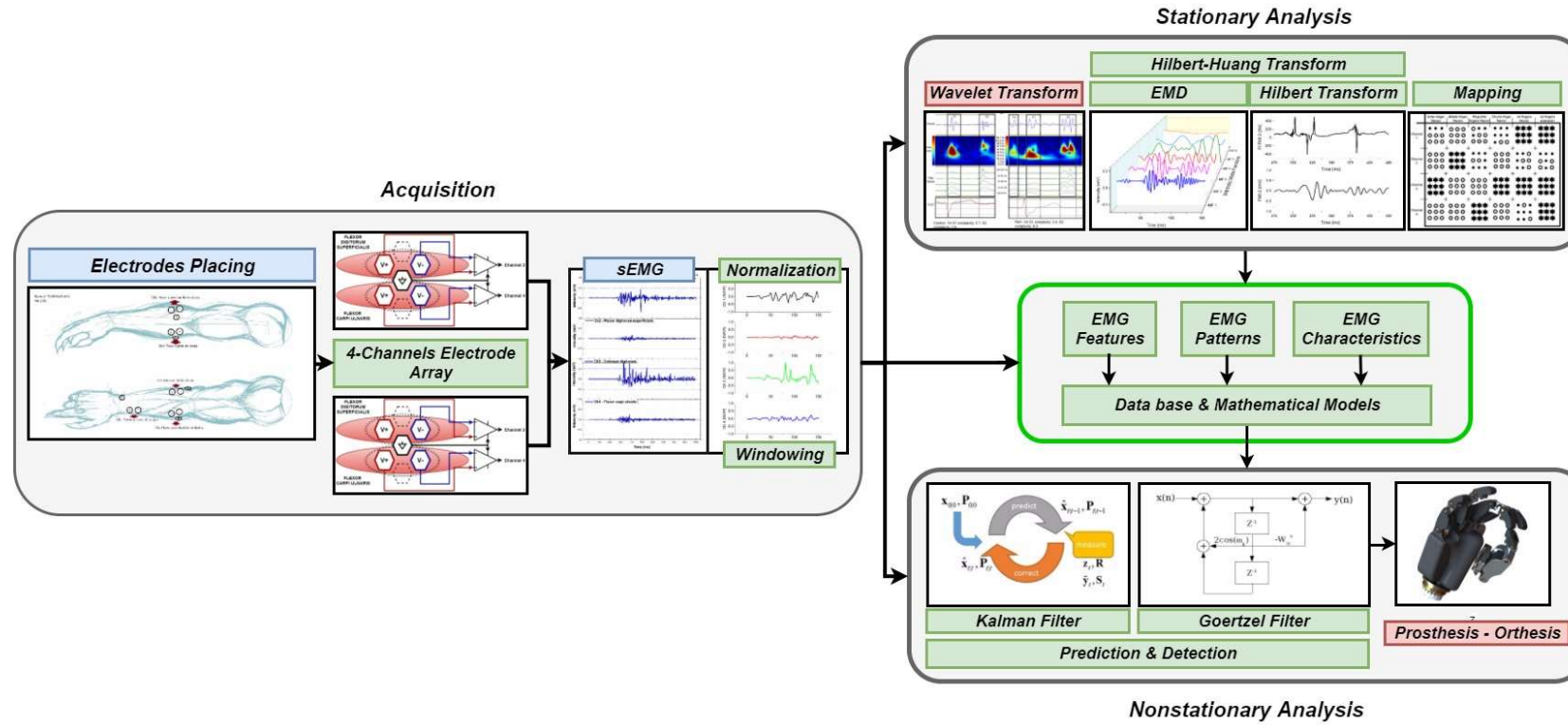


Figure 1. EMG prediction system block diagram.

CHAPTER 1

MUSCLES AND BIOPOTENTIALS

The aim of this chapter is to provide some basic and general information related to the physiology of the muscles and the biosignals, the EMG signals. This chapter is divided in three main sections. First, is about the anatomy and physiology of the muscles. In the second section, the basis of biopotential recording, i.e. electrodes, artifacts and safety. In the third section, some general properties of EMG signals.

1.1 MUSCLE ANATOMY AND PHYSIOLOGY

In electrodiagnostic, to understand the events that occur at molecular level it is important to understand the basic anatomy and physiology. Knowledge of gross nerve and muscle anatomy is required to know the locations of each of these.

1.1.1 Anatomy

The strict definition of the peripheral nervous system includes that part of the nervous system in which the Schwann cell is the major supporting cell, as opposed to the central nervous system in which glial cells are the major support cells. The peripheral nervous system is a group of nerve roots, peripheral nerves, primary sensory neurons, neuromuscular junctions (NMJs), and muscles (Figure 2).

1.1.2 Physiology

The primary role of nerve is to transmit information reliably from the anterior horn cells to muscles for the motor system and from the sensory receptors to the spinal cord for the sensory system. Although functionally nerves may seem like electrical wires, there are vast differences between the two. At the molecular level, a complex set chemical and electrical events allows nerve to propagate an electrical signal.

The axonal membrane of every nerve is electrically active. This property results from a combination of a specialized membrane and the sodium/potassium (Na^+/K^+) pump (Figure 3).

The specialized axonal membrane is semipermeable to electrically charged molecules (anions and cations). The membrane is always impermeable to large negatively charged anions, and it is relatively impermeable to sodium in the resting state. This semipermeable membrane, in conjunction with an active Na^+/K^+ pump that moves sodium outside in exchange for potassium, leads to concentration gradients across the membrane. The concentration of sodium is larger outside the membrane, whereas the concentration of potassium and larger anions is greater inside. The combination results in forces that create a resting equilibrium potential. At the nerve cell soma, this resting membrane potential is approximately 70 mV negative inside compared with the outside; distally in the axon it is approximately 90 mV negative.

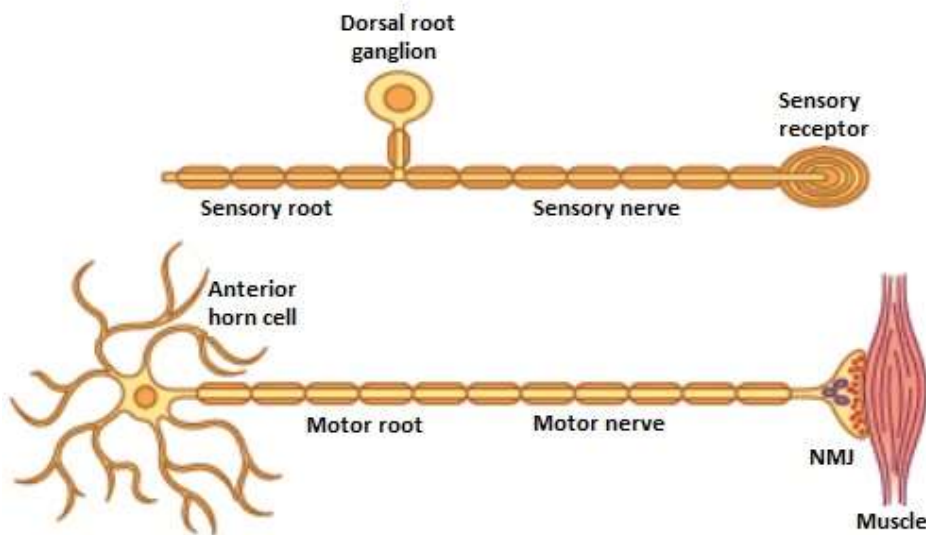


Figure 2. Elements of the peripheral nervous system. The peripheral nervous system includes the peripheral motor and sensory nerves their primary neurons, the anterior horn cells, and dorsal root ganglia; the neuromuscular junctions (NMJs); and muscle. The dorsal root ganglion, a bipolar cell located distal to the sensory root, is anatomically different from the anterior horn cell. Consequently, lesions of the nerve roots result in abnormalities of motor nerve conduction studies but do not affect sensory conduction studies, as the dorsal root ganglion and its peripheral nerve remain intact (Preston, 2013).

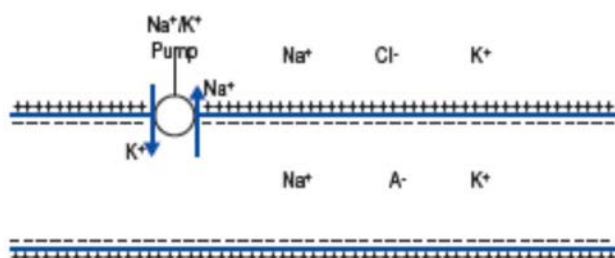


Figure 3. Resting membrane potential. At rest, the axonal membrane is negatively polarized, inside compared to outside. This resting potential results from the combination of a membrane that is semipermeable to charged particles and an active Na^+/K^+ pump. At rest, the concentration of Na^+ and large anions A^- greater inside the axon (Preston, 2013).

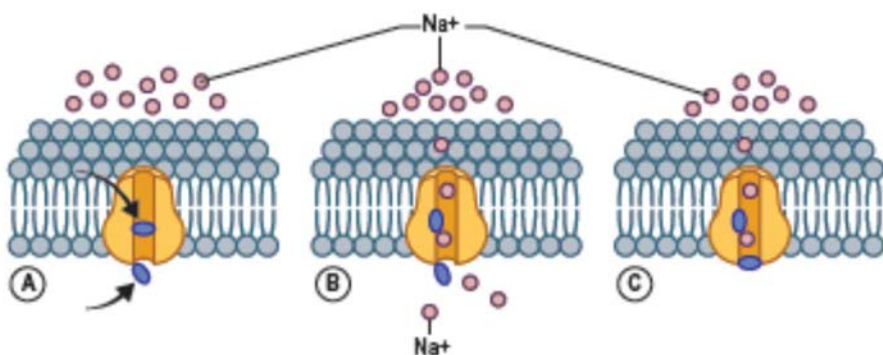


Figure 4. Voltage-gated sodium channel. The axonal membrane is lined with voltage-gated sodium channels. These channels are molecular pores with gates that open and close; when open, gates are selective for sodium A (Preston, 2013).

The membrane of the axon is lined with voltage-gated sodium channels, as shown in Figure 4. These structures are essentially molecular pores with gates that open and close. For many ion channels, gates open in response to molecules that bind to the channel. In the case of the voltage-gated sodium channel, the gate is controlled by a voltage sensor that responds to the level of the membrane potential. If current is injected into the axon, depolarization occurs, i.e. the axon becomes more positive internally. Voltage sensors within the sodium channel respond to the depolarization by opening the gate to the channel and allowing sodium to rush into the axon, driven, both by concentration and by electrical gradients.

Every time, a depolarization of 10 mV to 30 mV occurs above the resting membrane potential, threshold, it creates an action potential and a cycle of positive feedback; further depolarization occurs and more sodium channels open.

Action potentials are always all-or-none responses, which then propagate away from the initial site of depolarization. The axon does not remain depolarized for long, however, because the opening of the sodium channels is time limited.

Sodium channels have a second gate, known as the inactivation gate. The inactivation of the sodium channel occurs within 1 ms to 2 ms. During this time, the membrane is not excitable and cannot be opened, i.e. refractory period. The refractory period limits the frequency that nerves can conduct impulses. It also ensures that the action potential continues to propagate in the same direction. The area of nerve behind the depolarization is refractory when the area ahead is not, so that the impulse will continue forward and will not return backwards.

In addition to sodium channel inactivation, depolarization also results in the opening of potassium channels, which also then drives the membrane voltage more negative. These factors, along with the Na^+/K^+ pump, then reestablish the resting membrane potential.

The conduction velocity of the action potential depends on the diameter of the axon: the larger the axon, the less resistance and the faster the conduction velocity. For axons, typically the conduction velocity is in the range of 0.2 m/s to 1.5 m/s, also conduction velocity could be increased in addition of myelin. Myelin insulation is present on all fast-conducting fibers and is derived from Schwann cells.

Myelinated human peripheral nerve fibers typically conduct in the range of 35 m/s to 75 m/s, far faster than could ever be achieved by increasing the diameter of unmyelinated fibers. Not all human peripheral nerve fibers are myelinated. For unmyelinated fibers, typically, conduction is between 0.2 m/s to 1.5 m/s. When an individual axon is depolarized, an action potential propagates down the nerve. Distally, the axon divides into many embranchments, each of which goes to an individual muscle fiber.

An axon, along with its anterior horn cell and all muscle fibers with which is connected, is known as a motor unit, which is shown in Figure 5. Depolarization of all muscle fibers in a motor unit creates an electrical potential known as the Motor Unit Action Potential (MUAP).

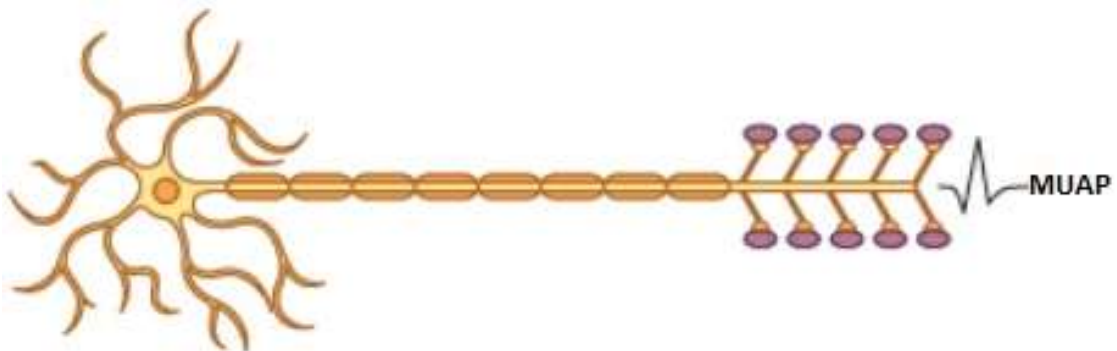


Figure 5. Motor unit is defined as one axon, its anterior horn cell, and all connected muscle fibers and neuromuscular junctions. A nerve fiber action potential normally always results in depolarization of all the muscle fibers of the motor unit creating an electrical potential known as the motor unit action potential (MUAP) (Preston, 2013).

When an action potential is generated, all muscle fibers in the motor unit are normally activated, again an all-or-none response. Before a muscle fiber can be activated, the nerve action potential must be carried across the NMJ.

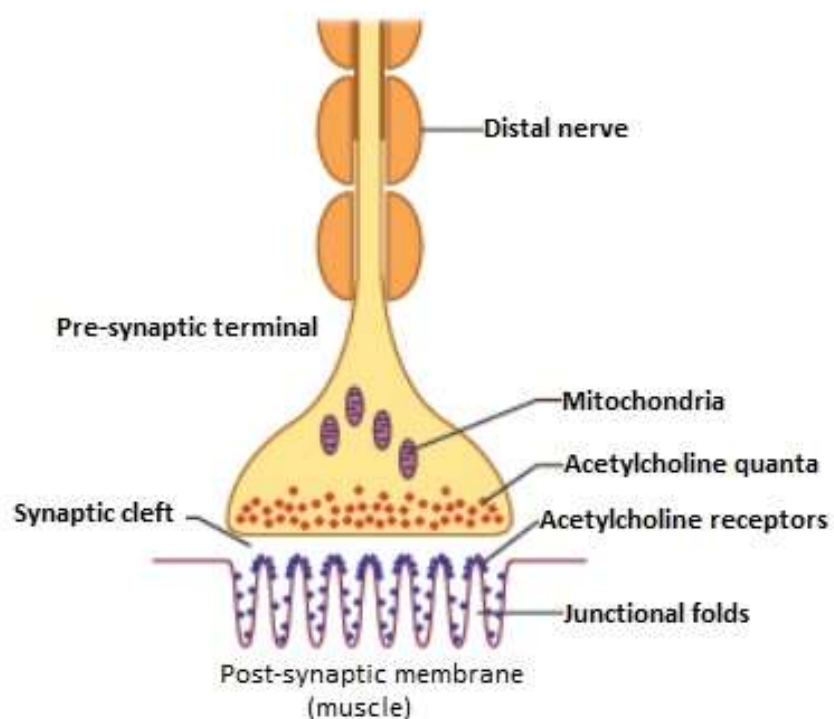


Figure 6. Neuromuscular junction. The neuromuscular junction is a specialized junction between the terminal axon and muscle fiber (Preston, 2013).

1.2 BIOPOTENTIAL RECORDING

Near-fields potentials can be recorded only close to their source, and the characteristics of the potential depend on the distance between the recording electrodes and the electrical source. With near-field potentials, a response generally is not seen until the source is close to the recording electrodes. The closer the recording electrodes are to the current source, the higher the amplitude. Compound muscle action potentials, sensory nerve action potentials, and motor unit action potentials recorded during routine motor conduction, sensory conduction, and surface myoelectric analyses, respectively, are essentially all volume-conducted near-field potentials. Volume-conducted, near-field potentials produce a characteristic triphasic waveform as an advancing action potential approaches and then passes beneath and away from a recording electrode.

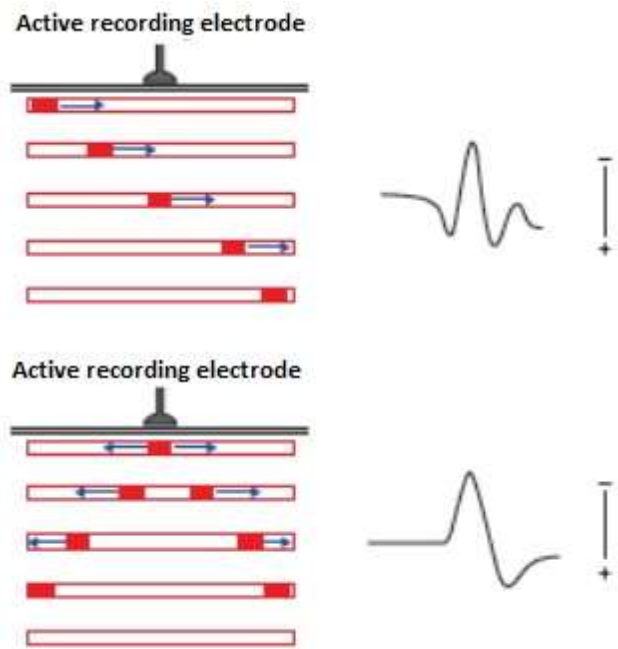


Figure 7. Volume conduction and waveform morphology. In *upper* image, an advancing action potential recorded by volume conduction will result in a triphasic potential that initially is positive, the is negative, and finally is positive again. In *lower* image, the depolarization occurs directly beneath the recording electrode, the initial positive phase is absent, and a biphasic, initially negative potential is seen. By convention, negative is up and positive is down in all nerve conduction and electromyographic traces (Preston, 2013).

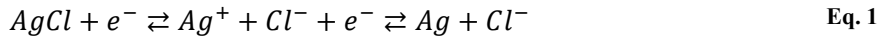
The electrical correlate of an action potential traveling toward, under, and then away from the recording electrode is an initial positive phase, followed by a negative phase and then a trailing positive phase, respectively. In Figure 7 upper shows that the first positive peak represents the time that the action potential is beneath the active electrode; this is the point at which the onset latency should be measured for nerve action potentials. The initial positive peak may be very small or absent with some sensory responses. In this case, the initial negative deflection best marks the true onset of the potential.

If a volume-conducted, near-field action potential begins directly under the recording electrode, the initial deflection is negative as seen in Figure 7 (*lower*).

1.2.1 The Ag/AgCl Electrode

To measure potential in solution, the Ag/AgCl electrode has become the standard system. The principle of this electrode is illustrated in Figure 8.

The charge carriers in wire are electrons e^- , in solution the chloride ion Cl^- . The electrode reaction is:



Due to the low solubility product K_L of $AgCl$ ($a_{Ag}^+ \cdot a_{Cl}^- = 1.7 \times 10^{-10}$), the KCl solution will be saturated but will have a very low activity of $Ag^+(a_{Ag}^+)$. The Ag/AgCl electrode will show a potential difference of:

$$E_{el} = E_0 + \frac{RT}{F} \ln a_{Ag}^+ = E_0 + \frac{RT}{F} (\ln K_L - \ln a_{Cl}^-) = E_0^* - \frac{RT}{F} \ln c_{Cl}^- \quad \text{Eq. 2}$$

with $E_0^* = 0.2222\text{ V}$ under standard conditions (25°C). The last equation shows that the Ag/AgCl electrode acts like a Cl^- -selective electrode. This is an important characteristic, which has severe consequences if the surrounding Cl^- concentration is altered.

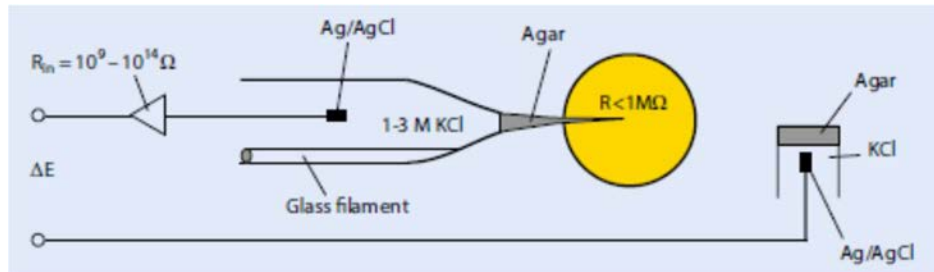


Figure 8. Arrangement of a Ag/AgCl microelectrode (Rettinger, et al., 2016)

1.3 sEMG SIGNALS

The myoelectric signal analysis requires advanced methods for detection, decomposition, processing, and classification, even when these signals will be used into basic or simple systems. To measure myoelectric signals, it is common to use detectors. These detectors are usually put over the skin, if this is the case; different signals from other motor units are collected at a time which may generate interaction between them. This is called superficial electromyographic signal (sEMG)

Electromyography is the study of muscle electrical signals. EMG is sometimes referred to as myoelectric activity. Muscle tissue conducts electrical currents like the way nerves do and the name given to these electrical signals in the muscle action potentials. For recording and detecting, there are two main issues of concern that influence the fidelity of the signal: Signal-to-noise ratio and distortion of the signal. The first one is the ratio of the energy in the EMG signals to the energy in the noise signal¹. The other issue is the distortion of the signal, meaning that the relative contribution of any frequency component in the EMG signal should not be altered.

For EMG muscle signals acquisition, two types of electrodes have been used: invasive electrode and non-invasive electrode. The combination of the muscle fiber action potentials from all the muscle fibers of a single motor unit is the motor action potential (MUAP) which can be detected by a skin surface electrode (non-invasive) located near this field, or by a needle electrode (invasive) inserted in the muscle (Basmajian & De Luca, 1985). When EMG is acquired from electrodes mounted directly on the skin, the signal is a composite of

¹ Noise signal: Is defined as electrical signals that are no part of the desired EMG signal, for this case.

all the muscle fiber action potentials occurring in the muscles underlying the skin. These action potentials occur at random intervals. So, at any moment, the EMG signal may be either positive or negative voltage. Individual muscle fiber action potentials are sometimes acquired using wire or needle electrodes placed directly in the muscle. Equation 3 shows a simple model of the EMG signal:

$$x(n) = \sum_{r=0}^{N-1} h(r)e(n-r) + w(n) \quad \text{Eq. 3}$$

where $x(n)$, modelled EMG signal, $e(n)$ m point processed, represents the firing impulse, $h(r)$, represents the MUAP, $w(n)$, zero mean additive white Gaussian noise and N is the number of motor unit firings.

The signal is picked up at the electrode and amplified. Typically, a differential amplifier is used as a first stage amplifier. Additional amplification stages may follow. Before being displayed or stored, the signal can be processed to eliminate low-frequency or high-frequency noise, or other possible artefacts. Consequently, the signal is frequently rectified and averaged in some format to indicate EMG amplitude.

A schematic representation of a general acquisition system is shown in Figure 9. Several physical magnitudes are usually measured from biologic systems. They include electromagnetic quantities (currents, potential differences, fields strengths etc.), as well as mechanical, chemical, or generally nonelectrical variables (pressure, temperature, movements, etc.). (Mainardi, et al., 2000)

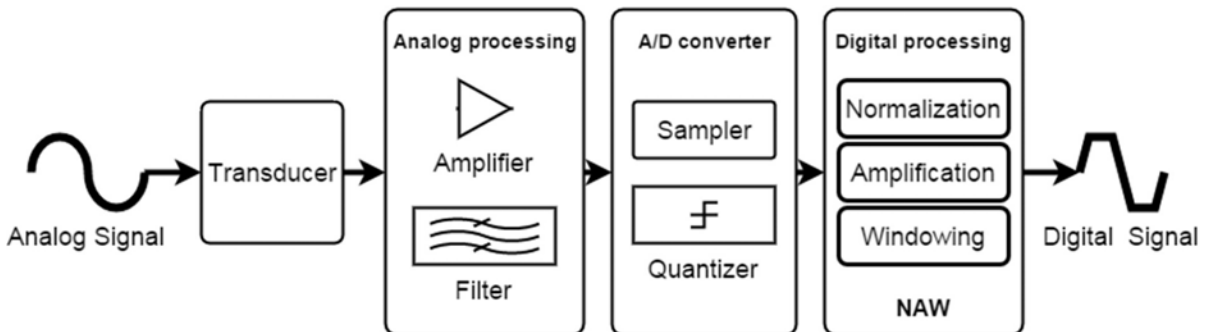


Figure 9. General block diagram of the acquisition procedure of a digital signal

An EMG signal is the train of Motor Unit Action Potential (MUAP) showing the muscle response to neural stimulation. The EMG signal appears random in nature and is generally modelled as a filtered impulse process where the MUAP is the filter and the impulse process stands for the neuron pulses, often modelled as a Poisson process (Basmajian & De Luca, 1985). Figure 10 shows the process of acquiring EMG signal and the decomposition to achieve the MUAPs.

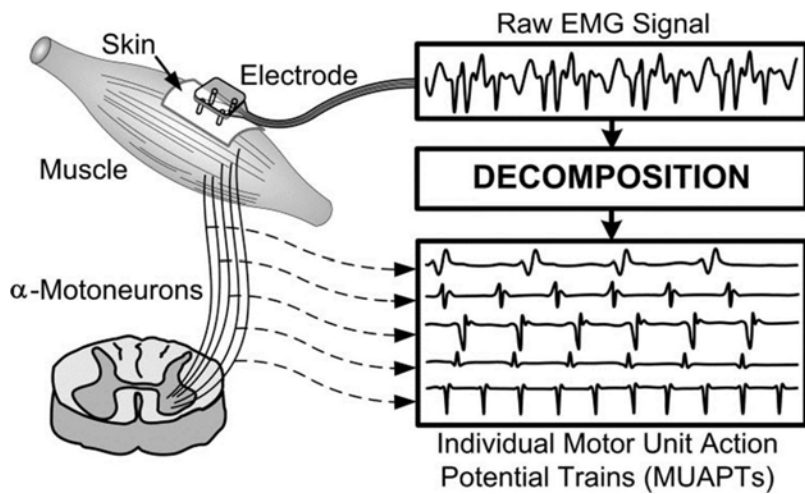


Figure 10. EMG signal and decomposition of MUAPs. (De Luca, et al., 2006)

1.3.1 EMG Features

To improve the performance of the classifier, researchers have been using different types of EMG features as an input to the classifier. To achieve optimal classification performance, the properties of EMG feature space, such as computational complexity, should be taken into consideration. There are three types of EMG features: time domain, frequency domain and time-frequency domain features. A carefully selected set of input features provides a higher classification rate than the raw EMG signal (Reddy, et al., 2009).

Time-frequency domain features are effective feature sets especially for transient myoelectric signal pattern classification.

1.3.2 On MUAP shape and its properties

The shape of the observed action potential will depend on the orientation of the recording electrode position with respect to the active muscle fibers. Electrodes must be placed in parallel to the muscular fibers, so then a biphasic shape and the sign of the phases will depend on the depolarization direction. From the right side, a depolarization is reflected as a negative phase and vice versa.

The amplitude of the MUAP depends on the diameter of the muscle fiber, distance of the electrodes and the electrode properties.

There can be even more than four phases on a MUAP, but one, two or three phases are considered normal into a healthy muscle, four phases appears in abnormal muscle tissue.

As a part of the MUAP, its electrical manifestation comes together with a shudder of the muscle fibers, this resulting sequence of MUAP's is known as Motor Unit Action Potential Train (MUAPT). There is a delay of few milliseconds between them, usually time duration of MUAP's is ranging from 1 ms to 24 ms.

1.3.3 EMG description over voltage dimension

We describe the EMG statistics regularity over voltage dimension by means of Frequency distribution on voltage. These are obtained by counting the number of signal samples, belonging to a long interval recording, occurring on each class in which arbitrarily we divided the range of the signal voltages.

Different segments of the same EMG have randomly shapes, histograms built from them are very similar, it means, statistical trend is maintained, regardless of the random fluctuation of the instantaneous values. This stationary effect is present only in short ranges, just until the muscle fatigue.

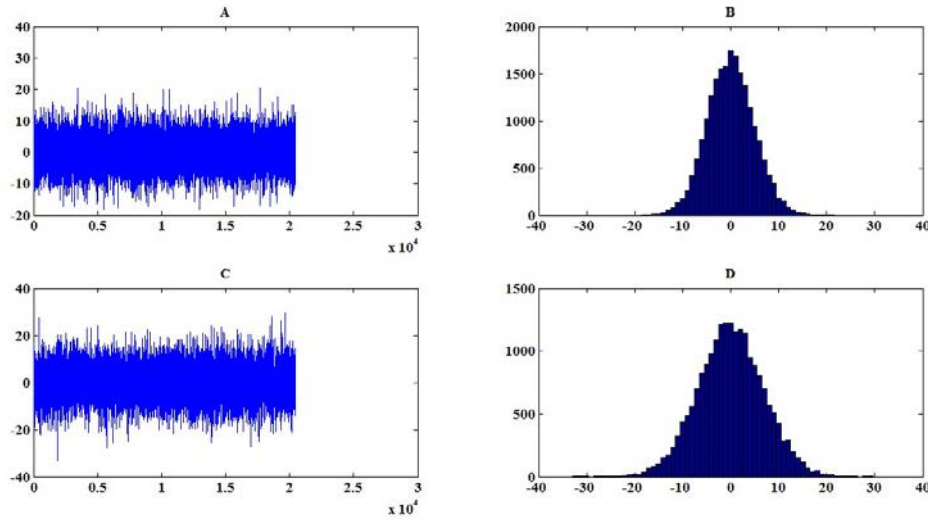


Figure 11 Histograms built from two different EMG signals (A, C) showing that statistical trend is maintained, regardless of the random fluctuation (B, D)

To describe distribution of the frequencies from voltage values were measure three parameters:

- Average: Indicate certain values tend to occur frequently.
- Variance: To indicate the instantaneous data variation from the average.
- Kurtosis: Indicating the degree of symmetry around the average.

For EMG signals the distribution is symmetric, null kurtosis, and average is zero (it is an AC signal). Also, the variance equation is:

$$S^2 = \frac{\sum(v_i - \bar{v})^2}{N} \quad \text{Eq. 4}$$

if the average (\bar{v}) is zero, equation 4 is reduced to a simple arithmetic average of the signal instantaneous values, squared.

In turn, Standard deviation (S), that is the Variance's root square and it serves to express the dispersion in the same dimension of the random variable, it is equally simplified, for this case is indicated as the Root Medium Square (RMS):

$$RMS = \sqrt{\frac{\sum(v_i)^2}{N}} \quad \text{Eq. 5}$$

Increased electrical activity of muscle is expressed by a higher standard deviation (R.M.S.); but the Average doesn't change, it remains at zero value.

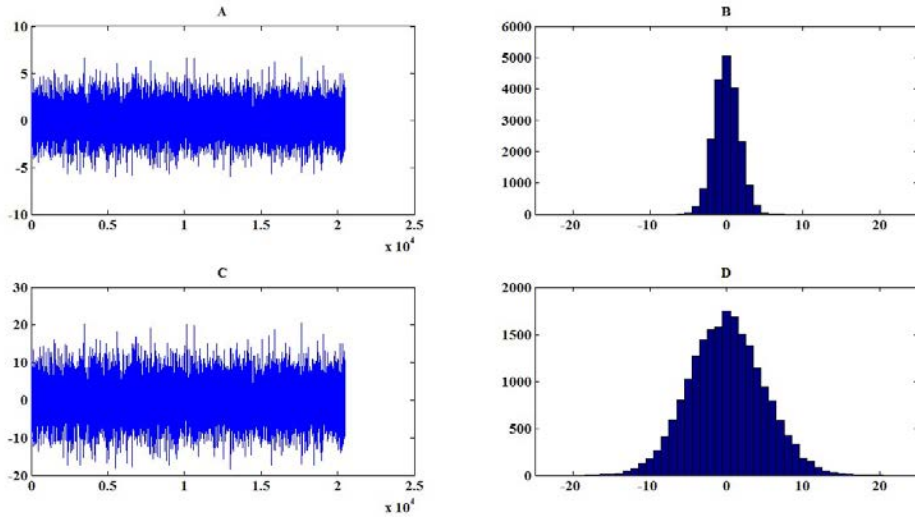


Figure 12 Increased electrical activity of muscle is expressed by a higher standard deviation, average didn't change.

A & C Images showed are the same EMG signal, but with different amplification.

A) EMG signal amplified 330 times, B) Histogram of EMG signal A.
C) EMG signal amplified 1000 times, D) Histogram of EMG signal C.

To refine statistical description of the random signal is necessary to fit the calculated histogram, computed from experimental data, with a mathematical model of frequency distribution. Gauss model, normal distribution, consists on a wrapped histogram bell shaped, with the symmetry axis over Average value and inflection points separated by a distance equal to Standard Deviation (R.M.S. value).

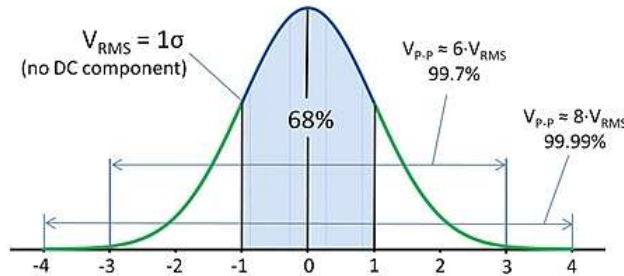


Figure 13 Normal Distribution or Gauss Model. Symmetry axis over Average value and inflection points separated by a distance equal to RMS value.

The Normal model is defined by the following equation that predicts Relative Density Frequency ($DF(V)$) with which signal samples of a given value (V) must occur:

$$DF(V) = \frac{1}{S\sqrt{2\pi}} \exp\left[\frac{1}{2}\left(\frac{V-\bar{V}}{S}\right)^2\right] \quad \text{Eq. 6}$$

In the last equation, Standard Deviation (S) is the only parameter, so that, having calculated this on a long EMG segment, fitting Normal model to experimental frequency distribution is too easy. This is a mathematical description for the behavior of a huge number of instantaneous values from EMG signal, it is not the value of a certain moment, and it is unpredictable because it is random.

1.3.4 EMG description on time dimension

There are two ways to characterize the statistical sequence regularity from voltage samples with the same value and sign: autocorrelation and spectrum.

1.3.4.1 Frequency Spectrum

Its visualization is not direct by the calculation mode, but physiological meaning is clearest. Both EMG representations have a relationship between each other through the Fourier direct and reverse transform.

The main mathematical concept of the spectral analysis is that all periodic signal could be constructed by the algebraic sum of sinusoidal functions series, each one with multiple frequencies (harmonic series), the first one is equal to the lower value present in the signal. Then, we assume that an EMG signal could be represented by harmonic series. This is considering that the complexity is of a higher level, so its spectrum too.

In the next figure, we could see the spectrum of an EMG signal captured over the skin surface.

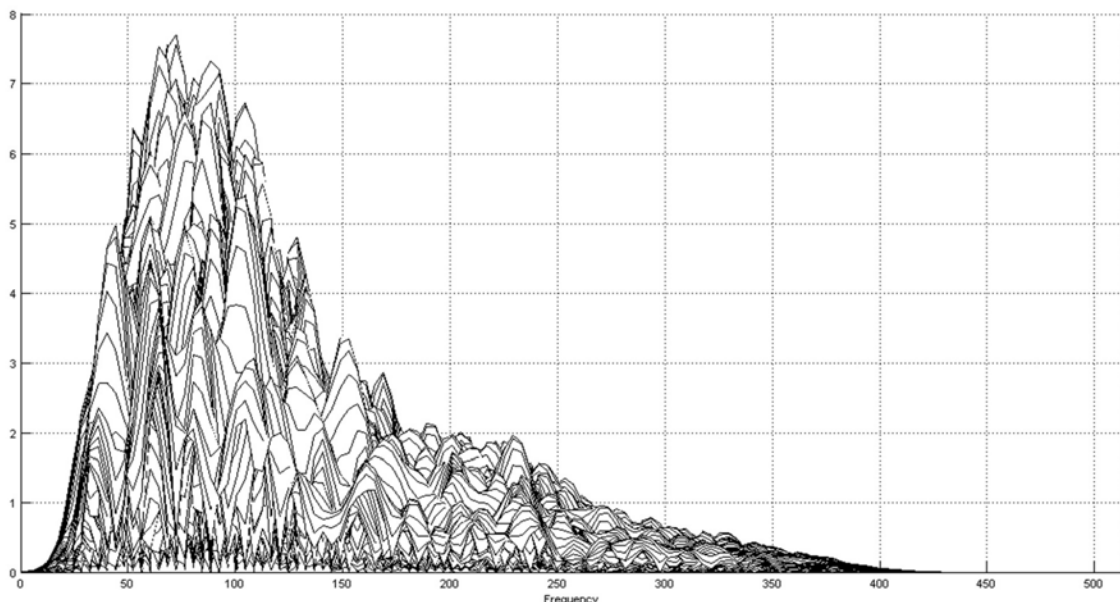


Figure 14 EMG spectrum contains significant frequency components, from 10 Hz to 450 Hz

The highest spectral peak occurs in the lower frequencies gamma, surrounding the 40 Hz to 120 Hz; these corresponding to motor-neurons discharge frequency that controls the muscle activation.

1.3.5 Electrical noise and factors affecting EMG signal

The amplitude range of EMG signal is 0 mV - 10 mV (± 5 mV) prior to amplification. EMG signals acquire noise while travelling through different tissue. It is important to understand the characteristics of the electrical noise. Electrical noise, which will affect EMG signals, can be categorized into the following types (Reaz, et al., 2006) - *Verbatim et literatim*:

1. “*Inherent noise in electronics equipment*: All electronics equipment generate noise. This noise cannot be eliminated; using high quality electronic components can only reduce it.
2. *Ambient noise*: Electromagnetic radiation is the source of this kind of noise. The surfaces of our bodies are constantly inundated with electric-magnetic radiation and it is virtually impossible to avoid exposure to it on the surface of earth. The ambient noise may have amplitude that is one to three orders of magnitude greater than the EMG signal.

3. *Motion artefact*: Motion artefact cause irregularities in the data. There are two main sources for motion artefact: 1) electrode interface and 2) electrode cable. Motion artefact can be reduced by proper design of the electronic circuitry and set-up.
4. *Inherent instability of signal*: The amplitude of EMG is random in nature. EMG signal is affected by the firing rate of the motor units, which, in most conditions, fire in the frequency region of 30 Hz to 60 Hz. This kind of noise is considered as unwanted and the removal of the noise is important.”

The factors that mainly affect the EMG signal can also be classified. This kind of classification is set so that EMG signal analysis algorithms can be optimized, and equipment can be designed in a consistent manner. Factors affecting EMG signal falls into three basic categories (Reaz, et al., 2006) *verbatim et literatim*:

1. “*Causative Factors*: This is the direct affect in signals.

Causative factors can be divided into two classes:

- i. *Extrinsic*: This is due to electrode structure and placement. Factors like area of the detection surface, shape of electrode, distance between electrode detection surface, location of electrode with respect to the motor points in the muscle, location of the muscle electrode on the muscle surface with respect to the lateral edge of the muscle, orientation of the detection surfaces with respect to the muscle fibers mainly influence EMG signal.
- ii. *Intrinsic*: Physiological, anatomical, biochemical factors take place due to number of active motor units, fiber type composition, blood flow, fiber diameter, depth and location of active fibers and amount of tissue between surface of the muscle and the electrode.

2. *Intermediate Factors*: Intermediate factors are physical and physiological phenomena influenced by one or more causative factors. Reasons behind this can be the band-pass filtering aspects of the electrode alone with its detection volume, superposition of action potentials in the detected EMG signal, conduction velocity of the action potential that propagate along the muscle fiber membrane. Even cross talk from nearby muscle can cause Intermediate Factors.
3. *Deterministic Factors*: These are influenced by Intermediate Factor, the number of active motor units, motor firing rate, and mechanical interaction between the muscle fibers have direct bearing on the information in the EMG signal and the recorded force. Amplitude, duration, and shape of the motor unit action potential can also be responsible.”

There are different ways to get the maximum quality of EMG signals, two of this are showed:

1. Signal-to-noise ratio should contain the highest amount of information from EMG signal and the minimum amount of contamination.
2. EMG distortion must be minimal without filtering.²

To analyze EMG signal, only the positive values are analyzed. The absolute value of each data point is used during full-wave rectification, this one is the most recommended to perform. (Reaz, et al., 2006).

1.4 sEMG SIGNAL DETECTION AND ACQUISITION

To detect the signal, a surface sensor array is put in over the skin above the muscle of interest³. The electrode must be placed with sufficient pressure to provide good electrical contact as evidence by the best signal-to-noise ratio of the detected signals (De Luca, et al., 2006). An important issue in EMG signal classification is the optimal sensor selection (Rafiee, et al., 2010).

1.4.1 sEMG Normalization

The voltage potential of the sEMG signal detected by the electrodes strongly depends on several factors, varying between individuals and over time within an individual.

² Notch Filters are not recommended (Reaz, et al., 2006)

³ No skin preparation or conductive gel is needed.

Thus, the amplitude of the sEMG itself is not useful in group comparisons, or to follow events over a long period of time (Mathiassen, 1997). The fact that the recorded EMG amplitude is never absolute is mainly because the impedance varies between the active muscle fibers and electrodes.

Therefore, when comparing amplitude variables measurements, normalization of some kind is required, i.e. the sEMG converted to a scale that is common to all measurements occasions.

1.4.2 EMG Filtering

Noise is the main issue into EMG signal, without it, characteristic quantification of the signal is more standard. There are many kinds of noises intrinsic to EMG signals caused by other muscles, interferences or artifacts.

The main challenges in analyzing the EMG signals are the inherent noise in the electrode, movement artifact, electromagnetic noise, cross talk, internal noise related to physiological and biochemical actions, inherent instability of the signal and electrocardiographic (ECG) artifacts (Chowdhury, et al., 2013).

1.4.3 EMG De-noising using Wavelets

The time-frequency plane is one of the most fundamental concepts in signal analysis. The Wavelet transform can essentially be divided into discrete and continuous forms. It transforms the signal in both time- and frequency domains. The Discrete Wavelet transform method has been successful in analyzing non-stationary signals, such as surface EMG (sEMG) signals.

Hussain and Mamun in 2012, proved that the wavelet Db45 shows the best contrast when they analyzed the sEMG signal using both power spectrum and bi spectrum compared to the other four wavelets (Haar, Db2, sym4 and sym5) within the range 50 Hz to 70 Hz over *rectus femoris* muscle during high speed walking (Hussain & Mamun, 2012).

Wavelet transform is traditionally used on de-noising process. Based on multi-resolution and multi-scale features of wavelet transform, we can use different energy distribution and the signal spectrum to eliminate the illusive components which corresponding to the noise in specific wavelet scale. The wavelet transform is used to reconstruct EMG pattern. The whole process could eliminate the noise of the signal (Jingtian, et al., 2007).

Wavelet transform is widely used as a traditional method to eliminate noise of ECG. But wavelet transform is based on Fourier transform theory. And Fourier transform is applied to the time-domain signal which is stationary or periodic. Therefore, using wavelet transform to do non-linear and non-stationary signal analysis is limited. Local parameter and basic local function are required to analyze non-stationary signal. Instantaneous frequency is the basic concept. The application of this algorithm needs the selection of five processing parameters (Phinyomark, et al., 2009):

1. Type of wavelet function
2. The scale
3. The threshold selection rule
4. The threshold rescaling method
5. The thresholding functions

Selection the right wavelet function is crucial of wavelet denoising, depends of a few factors, such as application and signal characteristics.

1.4.4 EMG De-noising using Hilbert-Huang Transform

The HHT method learn many advantages of wavelet transform like multi-resolution and overcome the difficulties like what wavelet transform need choose basic function (Jing-tian, et al., 2007).

Empirical Mode Decomposition has into its advantages that with a low level of SNR of the processed signal, method provided the best surface EMG de-noising performance compared to other methods

By studying the sEMG signals analysis using EMD technique, this offers the most successful results for attenuation of specific noises of sEMG signals, especially in cases of power-line noises, white Gaussian noise, baseline wandering and artifacts.

The noise filtering and the de-noising can be solved with HHT (Huang, et al., 1998), especially for the real-time analysis (Meeson, 2005). We will apply this method to the EMG de-noising in this thesis.

Signal de-noising in one dimension can be divided into three steps. That is decomposition, threshold and signal reconstruction. Here, HHT is adapted to EMG de-noising. Three steps are similar with traditional method. The clincher of this process is the EMD. The time-space filtering is constructed by using multi-revolution analysis and multi-scale filtering of EMD (Chung & Dong-ling, 2004). The advantage of the time-scale filtering is that can retain inherent characteristics of the non-linear and non-stationary. We will use EMD method to break down EMG signal into different time scale; it shows different information of signal and noise.

1.4.5 EMG signal decomposition

EMG signals are the superposition of activities of multiple motor units. It is necessary to decompose the EMG signal to reveal the mechanisms pertaining to muscle and nerve control. Decomposition of EMG signals has been done by wavelet spectrum matching and principle component analysis of wavelet coefficients.

According to Jianjung Fang (Fang, et al., 1997), more than one single motor unit (SMU) potential will be registered at same time overlapping with each other, especially during a strong muscle contraction. In 1997, they develop a technique using wavelet transform to classify SMU potentials and to decompose EMG signals into their constituent SMU potentials. The distinction of this technique is that it measures waveform similarity of SMU potentials from wavelet domain, which is very advantageous. This technique was based on spectrum matching in wavelet domain. Spectrum matching technique is sometimes considered to be more effective than waveform matching techniques, especially when the interference is induced by low frequency baseline drift or by high frequency noise. The technique, developed for multi-unit EMG signal decomposition, consists of four separate procedures: signal de-noising procedure, spike detection procedure, spike classification procedure and spike separation procedure.

According to Daniel Zennaro (Zennaro, et al., 2003), wavelet coefficients of lower frequency bands are more important in the differentiation of motor unit action potential (MUAP) characterization than higher bands.

On the other hand, Rie Yamada (Yamada, et al., 2003), showed that high frequency information, which were not considered, are also important for MUAP's classification. Their experiments were made proposing another method using principle components analysis (PCA) for wavelet coefficients. The decomposition algorithm consists of four processing stages: *segmentation, wavelet transform, PCA, and clustering*. The advantage of this method is that it does not require manual selection of coefficients, and takes all frequency information in account.

According to De Luca (De Luca, et al., 2006) - *verbatim et literatim*, a technique named *Precision Decomposition I (PDI)* was designed to enable physiological experiments and it was described by De Luca. "The technique has been useful for decomposing indwelling EMG (iEMG) signals detected by needle sensors during isometric contractions and has been used in various physiological studies (Adam & De Luca, 2003) (Adam, et al., 1998) (Masuda & De Luca, 1991). This technique consists of identifying action potentials in the iEMG signal and assigning them to specific motor units by classifying the shapes and amplitudes of the action

potentials. The assignments of the action potentials are based on template matching and the probability of firing of the individual motor units being tracked. Superposition of action potentials are resolved.

The decomposition accuracy for the i^{th} decomposable motor unit train is defined as

$$A(i) = \frac{N_{FIR}(i) - N_{FN}(i) - N_{FP}(i)}{N_{FIR}(i)} \times 100 \quad \text{Eq. 7}$$

where $N_{FIR}(i)$ is the number of the firings of the MU and $N_{FN}(i)$ and $N_{FP}(i)$ are respectively the number of false positives produced by the decomposition algorithm for that motor unit (MU). The term “*true firings*” refers to the firings that we obtained by an expert operator using a manual or automatic decomposed data.

The overall decomposition accuracy for a signal with N decomposable MU trains is then obtained as

$$A = \frac{1}{N} \sum_{i=1}^N A(i) \quad \text{Eq. 8}$$

The rationale behind this unweighted average is that the accurate decomposition of any MU train is of the same significance as that of any order MU train regardless of its duration, number of firings, and so forth.”

1.4.5.1 Challenges of sEMG decomposition

(De Luca, et al., 2006) *Verbatim et literatim*

Any approach for decomposing EMG signals must be able to deal with four major complexities that occur within the signal. These complexities are shown in Figure 15:

- 1) *Superposition* of action potentials from different MU’s,
- 2) *Large dynamic range* of the amplitudes among the action potentials of different MUs of interest,
- 3) *Shape changes* across the different action potentials of each MU (arising from slight movement between the sensor and muscle fibers and/or intracellular process), and
- 4) *Similarity of shape* at various times among the action potentials of different MUs. These phenomena may also act in concert with each other to make the decomposition task more difficult.

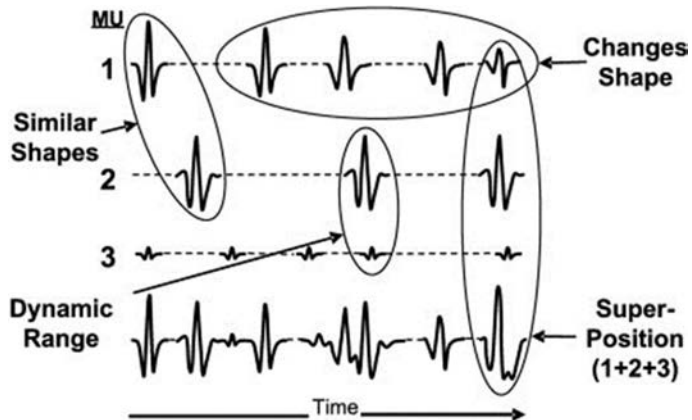


Figure 15. Stylized examples of the various challenges presented by the realistic behavior of EMG signals detected with indwelling sensors with small detection volume and susceptible to movement (De Luca, et al., 2006).

CHAPTER 2

MATHEMATICAL FRAMEWORK

2.1 SIGNALS

The term signal refers to a physical quantity that carries certain type of information and serves as a means for communication.

2.1.1 Classification of signals

In general, any signal can be broadly classified as being either deterministic or nondeterministic. Deterministic signals are those that can be defined explicitly by mathematical functions. Nondeterministic signals are random in nature and are described in statistical terms. A signal that can be generated repeatedly with identical results is deterministic, otherwise it is nondeterministic.

2.1.1.1 Deterministic Signal

There are two types of deterministic signals: periodic and transient. Periodic signal is defined as a function that repeats itself exactly after a certain period, or cycle. Transient signal is defined as a function that lasts a short period of time.

2.1.1.2 Nondeterministic Signal

Nondeterministic signals, also called random signals, do not follow explicit mathematical expressions. They are divided in two categories: stationary and nonstationary. Stationary signal is considered when none of its statistical properties change with time. Generally, wide-sense stationary is used to characterize the signal. This requires that it satisfies the following conditions on its mean function:

$$E\{x(t_1)\} = m_x(t_1) = m_x(t_1 + \tau) \quad \tau \in \mathbb{Z} \quad \text{Eq. 9}$$

and the correlation function

$$E\{x(t_1), x(t_1 + \tau)\} = \mathcal{R}_{xx}(t_1, t_1 + \tau) = \mathcal{R}_{xx}(0, \tau) \quad \tau \in \mathbb{R} \quad \text{Eq. 10}$$

Symbol τ is the real number, \mathcal{R}_{xx} is the autocorrelation function of the signal $x(t)$. The mean function and autocorrelation function of a signal can be obtained by time-averaging over a short time interval T as follows:

$$E\{x(t_1)\} = \frac{1}{T} \int_{t_1}^{t_1+T} x(t) dt \quad \text{Eq. 11}$$

and

$$E\{x(t_1), x(t_1 + \tau)\} = \frac{1}{T} \int_{t_1}^{t_1+T} x(t) dt \quad \text{Eq. 12}$$

A signal whose statistical properties change with time is called a nonstationary signal. Also, does not satisfy the conditions specified above.

2.2 WAVELET AND HILBERT-HUANG TRANSFORMS

All transforms of the signal $f(t)$ described in this section share a common computation principle: The signal is multiplied with a certain “analysis function” and integrated about the domain. In a symbolic notation, the description for performing a transform is:

$$f(t) \xrightarrow{\text{transform}} \int_{-\infty}^{+\infty} f(u) \overline{g(u)} du \quad \text{Eq. 13}$$

The analysis function $g(u)$ characterizes the chosen transform. In general, it may be a complex function, the overline denotes the complex conjugate entity. $g(u)$ in a certain way depends on the parameters, i.e. frequencies or detail sizes, to be measured. Thus, by the computation principle given above the transformed entity will depend on these parameters. In other words: the transformed entity again will be a function. These functions we shall denote with transformed signal.

2.2.1 Wavelet Transform

The wavelet transform has such a zooming property. In contrast to the Fourier transform, the wavelet transform does not look for circular frequencies but rather for detail sizes S at a certain time τ (Stark, 2005).

High frequencies correspond to small details and vice versa, thus, when comparing wavelet with Fourier transforms there is an inverse proportion between frequencies and detail sizes, so then, there is a constant β such that:

$$S = \frac{\beta}{\omega} \quad \text{Eq. 14}$$

We shall now briefly indicate, how the wavelet transform is computed.

Consider a, real or complex, analysis function ψ , oscillating around the t -axis

$$\int_{-\infty}^{+\infty} \psi(t) dt = 0 \quad \text{Eq. 15}$$

and decreasing rapidly for $t \rightarrow \pm\infty$. Such a function is called a Wavelet. Whereas relating scale factors with frequencies, the constant β depends on ψ .

Wavelet transform is generally divided into either a discrete and or continuous form. The continuous wavelet transform (CWT) of a signal $s(t)$ and the daughter wavelets, which are the time translation and scale expansion/compression versions of a mother wavelet function $\psi(t)$. Equivalent to a scalar production, this calculation generates continuous wavelet coefficients CWC (a, b), which determine the similarity between the signal and the daughter wavelets located at position b (time shifting factor) and positive scale a :

$$CWC(a, b) = \int_{-\infty}^{+\infty} s(t) \frac{1}{\sqrt{a}} \psi^* \left(\frac{t-b}{a} \right) dt \quad \text{Eq. 16}$$

where $*$ stands for complex conjugation and $\psi \in L^2$.

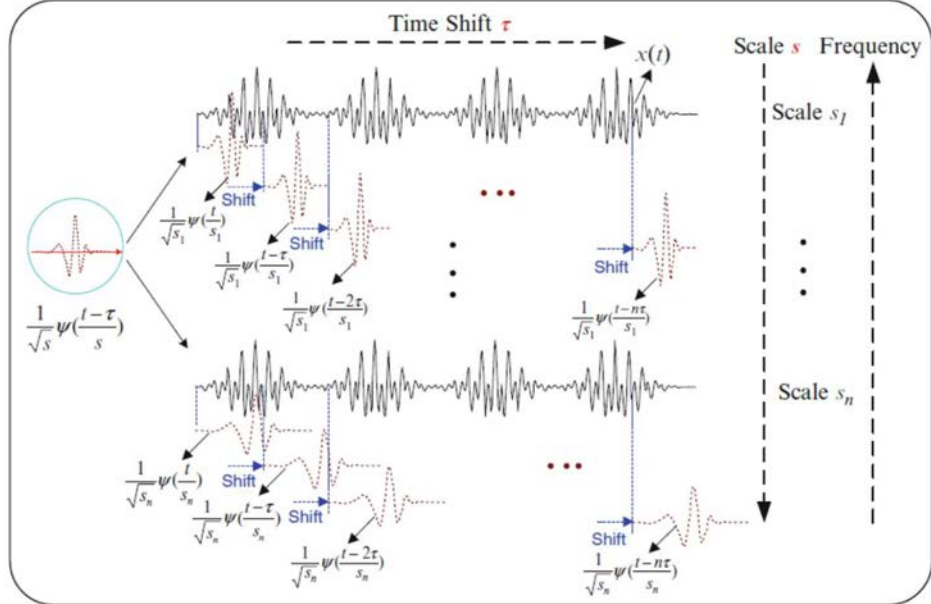


Figure 16. Representation of Wavelet transform (Gao & Yan, 2011)

2.2.1.1 Meyer Wavelet

The Meyer wavelet is orthogonal and symmetric. However, it does not have a finite support. The Meyer wavelet has explicit expression and is defined in the frequency domain as follows:

$$\Psi_{Meyer}(f) = \begin{cases} \sqrt{2\pi} e^{i\pi f} \sin \left[\frac{\pi}{2} v(3|f| - 1) \right] & \frac{1}{3} \leq |f| \leq \frac{2}{3} \\ \sqrt{2\pi} e^{i\pi f} \cos \left[\frac{\pi}{2} v \left(\frac{3}{2}|f| - 1 \right) \right] & \frac{2}{3} \leq |f| \leq \frac{4}{3} \\ 0 & |f| \notin \left(\frac{1}{3}, \frac{4}{3} \right) \end{cases} \quad \text{Eq. 17}$$

where $v(\cdot)$ is an auxiliary function, expressed as:

$$v(\alpha) = \alpha^4(35 - 84\alpha + 70\alpha^2 - 20\alpha^3), \quad \alpha \in (0,1) \quad \text{Eq. 18}$$

The Meyer wavelet with its magnitude spectrum is shown below in Figure 17. Typical applications of Meyer wavelet are signal denoising and MUAPs detection (Chowdhury, et al., 2013).

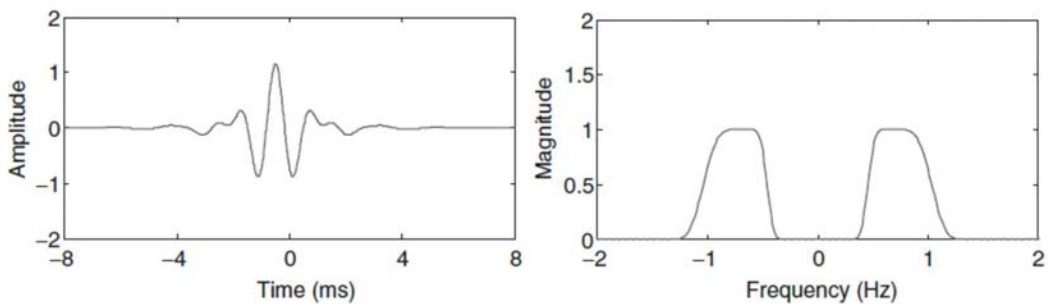


Figure 17. Wavelet Meyer (left) and its magnitude spectrum (right)

2.2.1.2 Daubechies Wavelet

The family of the Daubechies wavelets is orthogonal, however, asymmetric, which introduces a large phase distortion. This means that it cannot be used in applications where a signal's phase information needs to be kept. It is also a compactly supported base wavelet with a given support width of $2N-1$, in which N is the order of the base wavelet. In theory, N can be up to infinity.

The Daubechies wavelets do not have explicit expression except for the one with $N=1$, which is the Haar wavelet. With an increase of the support width, i.e., an increase of the base wavelet order, the Daubechies wavelet becomes increasingly smoother, leading to better frequency localization. Therefore, the magnitude spectra for each of the Daubechies wavelets decay quickly, as shown in Figure 18, where the Daubechies 2 base wavelet and Daubechies 4 base wavelet are used as examples.

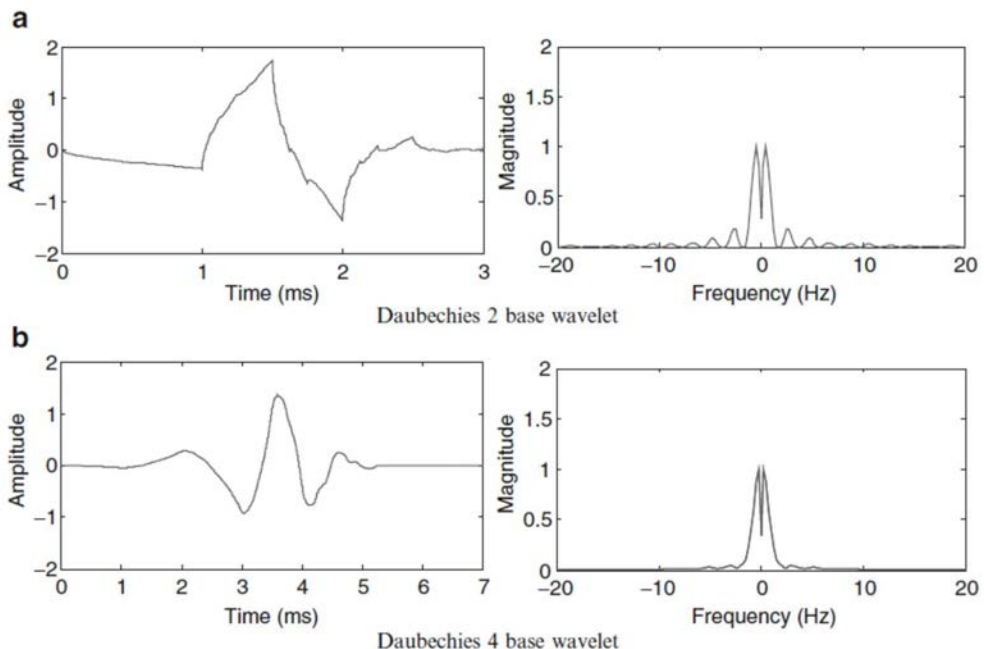


Figure 18. Daubechies wavelet (*left*) and its magnitude spectrum (*right*). a) Daubechies 2 base wavelet and b) Daubechies 4 base wavelet.

2.2.2 Hilbert-Huang Transform

In 1996 Norden E. Huang proposed the Hilbert Huang Transform (HHT). HHT can be used for processing non-stationary and non-linear signals, such as noise filtering and de-noising (Huang, et al., 1998). Is an empirically based data-analysis method. Its basis of expansion is adaptive, so that it can produce physically meaningful representations of the data from non-linear and non-stationary processes.

Empirical mode decomposition (EMD) and Hilbert spectral analysis (HSA) represent a desperate attempt to break the suffocating hold on data analysis by the twin assumptions of linearity and stationary. The EMD-HSA is truly an adaptive time-frequency analysis. It does not require an a priori functional basis.

This method is potentially viable for time-frequency-energy representations. It has been tested and validated exhaustively, but not empirically (Huang, 2005). In all the cases studied, the HHT gave results sharper than other methods; HHT revealed true physical meanings in many of the data examined.

Decomposition for non-stationary signal is necessary when the analysis is based on instantaneous frequency. Instantaneous frequency is defined as the time derivative of phase of the analytic signal and would be meaningful only to narrow-band signal⁴. The general process is the following:

2.2.2.1 Empirical Mode Decomposition (The sifting process)

The empirical mode decomposition (EMD) (Huang, et al., 1998) is a technique to decompose a given signal into a set of elemental signals called “intrinsic mode functions” (IMF’s). The EMD is the base of the so-called “Hilbert-Huang Transform” that comprises the EMD and the Hilbert spectral analysis that performs a spectral analysis using the Hilbert transform (HT) followed by an instantaneous frequency computation.

The algorithm is simple and gives good results in situations where other methods fail. However, it has some drawbacks, tied with some of the assumptions needed to implement the algorithm, leading to unexpected results (Rato, et al., 2008).

The first step decomposes the signal to a set of intrinsic mode functions (IMF). The second step is to get the instantaneous frequency and spectrum. IMF is a single signal which should satisfy the following conditions:

- 1) The number of zero and extreme crossing must be equal or up to one in the whole data set.
- 2) The mean value of two envelope curves which are defined by local maximum and minimum would be zero at the random time. The envelope is symmetry with time axis.

The decomposition that any data consists of different simple intrinsic modes of oscillations. Each intrinsic mode, linear or nonlinear, represents a simple oscillation.

An IMF represents a simply oscillatory mode as a counterpart to the simple function, but it is more general: instead of constant amplitude and frequency, as in a simple harmonic component, the IMF can have a variable amplitude and frequency as functions of time.

To decompose any function, we follow the next procedure: take the test data $x(t)$ as given in Figure 19; identify all the local extrema, then connect all the local maxima by cubic spline, do the same with the local minima.

Cubic spline fitting is used to gain the up and down signal envelopes, this calculates the mean value in all envelops points as shown in Figure 20. The average value makes a new curve that is named m_1 (Figure 21). Then we must determine if h_1 satisfy the two conditions mentioned above.

Ideally, h_1 should satisfy the definition of an IMF. The sifting process serves two purposes: 1) to eliminate riding waves, and 2) to make the wave profiles more symmetric (Huang, 2005). The first is achieved with the Hilbert transform to give instantaneous frequency, and the second purpose is achieved in case the neighboring wave amplitudes have too large a disparity. Toward these ends, the sifting process must be repeated as many times as is required to reduce the extract signal to an IMF.

⁴ Narrow-band signal: a signal who have a small bandwidth.

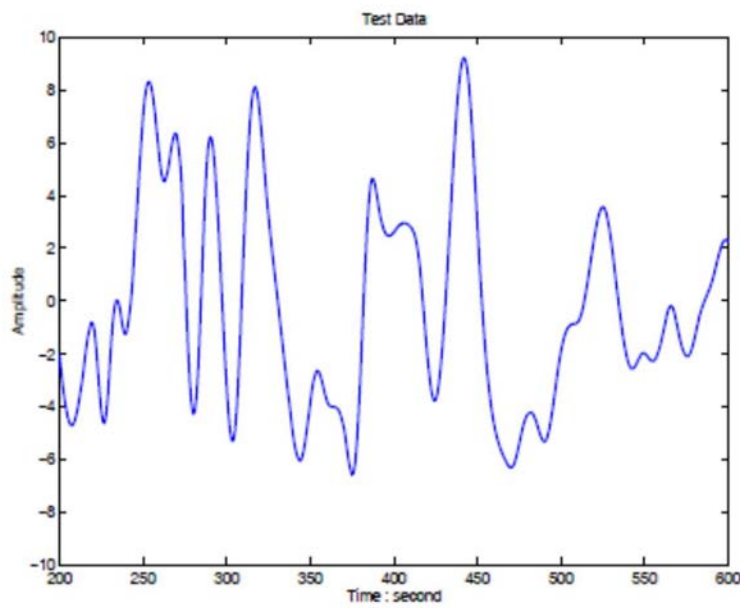


Figure 19. Test data $x(t)$ (Huang, 2005)

$$x(t) - m_1 = h_1$$

Eq. 19

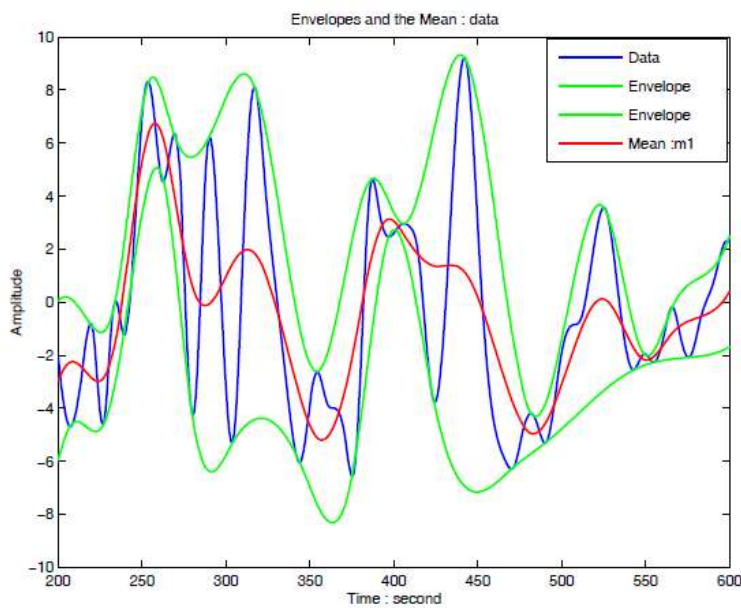


Figure 20. The data (blue), upper and lower envelopes (green) defined by the local maxima and minima, respectively, and the mean value of the upper and lower envelopes given in red. (Huang, 2005)

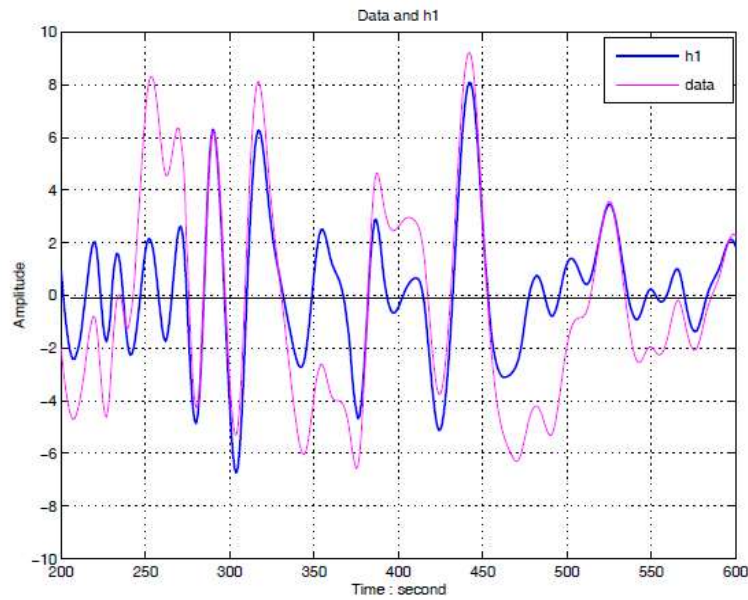
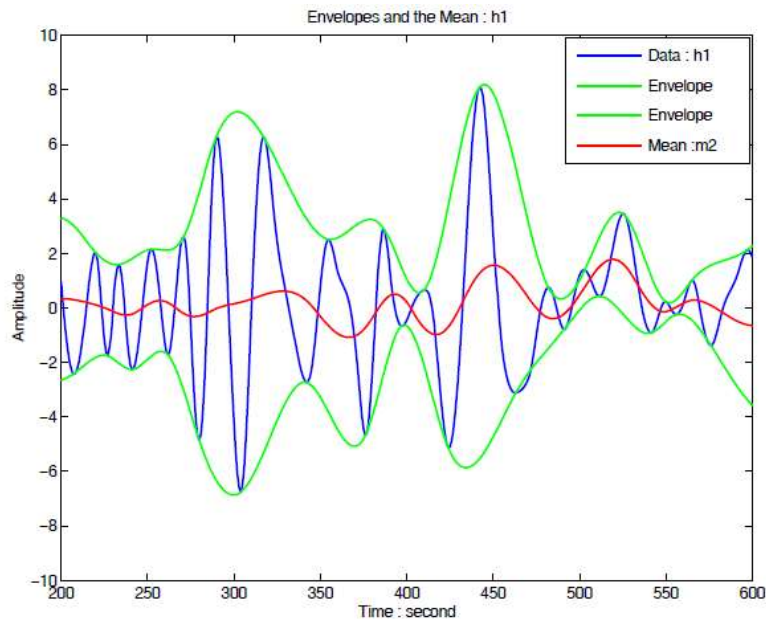


Figure 21. The data (pink) and h_1 (blue). (Huang, 2005)

But, if h_1 does not satisfy the conditions, in the subsequent sifting processes, h_1 can be treated only as a proto-IMF. In the next step, h_1 is treated as the data, then we continue doing the sifting process.

$$h_1 - m_1 = h_2 \quad \text{Eq. 20}$$



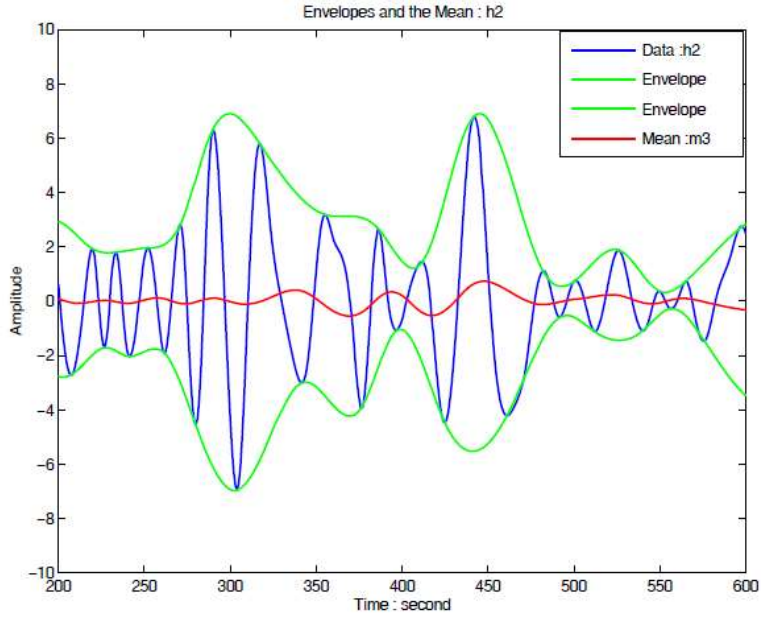


Figure 22. (A, top) Repeated sifting steps with h_1 and m_2 .
(B, bottom) Repeated sifting steps with h_2 and m_3 . (Huang, 2005)

This process must be repeated k times, until we find a h_k function that satisfy the IMF conditions. The general equation for this process is:

$$h_{(k-1)} - m_k = h_k \quad \text{Eq. 21}$$

Take h_k as c_1 , where c_1 is the first IMF of the signal, i.e. as shown in Figure 23

$$c_1 = h_k \quad \text{Eq. 22}$$

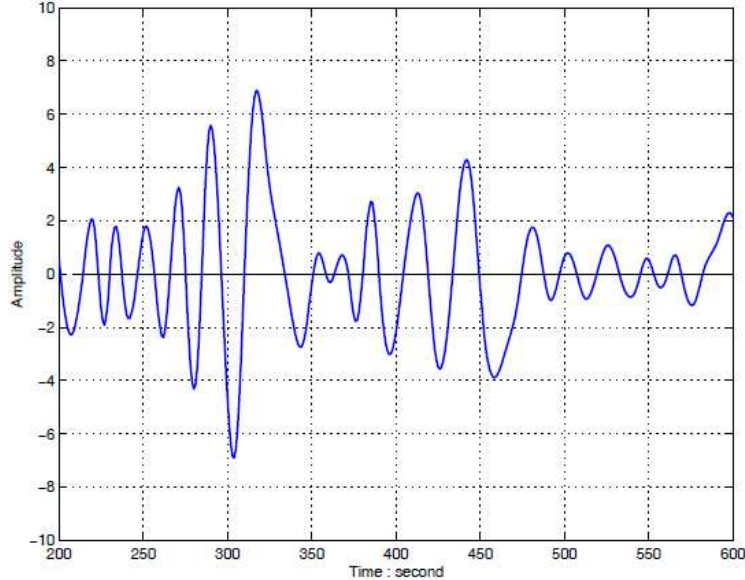


Figure 23. The first IMF component c_1 after 12 steps. (Huang, 2005)

take c_1 component out of the original data, the residue is:

$$x(t) - c_1 = r_1 \quad \text{Eq. 23}$$

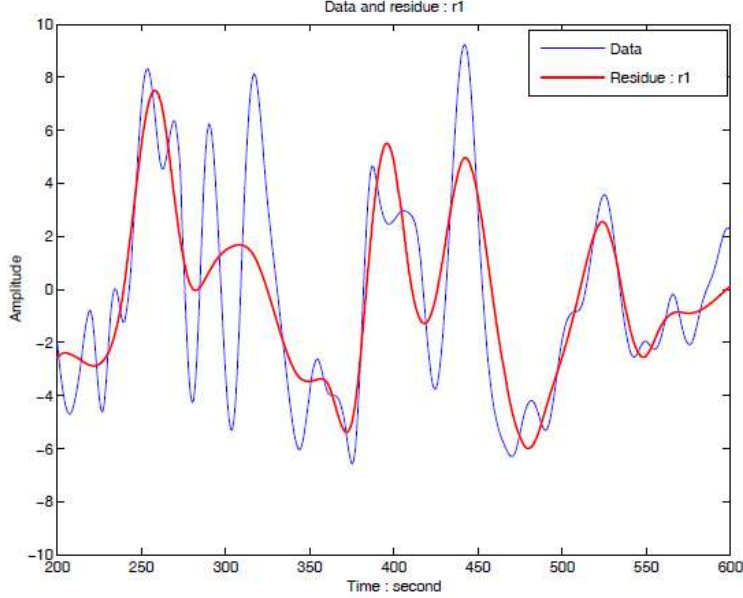


Figure 24. The original data (blue) and the residue r_1 (red). (Huang, 2005)

As the residue also includes the long-cycle information, we should take it as a “other” new signal and we must apply the filtering process as above. The residue of each sifting process is named r_i ,

$$r_1 - c_2 = r_2, \dots, r_{n-1} - c_n = r_n \quad \text{Eq. 24}$$

When r_n becomes a single function (or merely, we cannot extract single component as IMFs from it), the whole sifting process is over. Then $x(t)$ can be expressed as:

$$x(t) = \sum_{i=1}^n c_i + r_n \quad \text{Eq. 25}$$

The EMD is considered as a scale-filtering process, each IMF shows the characteristic of each scale, and in other words it shows the intrinsic mode characteristic of non-linear and non-stationary signal.

The IMF eliminates the non-stationary components of the original data. Because each sifting process is based on the residue of the previous process, then the main function of the process is variable and the decomposition is adaptive.

“Sifting” is the central signal separation process of the HHT algorithm. The traditional way of filtering, with appropriate real-time adjustments to parameters, could be substituted for Huang’s sifting process, but this suggestion is not supported yet (Meeson, 2005).

2.2.2.2 Hilbert Transform

The second part of the HHT process is the Hilbert transform. Having obtained the intrinsic mode function components, one will have no difficulty in applying the Hilbert transform to each IMF component, and in computing the instantaneous frequency as follows (equations 26-30).

For an arbitrary time series, $x(t)$ is given; $y(t)$ is equal to Hilbert transform of $x(t)$:

$$y(t) = \frac{1}{\pi} P \frac{\int x(t') dt'}{t - t'} \quad \text{Eq. 26}$$

where P indicates the Cauchy principal value. This transform exists for all functions of class L^p .⁵

Now with this definition, if we consider the signal $z(t)$ as an analytic signal, where $x(t)$ is the real part and $y(t)$ is the imaginary component.

$$z(t) = x(t) + iy(t) = a(t)e^{j\theta t} \quad \text{Eq. 27}$$

So, applying the operations to get the amplitude and phase of $z(t)$, we have:

$$\text{Amplitude} \quad a(t) = \sqrt{x^2(t) + y^2(t)} \quad \text{Eq. 28}$$

$$\text{Phase} \quad \theta(t) = \arctg \left(\frac{y(t)}{x(t)} \right) \quad \text{Eq. 29}$$

With this $\theta(t)$ function, we can obtain the instantaneous frequency, we just only apply the derivation to it:

$$\text{Instantaneous frequency} \quad \omega = \frac{d\theta}{dt} \quad \text{Eq. 30}$$

After performing the Hilbert transform on each IMF component, the original data can be expressed as the real part Re in the following form:

$$x(t) = \text{Re} \sum_{j=1}^n a_j(t) e^{j \int \omega_j dt} \quad \text{Eq. 31}$$

Equation 31 shows that HHT (Hilbert-Huang Transform) is an extended form of Fourier Transform.

$$x(t) = \text{Re} \sum_{j=1}^n a_j(t) e^{i \omega_j(t) t} \quad \text{Eq. 32}$$

⁵ In mathematics, the L^p spaces are function spaces defined using a natural generalization of the p -norm for finite-dimensional vector spaces. They are sometimes called *Lebesgue* spaces. (Maddox, 1988).

The contrast between equations 31 and 32 is clear: the IMF represents a generalized Fourier expansion. The variable amplitude and the instantaneous frequency have not only greatly improved the efficiency of the expansion, but also enabled the expansion to accommodate nonlinear and nonstationary data.

Table 1. Comparison between Fourier, Wavelet and HHT analysis.

	Fourier	Wavelet	HHT
Basis	a priori	a priori	a posteriori, Adaptive
Frequency	Convolution: global, Uncertainty	Convolution: regional, Uncertainty	Differentiation over local domain, Certainty
Presentation	Energy-frequency	Energy-time-frequency	Energy-time-frequency
Nonlinearity	No	No	Yes
Nonstationarity	No	Yes	Yes
Feature Extraction	No	Discrete: Yes Continuous: Yes	Yes
Theoretical base	Theory complete	Theory complete	Empirical

2.3 THE GOERTZEL ALGORITHM

The most common application of this process is to detect the presence of a single continuous wave sinusoidal tones produced by the buttons pushed on a telephone keypad.

2.3.1 Summary

Verbatim et literatim (Engelberg, 2008)

We know that Fast Fourier Transform allows one to calculate the Direct Fourier Transform (DFT) of an N -term sequence in $O(N \ln(N))$ steps. As calculating a single element of the DFT requires $O(N)$ steps, is clear that when one does not need too many elements of the DFT, one is the best off calculating individual elements, and not the entire sequence. The Goertzel algorithm calculate individual elements of the DFT.

Consider the definition of the DFT

$$Y_m = DFT(\{y_k\})(m) \equiv \sum_{k=0}^{N-1} e^{-\frac{2\pi j m k}{N}} y_k \quad \text{Eq. 33}$$

The calculation of any given coefficient, Y_m , takes $O(N)$ steps. Thus, if one only needs a few coefficients (fewer than $O(\ln(N))$ coefficients), the it is best to calculate the coefficients and not bother with more coefficients of FFT algorithm, which calculates all the Fourier coefficients). The Goertzel algorithm is a simple way of calculating an individual Fourier coefficient. It turns calculating a Fourier coefficient into implementing a second-order filter and using that filter for a fixed number of steps. The Goertzel algorithm is somewhat more efficient than an exhaustive implementation of the DFT.

2.3.2 First-order Filters

Consider the solution of the equation

$$r_n = \alpha r_{n-1} + x_n \quad \text{Eq. 34}$$

This corresponds to calculating the response of the filter whose transfer function is

$$\frac{R(z)}{X(z)} = \frac{z}{z - \alpha} \quad \text{Eq. 35}$$

Making use of the variation of parameters idea, we guess that the solution of r_n is of the form

$$r_n = \alpha^n z_n \quad \text{Eq. 36}$$

We find that we must produce a z_n for which

$$\begin{aligned} r_n &= \alpha^n z_n \\ &= \alpha r_{n-1} + x_n \\ &= \alpha(\alpha^{n-1} z_{n-1}) + x_n \\ &= \alpha(\alpha^{n-1}(z_n + (z_{n-1} - z_n))) + x_n \\ &= \alpha^n z_n + \alpha^n(z_{n-1} - z_n) + x_n \end{aligned} \quad \text{Eq. 37}$$

For equality to hold, we find that

$$z_n = z_{n-1} + \alpha^{-n} x_n \quad \text{Eq. 38}$$

Assuming that $r_n = x_n = 0$ for $n < 0$, implies that

$$z_n = \sum_{k=0}^n \alpha^{-k} x_k \quad \text{Eq. 39}$$

Finally, we find that

$$r_n = \alpha^n z_n = \sum_{k=0}^n \alpha^{n-k} x_k \quad \text{Eq. 40}$$

2.3.3 Comparing FFT vs Goertzel algorithm

If one performs a brute force calculation of Y_m , one must multiply $e^{-2\pi jm/N}$ by y_k for N values of k . As the complex exponential is essentially a pair of real numbers, this requires $2N$ real multiplications. Additionally, the sum requires that $2(N - 1)$ real sums be calculated. When using the Goertzel algorithm, the recurrence relation requires two real additions and one real multiplication at each step. The FIR filter that is used in the final stage requires two real multiplications and one addition. In sum, the Goertzel algorithm requires $N + 2$ real multiplications and $2N + 1$ real additions. We find that the Goertzel algorithm is somewhat more efficient than the exhaustive calculation.

2.4 KALMAN FILTER

Kalman filter is an optimal state estimation process applied to a dynamic system that involves random perturbations. Kalman filter gives a linear, unbiased, and minimum error variance recursive algorithm to optimally estimate the unknown state of a dynamic system from noisy data taken at discrete real-time. It is used in a wide range of engineering and econometric applications and is an important topic in control theory and control systems engineering.

The Kalman filters are based on linear dynamical systems discretized in the time domain. They are modelled on a Markov chain built on linear operators perturbed by errors that may include Gaussian noise. The state of the system is represented as a vector of real numbers. At each discrete time increment, a linear operator is applied to the state to generate the new state, with some noise mixed in, and optionally some information from the controls on the system are known. Then, another linear operator mixed with more noise generates the observed outputs from the hidden state. The Kalman filter may be regarded as analogous to the hidden Markov

model, with the difference that the hidden state variables take values in a continuous space (as proposed to a discrete state space as in the hidden Markov model).

In order to use the Kalman filter to estimate the internal state of a process given only by a sequence of noise observations, the process should model in accordance with the framework of the Kalman filter. The following matrices must be specified: A_k , the state-transition model; C_k , the observation model; Q_k , the covariance of the process noise; R_k , the covariance of the observation noise; and B_k , the control input model, for each step k .

2.4.1 The Model

Verbatim et literatim (Chi & Chen, 2009)

Consider a linear system with state-space description

$$\begin{cases} x_{k+1} = A_k x_k + B_k u_k + \Gamma_k \underline{\xi}_k \\ w_k = C_k x_k + D_k u_k + \underline{\eta}_k \end{cases} \quad \text{Eq. 41}$$

Where $A_k, B_k, \Gamma_k, C_k, D_k$ are $n \times n$, $n \times m$, $n \times p$, $q \times n$, $q \times m$ (known) constant matrices, respectively, with $1 \leq m, p, q \leq n$, $\{u_k\}$ a known sequence of m -vectors, called a deterministic input sequence, and $\{\underline{\xi}_k\}$ and $\{\underline{\eta}_k\}$ are, respectively, (unknown) system and observation noise sequences, with known statistical information such as mean, variance, and covariance. Since both the deterministic input $\{u_k\}$ and noise sequences $\{\underline{\xi}_k\}$ and $\{\underline{\eta}_k\}$ are present, the system is usually called a linear deterministic/stochastic system. This system can be decomposed into the sum of a linear deterministic system:

$$\begin{aligned} z_{k+1} &= A_k z_k + B_k u_k \\ s_k &= C_k z_k + D_k u_k \end{aligned} \quad \text{Eq. 42}$$

and a linear stochastic system:

$$\begin{aligned} x_{k+1} &= A_k x_k + \Gamma_k \underline{\xi}_k \\ v_k &= C_k x_k + \underline{\eta}_k \end{aligned} \quad \text{Eq. 43}$$

With $w_k = s_k + v_k$ and $y_k = z_k + x_k$. The advantage of the decomposition is that the solution of z_k in the linear deterministic system is well known and is given by the so-called transition equation

$$z_k = (A_{k-1} \dots A_0) z_0 + \sum_{i=1}^k (A_{k-1} \dots A_{i-1}) B_{i-1} u_{i-1} \quad \text{Eq. 44}$$

Hence, it is sufficient to derive the optimal estimate \hat{x}_k of x_k in the stochastic state-space description, so that

$$\hat{x}_k = z_k + \hat{x}_k \quad \text{Eq. 45}$$

becomes the optimal estimate of the state vector y_k in the original linear system. Of course, the estimate has to depend on the statistical information of the noise sequences. In this work, we will only consider zero-mean Gaussian white noise processes.

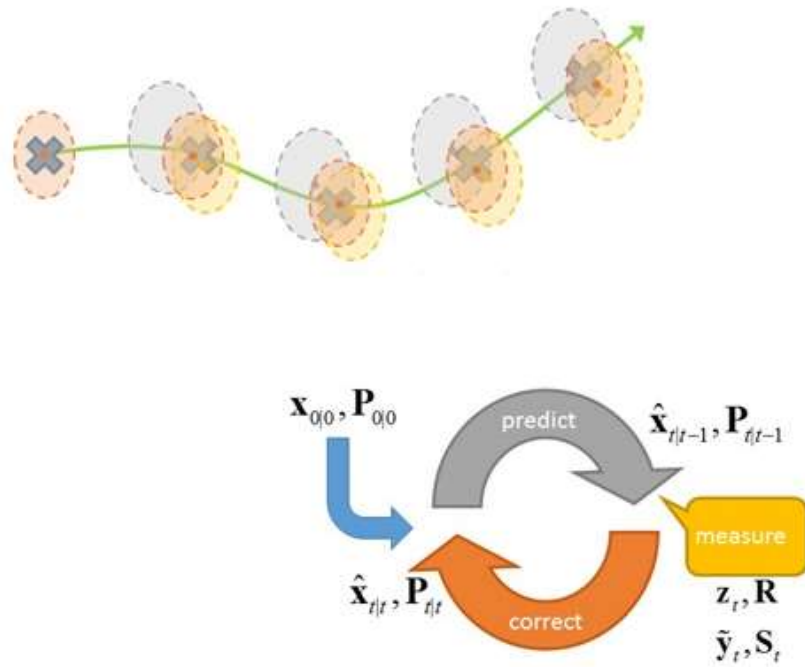


Figure 25. Kalman filter predicts, measure, corrects cycle iteratively and estimates the state at each time step.

CHAPTER 3

METHODOLOGY

This chapter is divided in tree main sections: Acquisition, Stationary Analysis and Nonstationary Analysis. In section 3, Acquisition stage, are reported the methods and techniques to acquire sEMG signals, placing electrodes, signal recording, normalization and windowing the signals. In section 3.2, Stationary Analysis, describes the methods and processes used to analyze the recorded data using Wavelet and Hilbert-Huang Transforms, also features, characteristics and patterns found using these techniques are described. In section 3.3, Nonstationary Analysis, propose the conditions, methods, techniques and processes to perform a quick filtering, under 100 ms, using Kalman and Göertzel Filters to identify the features, characteristics or patterns identified in Stationary Analysis. Acquisition system is basic in both stationary and nonstationary analysis, but equal. Figure 26 and Figure 27 show two similar processes resulted of this work.

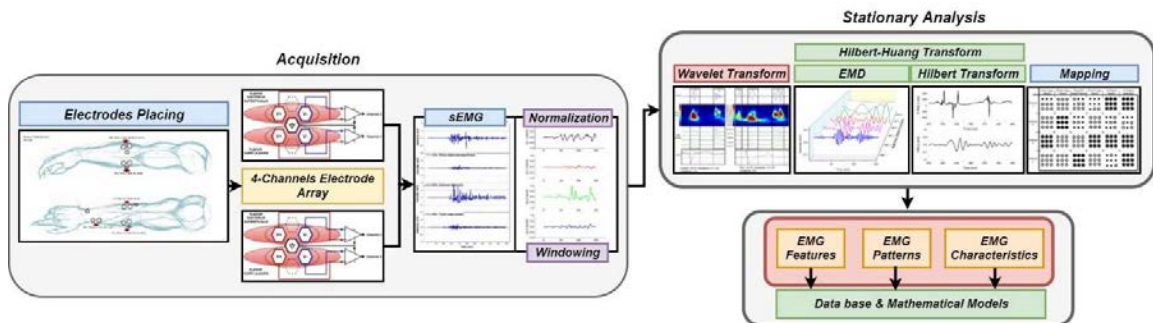


Figure 26. Block diagram of the Stationary Analysis. For Stationary Analysis is necessary the acquisition stage that comprises the electrode placing, 4-channels array acquisition system, recording data base, normalization and windowing of the signals.

After acquisition, the analysis stage is based on Wavelet and Hilbert-Huang transforms used to identify the features, characteristics and patterns into the myoelectric signals. Result of these processes are databases and mathematical models that describes myoelectric signals in time and frequency.

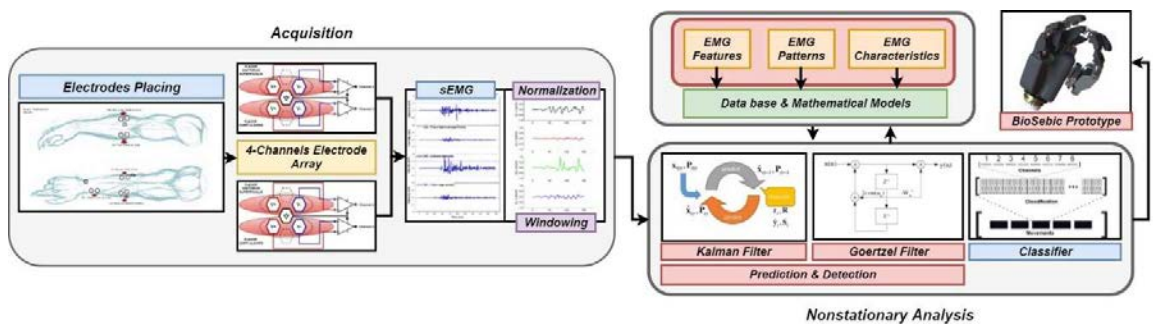


Figure 27. Block diagram of the Nonstationary Analysis. For Nonstationary Analysis is necessary the acquisition stage, that comprises the electrode placing, 4-channels array acquisition system, sampling, normalization and windowing to buffer the signals in a small-time slot. After acquisition, the filtering stage is a Kalman and Goertzel filters algorithms matching the input signals to predict, correct and identify the feature, characteristic or pattern of the de the myoelectric signals, these filters use the databases and mathematical models obtained in the Stationary Analysis.

3.1 ACQUISITION

In this section, the signals are acquired by placing Ag/AgCl surface electrodes over five forearm link-finger muscles of the subjects. Using a 4-channel electrode array configuration, these signals were sampled and recorded. Then, signals were normalized and windowed before the analyzing steps. Database for six movements of the fingers were obtained.

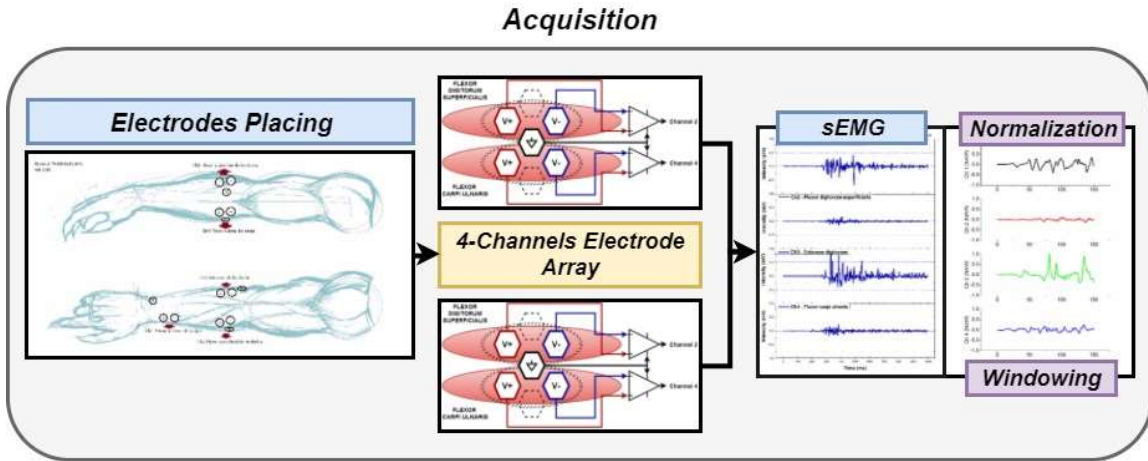


Figure 28. Block Diagram of Acquisition Stage. Acquisition of the signals consists in placing the electrodes over five forearm muscles of each subject using the 4-channels electrode array, signals from the muscles were sampled and recorded, and finally recorded signals were normalized and windowed before analyzing.

Using the BIOPAC MP35 acquisition system with 4-Channels were recorded the superficial myoelectric signals from five volunteers aged between 21 years-old and 30 years-old, without physiological or neurological problems.

The signals for the data base were recorded by BLS PRO 3.7 software under the following conditions: 2 kHz sampling frequency and a gain of 1000. The system is restricted to maximum 4 analog channels. BIOPAC system has a default IIR Chebyshev 2 bandwidth 6th order filter, it was set to 10 Hz to 500 Hz. Each channel has differential-mode configuration based on instrumentation amplifier with an external reference.

Obtained signals were relative to six movements of the fingers only. Considering that if finger 1, can reach the tip of the other four fingers, then is possible to perform 27 combinations between them (Altamirano-Altamirano, et al., 2013). Simplifying all finger movements in just 6: 1) Index Flexion (finger II), 2) Middle finger flexion (finger III), 3) Ring and Little fingers flexion (fingers IV-V), 4) Thumb finger flexion (Finger I), 5) All fingers flexion (Closing) and 6) All fingers extension (Opening).



Figure 29. Finger movements. 1) Finger II flexion, 2) Finger III flexion, 3) Fingers IV-V flexion, 4) Finger I flexion, 5) All fingers flexion, and 6) All fingers extension.

After reviewing the anatomical muscle distribution (Tortora & Derrickson, 2014), were determine the associated superficial muscles to the six movements. The muscles were 1) *Pollicis brevis* & *Pollicis Longus*, 2) *Flexor digitorum superficialis*, 3) *Extensor digitorum* and 4) *Flexor Carpi Ulnaris*. Having determined these muscles were linked to one channel, respectively.

A special name codification was used to save each record. To automate the processing in the programmed algorithms, wavelet and Hilbert-Huang algorithms, a sequence of letters and numbers was applied with the following order: *CBA4_XYZ*

Table 2. CBA4_XYZ code meaning for records names.

C	CINVESTAV		
B	BIOELECTRONICS	X	Subject number: 1 to 5
A	Researcher: ALTAMIRANO	Y	Movement number: 1 to 6
4	Number of channels	Z	Record number: 0 to 9

3.1.1 Electrodes array

Figure 30 shows the electrode array as a focal-vertex point distribution per channel, related to the parts of an ellipse. Two differential electrodes are in the focal points, one per point, and the reference electrode could be placed in one of the minor axis vertex (up or down). Reference electrode position depends of other channel position, this is to use the lowest references positions against highest number of channels, without disrupting the focal-vertex basis.

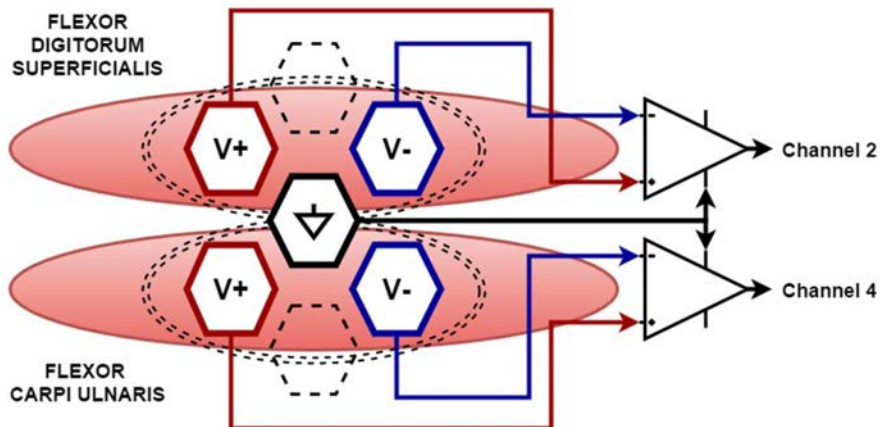


Figure 30. Electrode configuration diagram with Vertex-focal distribution. Differential electrodes (V+ & V-) and Reference electrode placed between the muscles to reduce to 1-reference. Other reference electrode position could be in the other extrema between the differential electrodes. These are distributed over larger surface of the muscle.

This array configuration allows to place each differential electrode throughout of each selected muscle, striving to place them on the larger surface of the muscle (Masuda & De Luca, 1991), placing 4 electrodes over 5 forearm muscles, respectively, as shown in Figure 31. Pediatric Ag/AgCl electrodes were used.

3.1.2 Recording protocol

The protocol for record the signals consisted to perform six mentioned movements, starting in relaxed position, this was, resting forearm into a table without any contraction, then

1. From a doss position of the hand, the person was seated and placing the right forearm over a table with the palm of the hand up.
2. Each record has a duration of eight seconds from the start to the end of the test. By movement.
3. In second four, the subject performs a movement of flexion and extension, without hold the contraction, to return immediately to doss position until the second eight, end the record.
4. For next movement, a new record starts, repeat step 3 nine times to obtain ten records per movement.
5. Repeat steps 3 and 4 all movements.

From this protocol were obtained 60 records per user ($6 \text{ mov} * 10 \text{ rec} = 60 \text{ rec/u}$); from five users were got 300 records. Each record is made up of signals from four channels with $4 \times 16,000$ elements each. These elements were used to perform wavelet analysis. To perform Hilbert-Huang analysis, these records were cut in one second length segment between 3.5 s and 4.5 s, so then $4 \times 2,000$ elements matrix is obtained. This segment corresponds to the voluntary muscular contraction and relaxation of the subjects.

The use of a data base with different size for Hilbert-Huang analysis than data base of for wavelets has foundation on two parameters: characteristics of the developed Hilbert-Huang code and the location of the information. Hilbert-Huang code was programmed for one second length segment, but also it can be adapted to other lengths. Relevant data location is in muscular activation not in the doss zones.

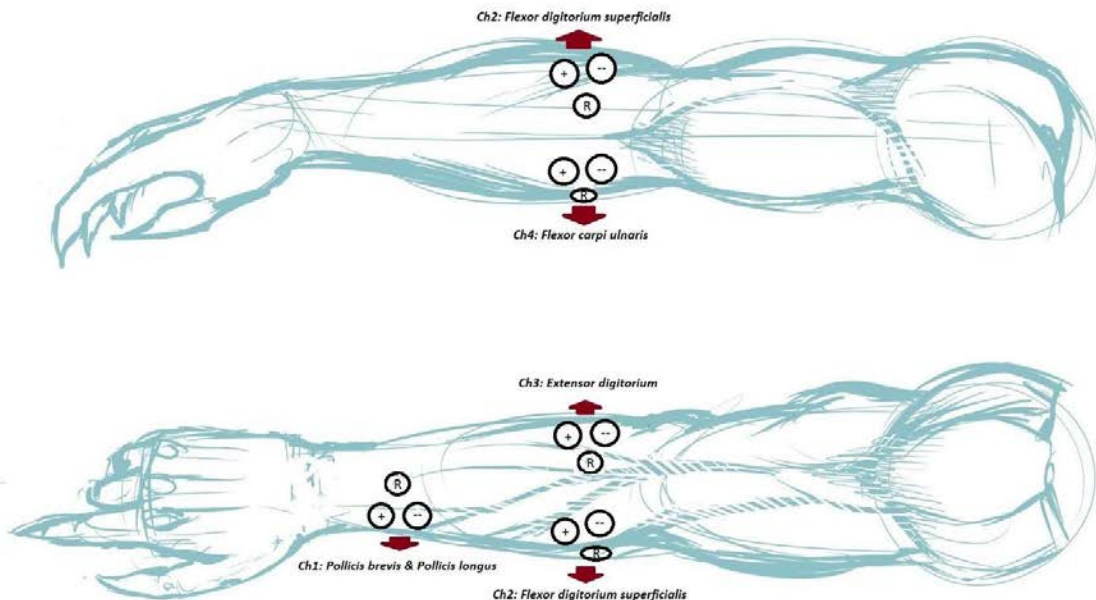


Figure 31. Channel electrode array with focal-vertex basis configuration.

3.1.3 Normalization

Normalization is fundamental in every signal processing method. For this work two normalization processes were used.

The first normalization is done by obtaining the factor α , that is reciprocal to the maximum absolute value of the myoelectric signal in each channel, in a 1000 ms sample.

$$V_{max_i} = \max[V_i(t)]; \quad i = 1, \dots, 4 \quad \text{Eq. 46}$$

$$\alpha_i = \frac{1}{V_{max_i}}; \quad i = 1, \dots, 4 \quad \text{Eq. 47}$$

where i is channel number.

Subsequently, each channel is amplified by its corresponding α_i factor, obtaining an amplitude normalization with an absolute maximum value of 1 V in all channels. With this process, the inherent noise into the channels is also amplified, intentionally, to identify its characteristics.

The second normalization is different, first the segment of the signal is windowed with a square window of 150 ms and within it were identify the absolute maximum element of each signal, simultaneously, for the four channels,

$$V_{max} = \max \left\| \begin{bmatrix} V_{Ch1}(t) \\ V_{Ch2}(t) \\ V_{Ch3}(t) \\ V_{Ch4}(t) \end{bmatrix} \right\| \quad \forall \quad (t, t + 150 \text{ ms}) \quad \text{Eq. 48}$$

followed by the β factor, that is

$$\beta = \frac{1 \text{ V}}{V_{máx}} \quad \text{Eq. 49}$$

Each channel was amplified β times, keeping original signal ratio with a maximum absolute value of 1 V.

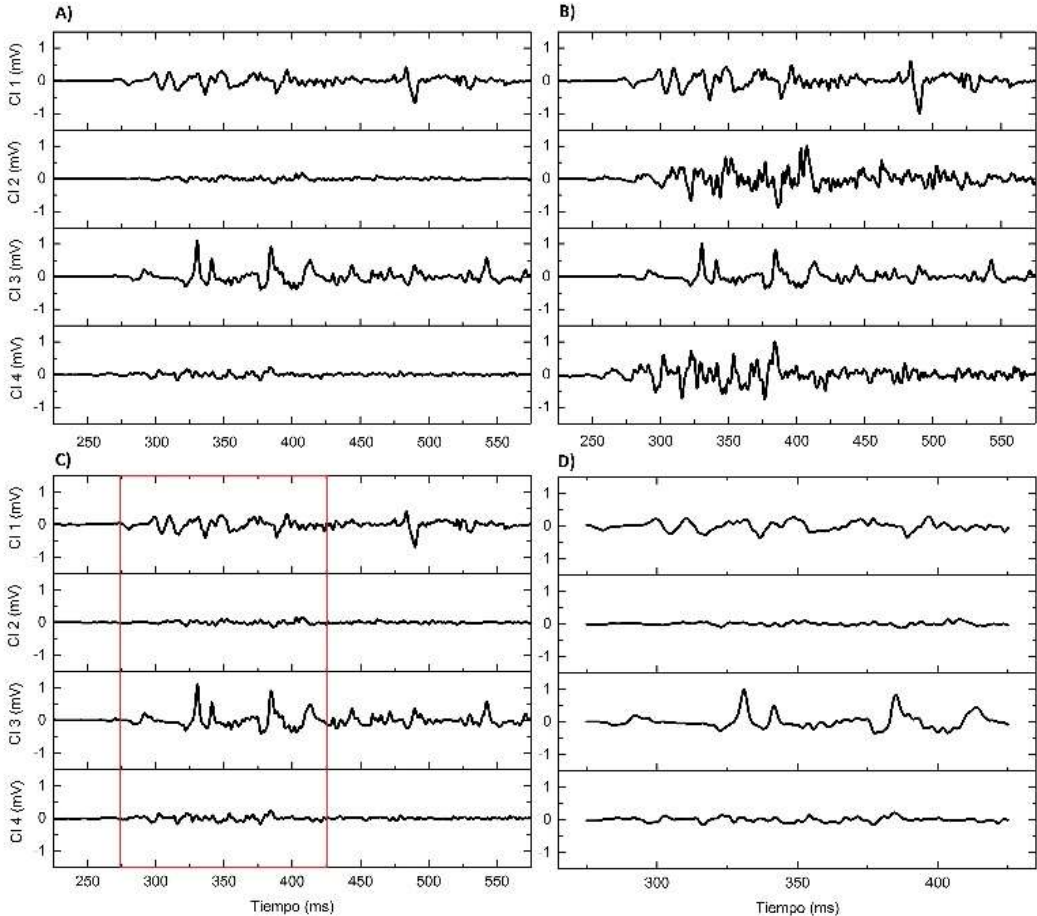


Figure 32. Normalization processes. A) and C) are original signals of four channels system. B) are the amplified signals by the α_i factors. D) shows the four channels in a 150 ms square window, as shown in figure C, amplified β times.

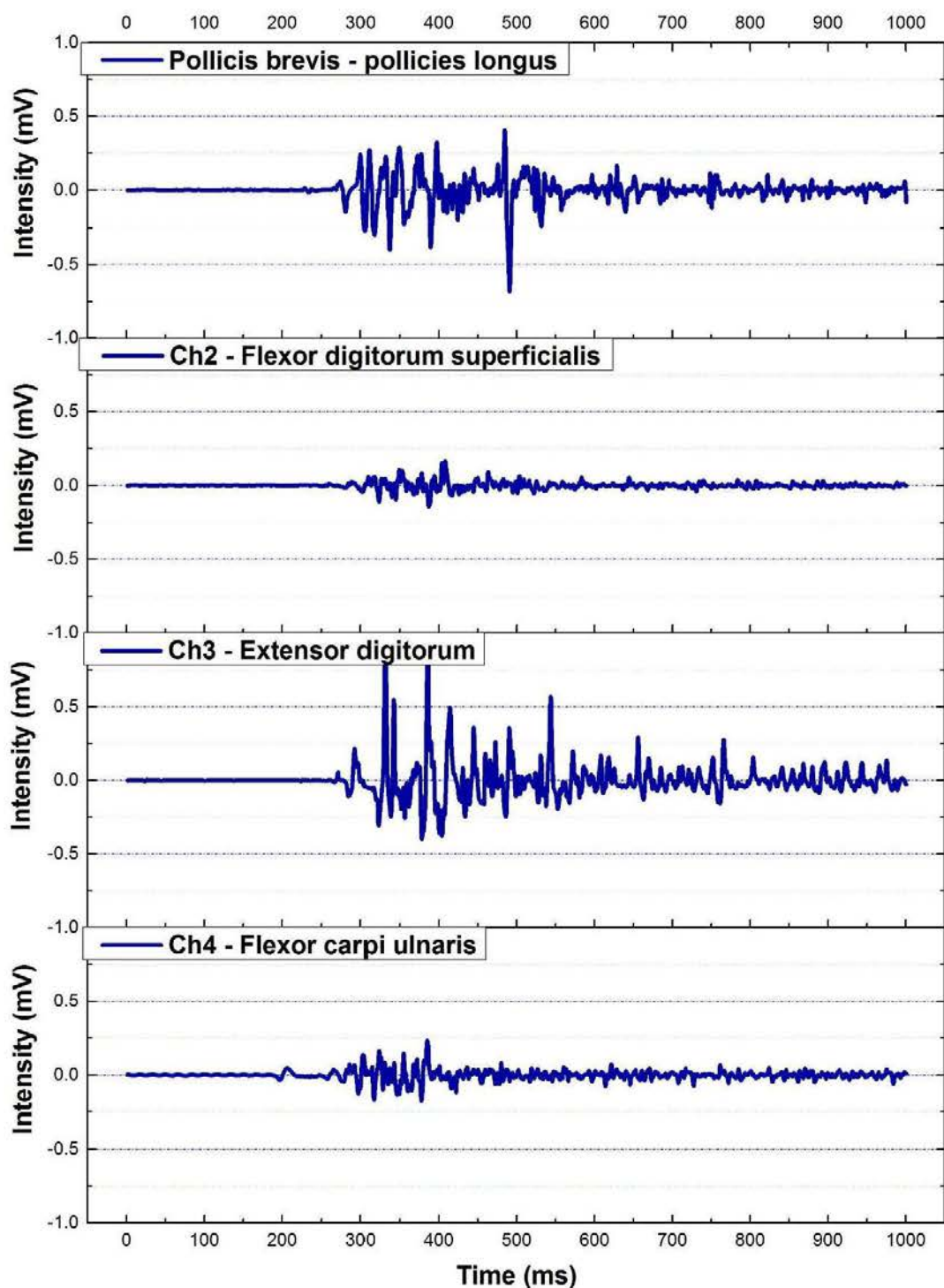


Figure 33. Record normalized -1V to 1V, filtered between 20 Hz -500 Hz and windowed between 3.5 s to 4.5 s concerning to its 8 s record number 3 of the user 1 for closing hand (CBA4_153)

3.2 STATIONARY ANALYSIS

Stationary analysis consists in the methods and processes proposed to analyze the recorded data using Wavelet and Hilbert-Huang Transforms. Features⁶, characteristics⁷ and patterns⁸ were found using these techniques. Scalograms and Statistical features are reported. Time and frequency patterns are described as mathematical models. An intrinsic characteristic of the muscular activity related with the intensity of the sEMG signal is also showed. Results are useful to propose a real-time filtering processes.

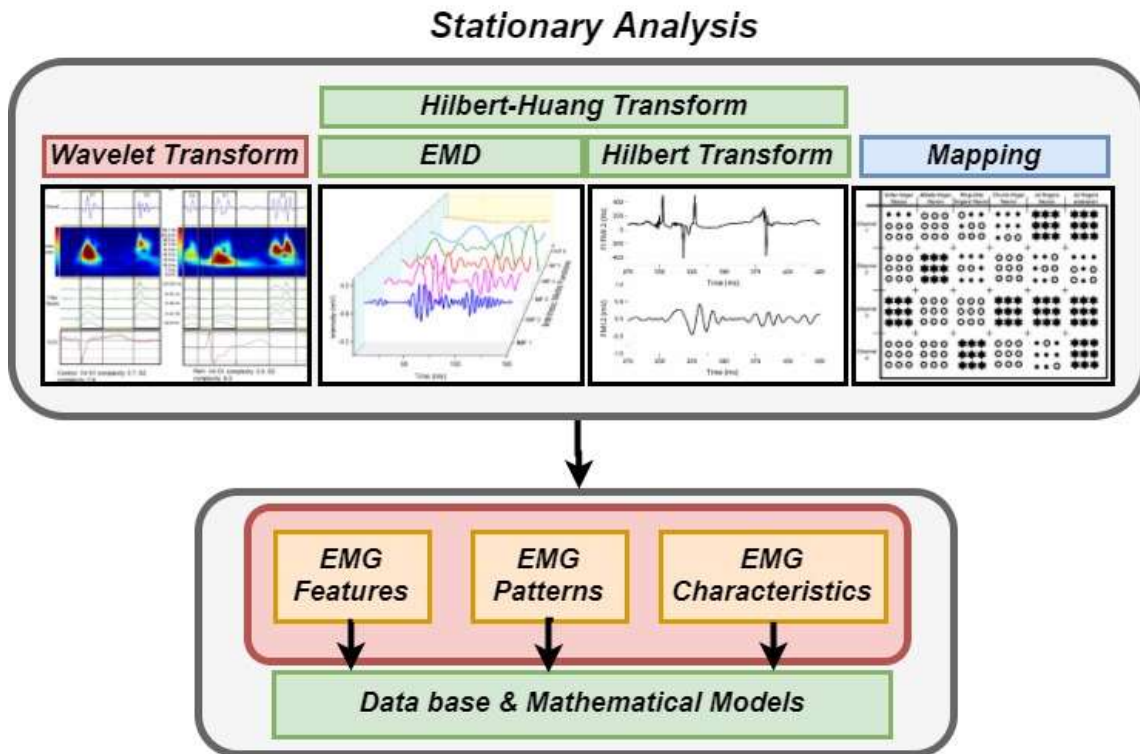


Figure 34. Block Diagram of the Stationary Analysis Stage. Stationary Analysis consist in the methods and processes used to analyze the recorded data using Wavelet and Hilbert-Huang Transforms. Features, characteristics and patterns were found, using these techniques are described, resulting in databases and mathematical models in time and frequency.

3.2.1 Wavelet Analysis

Both the time and frequency domain approaches have been attempted with diverse methods. The Wavelet Transform (WT) is an efficient math tool for nonstationary signals.

If the wavelet analysis is chosen to match the shape of the MUAP, the resulting wavelet transform yields a very good possible energy localization in the time-scale plane (Guglielminotti & Meletti, 1992). There are several factors that should be considered when choosing the wavelet function (Phinyomark, et al., 2009).

Time-frequency analysis of the acquired myoelectric signals was done with the Continuous Wavelet Transform. For this analysis, two wavelet basis were used: Daubechies 44 (db44, Figure 35) and Meyer (Figure 36), both reported for sEMG analysis (Rafiee, et al., 2011) (Reaz, et al., 2006) (Chowdhury, et al., 2013). Daubechies and Meyer wavelets are orthogonal, but Daubechies 44 is not symmetric.

⁶ Feature: An interesting or important part or quality of something.

⁷ Characteristic: A special quality that makes something different from others.

⁸ Pattern: Is something repetitive or regular way in which something happens or is done.

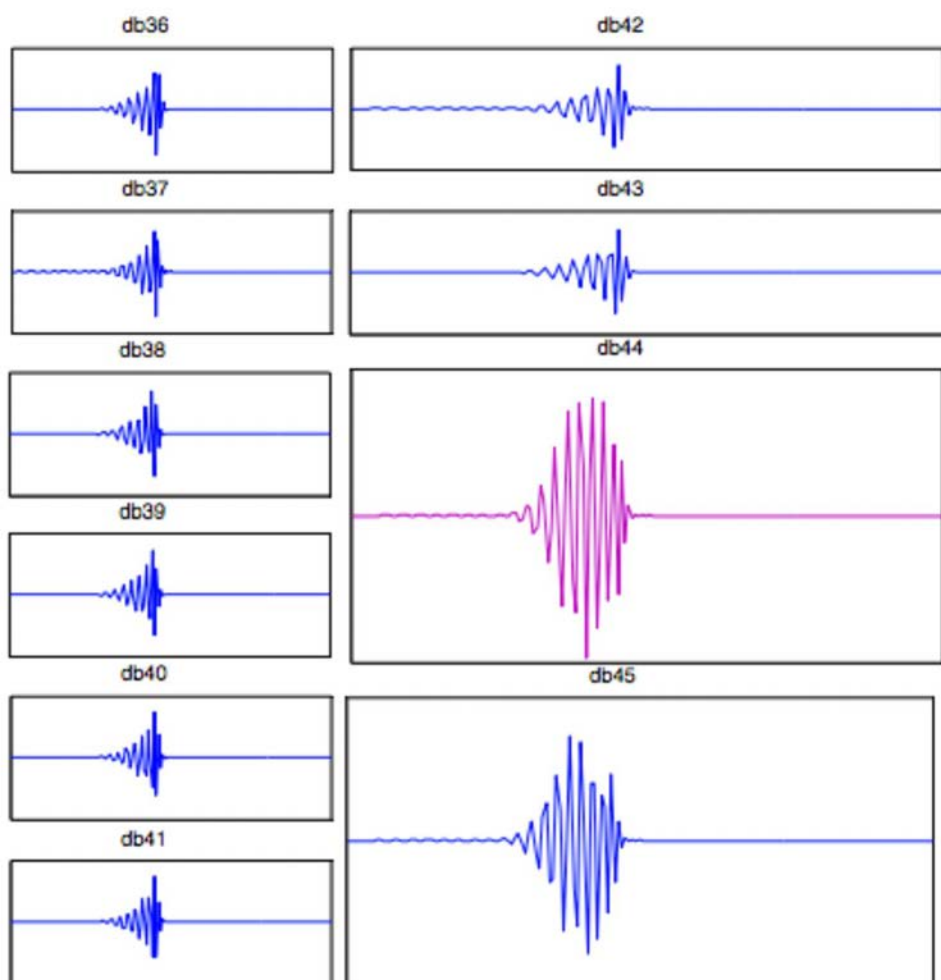


Figure 35. Wavelet Daubechies. High order wavelets. Db44 (*highlighted*) was used in this work. (Rafiee, et al., 2011)

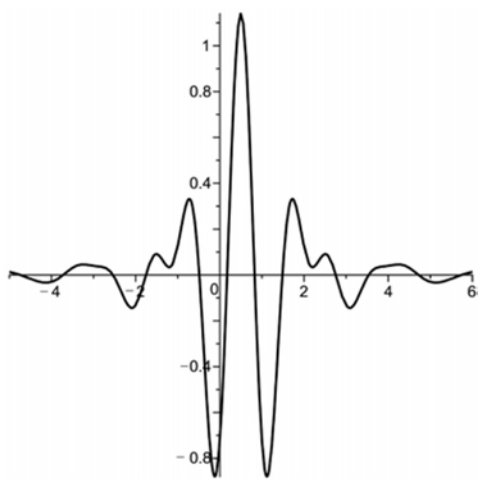


Figure 36. Wavelet Meyer

Daubechies wavelets are a set of orthogonal and nonsymmetrical functions, however, Daubechies 44 is almost symmetric. This characteristic allows it to be used in biomedical signal processing like in ECG, EMG, EEG and etcetera (Rafiee, et al., 2011).

The Continuous Wavelet Transform was applied using the “cwt” function in Matlab with a logarithmic scale vector to create the spectrograms. Figure 37 shows the logarithmic scale associated to frequency distribution.

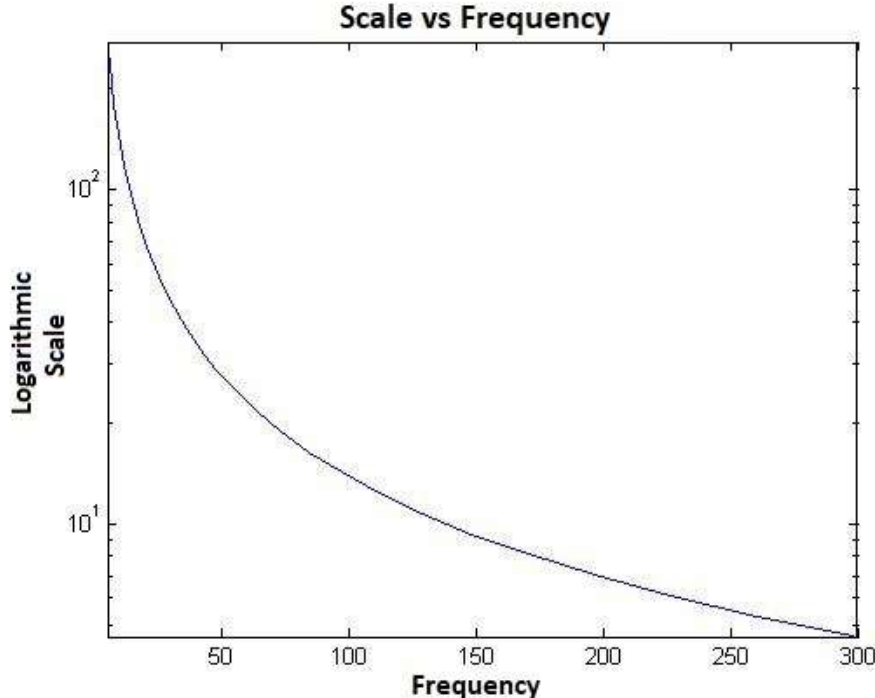


Figure 37. Wavelet logarithmic scale vs frequency for spectrogram description

CWT function computes the continuous wavelet transform coefficients of the real-valued signal x at real, positive scales. The analyzing wavelet can be real or complex. Resulting of this function is a coefficients wavelet matrix $l_a \times l_x$, where l_a is the length of the scales and l_x is the length of the input x . After obtaining the CWT coefficients, scalograms where plotted as shown in Figure 38. There were obtained 1200 scalograms, 300 by channel. The best match for each mother wavelet basis were identified in the scalogram, related directly with the original signal, highlighted in red color. Algorithm for this process is in Appendix.

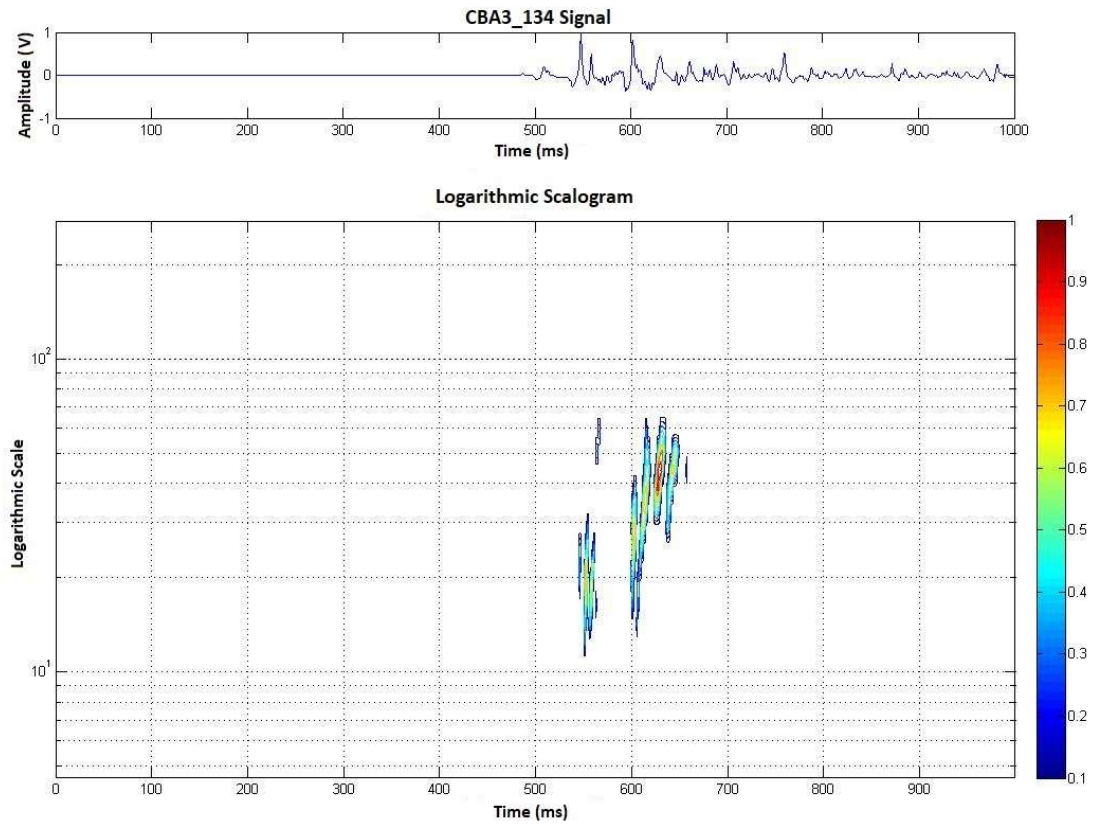


Figure 38. sEMG signal from channel 3 in 1 second timeslot (**upper**) with the logarithmic scalogram for Meyer wavelet coefficients (**lower**).

Using these locations for each signal and for all channels, some frequencies were identified. Frequency vectors were obtained to be analyzed by statistics methods, histograms and variance analysis (ANOVA).

3.2.1.1 *Histograms*

For each channel, groups of frequencies were obtained, and their histograms were plotted as shown in Figure 39.

As a complement to these histograms, a box plot for each were obtained. The means were calculated.

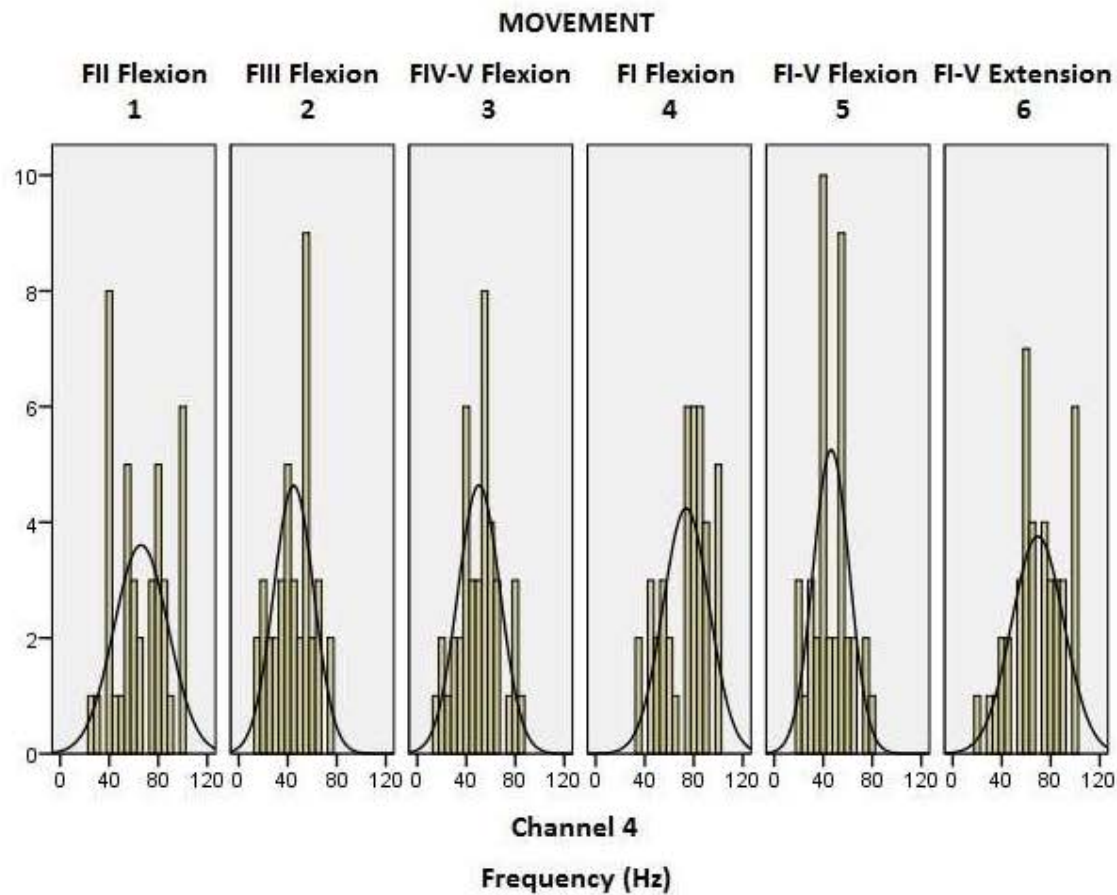


Figure 39. Histogram of frequencies channel 4, obtained from the scalogram

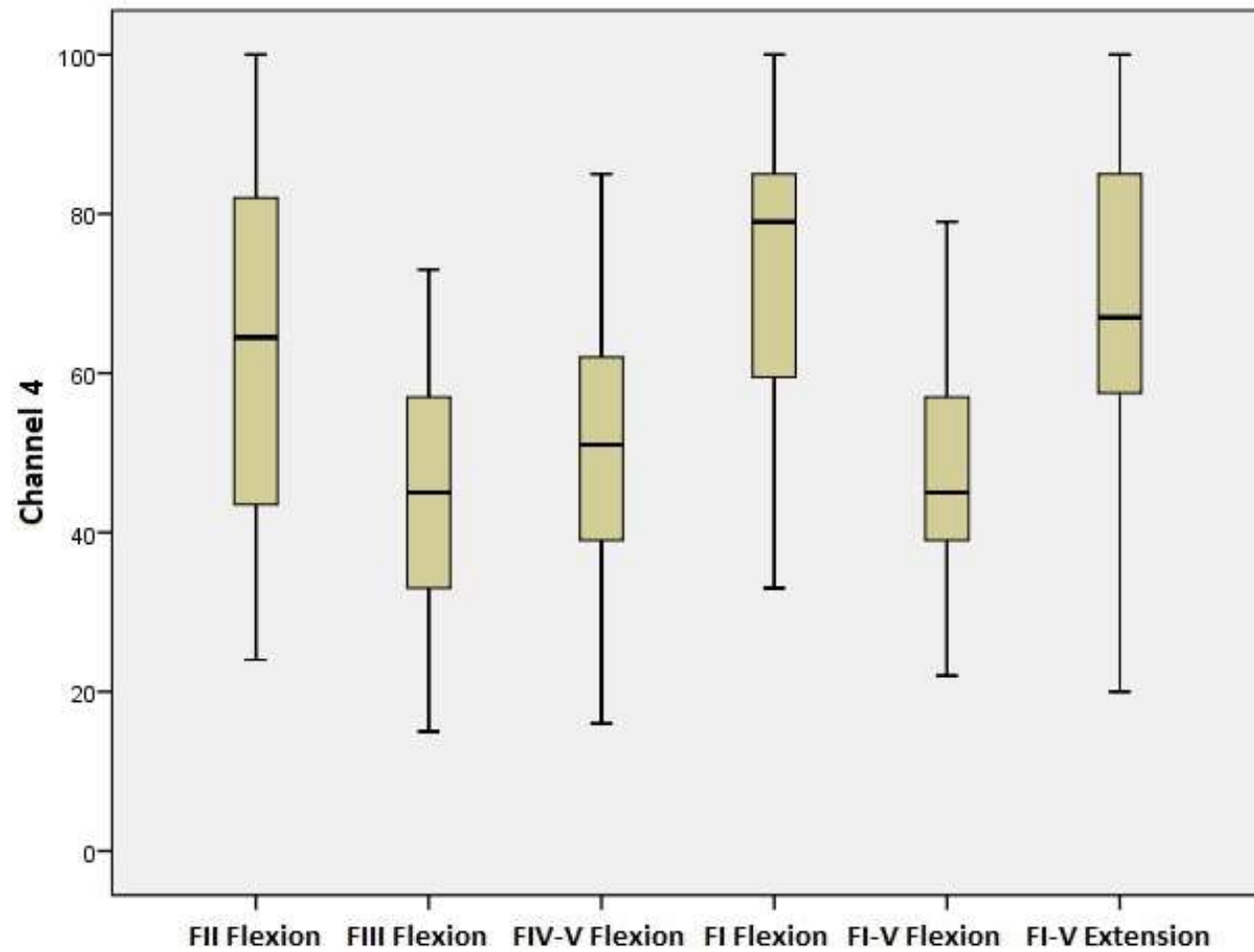


Figure 40. Box plot of the frequencies for channel versus movement

3.2.2 Statistics: ANOVA, Levene & post hoc tests.

The groups of frequencies were analyzed via variance of the means using ANOVA statistics. If significant difference exists between the frequencies, then data obtained could be useful to classify movements only with the means.

Homogeneity trial was applied to data. Levene's test is an inferential statistic used to assess the equality of variances for a variable calculated for two or more groups. Some statistical procedures assume that variances of the populations from which different samples are drawn are equal, Levene's test assesses this assumption. If the resulting *a-value* of Levene's test is less than 0.05, the obtained differences in sample variances are unlikely to have occurred based on random sampling from a population with equal variances. Thus, the null hypothesis of equal variances is rejected, and it is concluded that there is a difference between the variances in the population. If data were homogeneous then a Ratio F is used, otherwise Brown-Forsythe test were used (Levene, 1960).

A final test, *post-hoc*, for data was performed to distinguish if there are statistical enough information between movements, likewise in which are not. *Post-hoc* analyses are usually concerned with finding patterns and/or relationships between subgroups of sampled populations that would otherwise remain undetected and undiscovered. A significant ANOVA test only reveals that not all the means compared in the test are equal. Bonferroni and Games Howell tests were used. Bonferroni test is used when performs many independent or dependent statistical tests at the same time. If data did not meet the homogeneity of variances assumption then Games Howell post hoc test were applied (Hochberg, 1988) (Ruxton & Beauchamp, 2008). All statistical analysis was calculated with IBM SPSS software⁹.

⁹ <https://www.ibm.com/analytics/us/en/technology/spss/> Last access: May 29th, 2015.

3.2.3 Hilbert-Huang Analysis

Time-frequency analysis is the process of determining what frequencies are present in a signal, their intensity and their time changing. Understanding this behavior of the frequencies respecting with time can explain much about the physical processes that generate or influence the sEMG signal.

The Hilbert-Huang Transform offers higher frequency resolution and more accurate timing of transient and non-stationary signal events than conventional integral transform techniques. This separates the complex signals into simpler component signals, each of which has a single, well-defined, time-varying frequency. Real-time HHT algorithms enable this enhanced signal analysis capability to be used in process monitoring and control applications (Huang & Shen, 2005).

Raw EMG offers us valuable information into a very “noisy” form. This information is useful if is quantified. To achieve this, we applied on a raw sEMG the Hilbert-Huang method.

The sEMG recognition system can be summarized as shown below, it is composed by five stages:

1. Collected signals will be segmented and normalized in time with 150 ms width window.
2. Decompose the segment into IMFs using Empirical Mode Decomposition (EMD) for each channel.
3. Apply Hilbert Spectral Analysis followed by an instantaneous frequency computation for each IMF.
4. Discrimination features will be calculated to build feature space.
5. A classifier used to recognize the movement.

The success of a pattern recognition system depends almost entirely on the choice of features representing data sequence (Huang & Chen, 1999). Although normal resting muscles show almost no change in their sEMG signals, when a sEMG from a contracting muscle is acquired it shows significant changes in their potentials.

3.2.3.1 Empirical Mode Decomposition

Empirical Mode Decomposition is a technique to decompose a given signal into a set of elemental signals called “intrinsic mode functions” (IMFs). The EMD is the base of the so-called “Hilbert Huang Transform (HHT)”. The algorithm is simple and gives good results in situations where other methods fail (Wavelets, Fourier and etcetera) (Huang, et al., 1998) . The EMD as proposed by Norden Huang is a signal decomposition algorithm on a successive removal of elemental signals: the IMFs.

3.2.3.1.1 Algorithm to calculate IMFs, proposed by Huang.

Given any signal, $x(t)$, the IMFs are found by an iterative procedure called *sifting algorithm* (Figure 41), which is described on the following steps:

- a) Find the local maxima, M_i , $i = 1, 2, \dots$, and minima, m_k , $k = 1, 2, \dots$, in $x(t)$.
- b) Compute the corresponding interpolating signals ; $(t) = f_M(M_i, t)$, and $m(t) = f_m(m_k, t)$. These signals are the upper and lower envelopes of the signal.
- c) Let $e(t) = \frac{(M(t)+m(t))}{2}$.
- d) Subtract $e(t)$ from the signal: $x(t) = x(t) - e(t)$.
- e) Return to step (a) – stop when $x(t)$ remains nearly unchanged.
- f) Once we obtain an IMF, $\varphi(t)$, remove it from the signal $x(t) = x(t) - \varphi(t)$ and return to (a) if $x(t)$ has more than one extremum (neither a constant nor a trend).

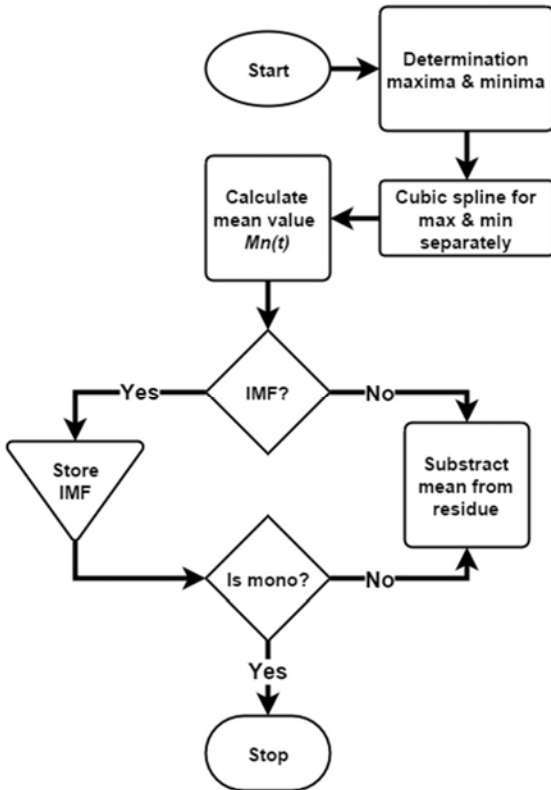


Figure 41. Flow chart for the sifting algorithm, basis of EMD method.

When the IMF component is a monotonic function, the process is finalized, and the original signal is reconstructed by adding all the IMF components along with the mean of final residue, m_{final} . The reconstructed signal can be represented as:

$$S(t) = \sum_{k=1}^n IMF_k + m_{final} \quad \text{Eq. 50}$$

where n is the number of IMFs.

The Matlab algorithm for EMD Decomposition is in Appendix: Empirical Mode Decomposition basis.

To show this step, for each channel were calculated their IMFs with the EMD algorithm to extract the symmetric components of the signal.

For channel 1, the figure shown below contains the IMFs corresponding to it: 9 IMFs.

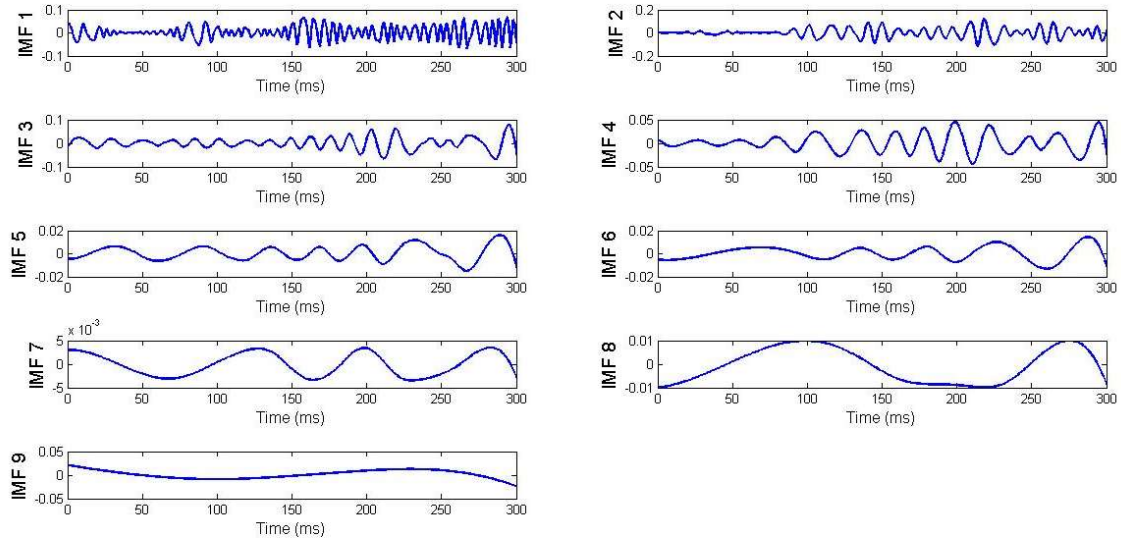


Figure 42. Intrinsic Mode Functions (IMFs) extracted from channel 1 for transitory stage of supination movement.

For channel 2, the figure shown below contains the IMFs corresponding to it: 8 IMFs.

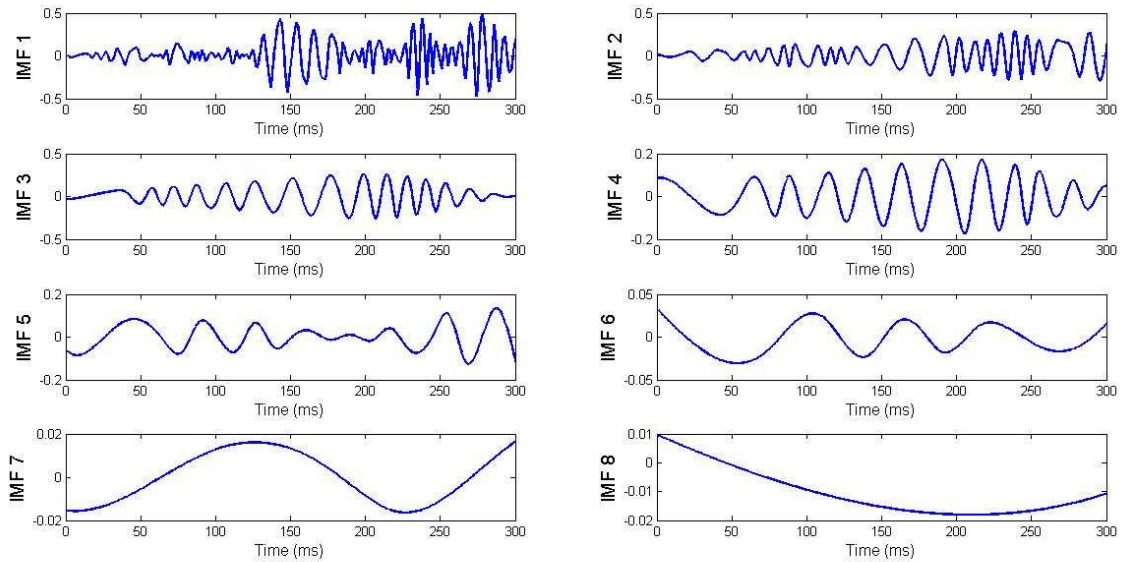


Figure 43. Intrinsic Mode Functions (IMFs) extracted from channel 2 for transitory stage of supination movement.

For channel 3, the corresponding IMFs are shown in the figure below: 10 IMFs.

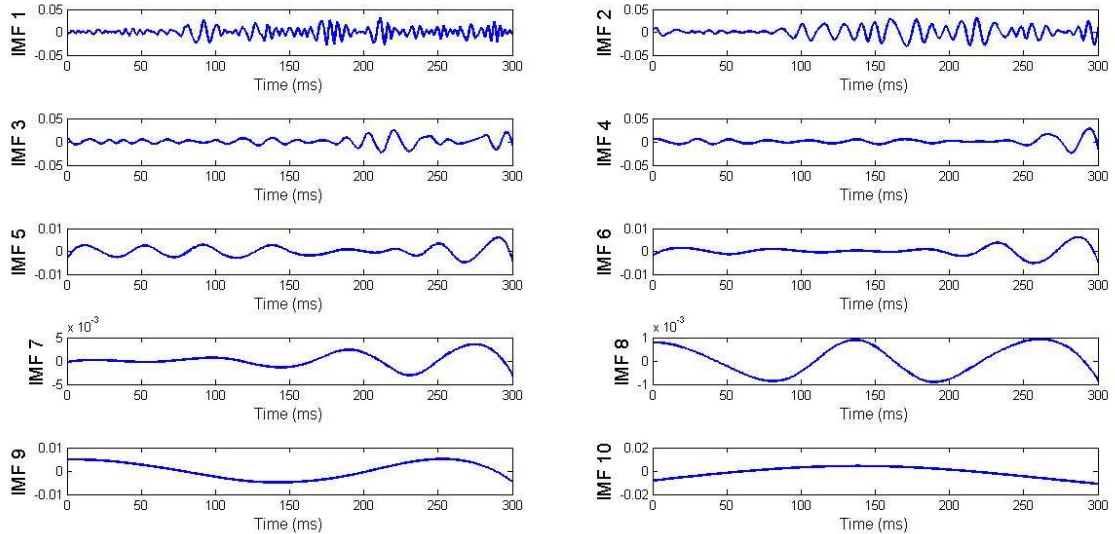


Figure 44. Intrinsic Mode Functions (IMFs) extracted from channel 3 for transitory stage of supination movement.

Finally, for channel 4, the corresponding IMFs are shown in the figure below: 8 IMFs.

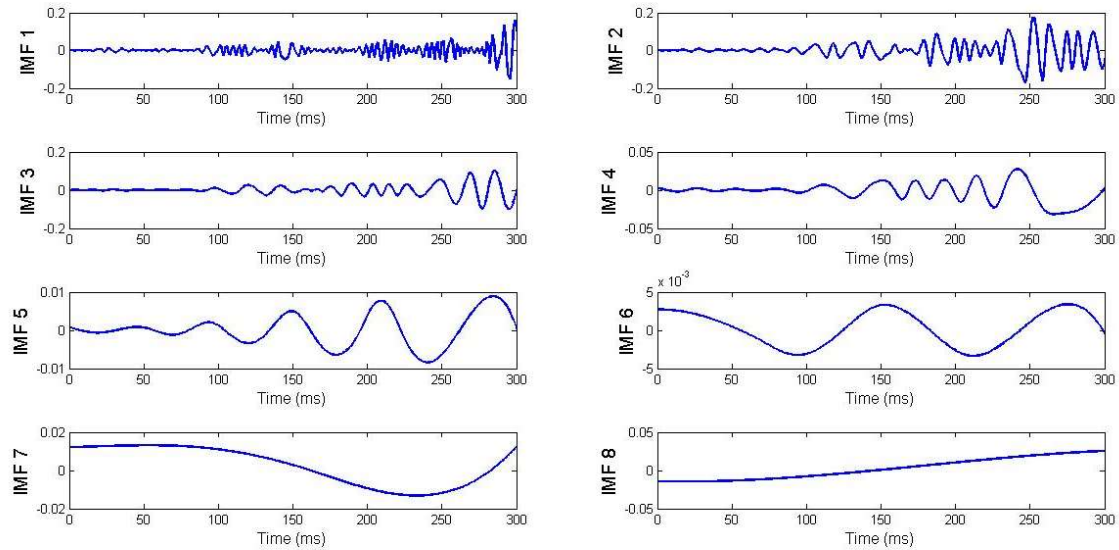


Figure 45. Intrinsic Mode Functions (IMFs) extracted from channel 4 for transitory stage of supination movement.

After decomposition, we analyze each IMF according to the original data. Baseline drift is reflected in higher-standards scales, like in IMFs 6-10. High-frequency noise is in the lower scales, like in IMF 1 and IMF 2.

By construction, the number of extrema should decrease when going from one IMF to the next, and the whole decomposition is expected to be completed with a finite number of IMFs. Conceptually, the algorithm: is simple; appears naturally, does not assume anything about the signal, mainly stationary and can be applied to a wide class of signals. For each channel, we calculated their IMFs to extract the main components of the signal. Figures 42 – 45 shown the AM/FM components from channels 1-4, respectively; those IMFs satisfy the following conditions:

- Resolution: 45dB between Signal and Bias energy $10 \log \frac{W_{signal}}{W_{bias energy}}$, normally they are in 40dB - 60dB.
- Residual energy: 45dB between Signal/Residual $10 \log \frac{W_{signal}}{W_{residual}}$, normally they are in 40dB-60dB.
- With these resolution, each channel has between 8 IMFs to 10 IMFs.
- Reconstruction of the signal with the obtained IMFs is the same as the original one.
- Every IMF could be filtrated or treated with hard thresholds to eliminate undesirable frequencies in lower and higher orders.

Most important steps into the algorithm is (Rato, et al., 2008): extrema locations, extrema interpolation, end effects, sifting stopping criterion and IMF removal.

Some suggestions for the development of the algorithm: remove the mean and normalize the signals to a unit power. This last procedure is important when dealing signals with very low amplitudes as in the case of biomedical signals. There is interdependence between the number of IMFs and resolution. The algorithm is simple, does not assume anything about the signal, can be applied to a wide class of signals.

This step was applied to all the segmented and normalized signals.

3.2.3.2 Hilbert Spectral Analysis

Spectral estimation is the second step of the HHT. This consists in computing the instantaneous frequency for each IMF using the Hilbert Transform (HT) and the analytic signal concept.

This is another drawback of the HHT, because the HT uses the whole signal (theoretically (from $-\infty$ to $+\infty$)). As we have finite segment of a signal, the window effect, rectangular window in this case, will distort its spectrum and consequently its HT. As we will show later, this may give poor frequency estimation. On the other hand, using HT it is not necessary to compute the instantaneous amplitude because we already have it.

3.2.3.2.1 Demodulating the IMF

Let $\varphi(t)$ be an IMF $y(t)$ the corresponding analytic signal.

$$\varphi(t) = Re\{|y(t)|e^{j\arg(y(t))}\} = |y(t)|\cos\theta(t) \quad \text{Eq. 51}$$

where $\theta(t) = \arg[y(t)]$. So, we obtained the instantaneous amplitude and an oscillating function that is a constant AM/FM signal (not necessarily a sinusoid). If $|y(t)|$ is known, we can perform an amplitude demodulation and obtain

$$s(t) = \cos[\theta(t)] \quad \text{Eq. 52}$$

such that

$$|s(t)| \leq 1 \quad \text{Eq. 53}$$

$s(t)$ can be considered as an FM signal. Its demodulation leads us to the instantaneous frequency.

3.2.3.2.2 Demodulated signal is an AM signal

At the end of the sifting procedure leading to the referred IMF, $\varphi(t)$, we also have its envelopes, $M(t)$ and $m(t)$. If these were true envelopes, they would be symmetric, and its difference would be the estimate of the amplitude modulating signal

$$\varphi(t) = A(t) \cdot s(t) \quad \text{Eq. 53}$$

and

$$A(t) = |y(t)| = M(t) - m(t) \quad \text{Eq. 54}$$

As $M(t)$ and $m(t)$ are not truly symmetric, we must look for a more reliable estimate of $A(t)$. This can be achieved by the following procedure:

- a) Make $g(t) = |\varphi(t)|$
- b) Compute the maxima of $g(t)$ and extrapolate them as described in
- c) Interpolate those maxima to obtain an estimate of $A(t)$.

Now, it is enough to divide $\varphi(t)$ by $A(t)$ to obtain an FM signal, $s_{FM(t)}$.

3.2.3.3 Instantaneous Frequency Estimation

Assume that the instantaneous frequency of $s_{FM(t)}$ is a slowly time varying signal, so that we may consider it to be constant over small intervals. Moreover, sample it to get a discrete-time signal that we can express as:

$$s_{FM(n)} \approx \cos[2\pi f(n_0)n] \quad \text{Eq. 55}$$

this for $n_0 - N \leq n \leq n_0 + N$.

Then, we assume that the frequency is constant in a window with length $2N + 1$, where N is a positive integer. In this situation, instantaneous frequency could be obtained from

$$\cos[2\pi f(n_0)] = \frac{\sum_2^{L-1} s_{FM}(n)[s_{FM}(n-1) + s_{FM}(n+1)]}{2 \sum_2^{L-1} s_{FM}^2(n)} \quad \text{Eq. 56}$$

where L is the number of available samples. For a pure sinusoid, this formula gives the correct value, provided we have at least three samples. So, for a FM signal we substitute $L = 2N + 1$, as referred above.

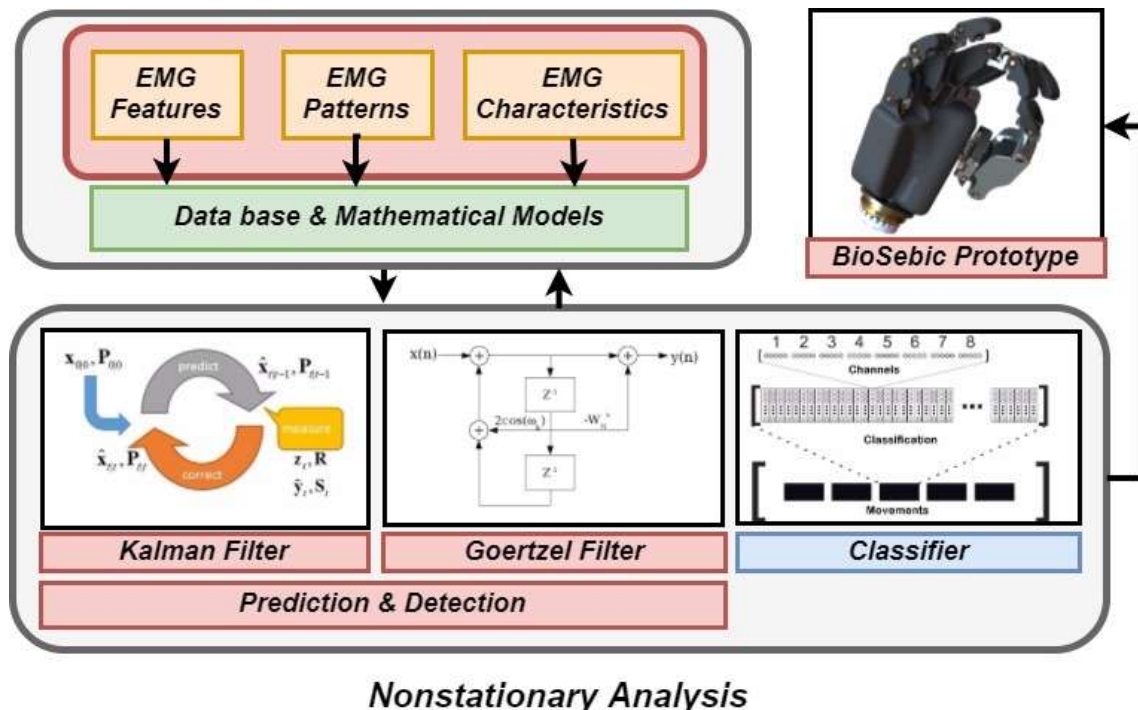
Each IMF appears as an AM/FM signal. In Huang et al. papers a Hilbert spectral estimation is used to estimate the instantaneous frequency.

Estimating the instantaneous frequencies corresponding to, almost, six hand movements, we will create a data base in matrix form to save corresponding numbers associated to the patterns. This will be a numerical model that we can use to compare the input patterns versus the saved patterns.

To show this step, we will use the IMF's extracted from the last procedure (EMD) for channel 1 to 4, corresponding to transient segment during all-fingers closing movement.

3.3 NONSTATIONARY ANALYSIS

In this section, Nonstationary analysis, is a proposal for the conditions, methods, techniques and processes to perform in short-time, or real-time under 100 ms of processing slot, using Kalman and Goertzel filters to identify the features, characteristics or patterns of the myoelectric signals. Kalman filter improves the denoising and reconstruction to predict the input signal, myoelectric signal. The output signal from Kalman Filter goes to the Goertzel filter, that detects specific signals using the Discrete Fourier Transform based on the modeled patterns. Results from these filters could be applied directly to the prosthetic system as a control signal or be applied to a classifier system, depending on the complexity of the acquisition system, channels or movements.



Nonstationary Analysis

Figure 46. Block Diagram of the Nonstationary Analysis Stage. Nonstationary Analysis, propose the conditions, methods, techniques and processes to perform in short-time, under 100 ms, using Kalman Filter and Goertzel filter to identify the features, characteristics or patterns of myoelectric signals. Resulting data could be applied to a classifier system.

3.3.1 Dynamical Reconstruction using Hybrid Kalman filter

To improve reconstruction accuracy, Kalman filter were proposed, which allows to fuse two information sources, i.e. the finger movement intensity mapping and the activity of the finger linked muscles, registered by the sEMG. Applying the Kalman filter, can convert four channels of myoelectric activity recorded from the forearm muscles into defined reconstructions of MUAP shapes. The filter operates in a causal manner and acts as a predictor using the sEMG signals from the past only, which makes the approach suitable for real-time operations.

Kalman filter is an algorithm that fuses two or more noisy signals to produce an estimate of the dynamical system state vector, which is optimal in the minimum squared error sense.

The algorithm works in two steps, prediction and correction. In the prediction step produces estimates of the current state variables, along with their uncertainties. Once the outcome of the next measurement, typically with random noise, is observed, these estimates are updated using a weighted average. The algorithm is

recursive, it can run in real time using only the present input measurements and the previously calculated state and its uncertainty matrix, no additional information is required.

Most physical systems are represented as continuous-time models while discrete-time measurements are frequently taken for state estimation via digital processor. Therefore, the system model and measurement model are given by

$$\dot{x}(t) = A(t)x(t) + B(t)u(t) + w(t) \quad \text{Eq. 57}$$

$$z_k = C_k x_k + v_k \quad \text{Eq. 58}$$

where $x_k = x(t_k)$

Initialize

$$\hat{x}_{0|0} = E[x(t_0)], \quad P_{0|0} = \text{Var}[x(t_0)] \quad \text{Eq. 59}$$

3.3.1.1 Prediction equations

The prediction equations are derived from those of continuous time Kalman filter without update from measurements, i.e. $K(t) = 0$. The predicted state and covariance are calculated respectively by solving a set of differential equations with the initial value equal to the estimate at the previous step.

$$\dot{\hat{x}}(t) = A(t)\hat{x}(t) + B(t)u(t), \quad \text{Eq. 60}$$

with

$$\begin{aligned} \hat{x}(t_{k-1}) &= \hat{x}_{k-1|k-1} \\ \hat{x}_{k|k-1} &= \hat{x}(t_k) \end{aligned} \quad \text{Eq. 61}$$

$$\dot{P}(t) = A(t)P(t) + P(t)F(t)^T + Q(t) \quad \text{Eq. 62}$$

with

$$\begin{aligned} P(t_{k-1}) &= P_{k-1|k-1} \\ P_{k|k-1} &= P(t_k) \end{aligned} \quad \text{Eq. 63}$$

3.3.1.2 Update equations

The update equations are identical to those of the discrete-time Kalman filter.

$$\begin{aligned} H_k &= P_{k|k-1}H_k^T(H_kP_{k|k-1}H_k^T + R_k)^{-1} \\ \hat{x}_{k|k} &= \hat{x}_{k|k-1} + K_k(z_k - H_k\hat{x}_{k|k-1}) \\ P_{k|k} &= (I - K_kH_k)P_{k|k-1} \end{aligned} \quad \text{Eq. 64}$$

3.3.2 Single tone detection with Goertzel algorithm

The Goertzel algorithm analyses one selectable frequency component from a discrete signal. Unlike direct DFT calculations, this algorithm applies a single real-valued coefficient at each iteration, using real-valued arithmetic for real-valued input sequences. For covering a full spectrum, the Goertzel algorithm has a higher order of complexity than fast Fourier transform algorithms, but for computing a small number of selected frequency components, it is more efficient numerically. The simple structure of the Goertzel algorithm makes it well suitable for embedded systems.

The main calculation in the Goertzel algorithm has the form of digital filter, and for this reason the algorithm is often called a Goertzel filter. The filter operates on an input sequence $x[n]$ in a cascade of two stages with a parameter ω_0 , giving the frequency to be analysed, normalized to radians per sample.

The first stage calculates an intermediate sequence, $s[n]$:

$$s[n] = x[n] + 2 \cos(\omega_0) s[n-1] - s[n-2] \quad \text{Eq. 65}$$

The second stage applies the following filter to $s[n]$, producing output sequence $y[n]$

$$y[n] = s[n] - e^{-j\omega_0} s[n-1] \quad \text{Eq. 66}$$

The first filter stage can be observed to be a second-order IIR filter with a direct-form structure. This structure has the property that its internal state variables equal the past output values from that stage. Input values $x[n]$ for $n < 0$ are presumed all equal to 0. To establish the initial filter state so that evaluation can begin at sample $x[0]$, the filter states are assigned initial values $s[-2] = s[-1] = 0$. To avoid aliasing hazards, frequency ω_0 is often restricted to the range 0 to π ; using a value outside this range is not meaningless, but is equivalent to using an aliased frequency inside this range, since the exponential function is periodic with a period of 2π in ω_0 . The Z transform for this stage is:

$$\frac{S(z)}{X(z)} = \frac{1}{1 - 2 \cos(\omega_0) z^{-1} + z^{-2}} = \frac{1}{(1 - e^{j\omega_0} z^{-1})(1 - e^{-j\omega_0} z^{-1})} \quad \text{Eq. 67}$$

The second stage filter can be observed to be a FIR filter, since its calculations do not use any of its past outputs. Z transform methods can be applied to study the properties of the filter cascade. The z-transform for this stage is:

$$\frac{Y(z)}{S(z)} = 1 - e^{-j\omega_0} z^{-1} \quad \text{Eq. 68}$$

The combined Z transform transfer function of the cascade of the two filter stages is then

$$\frac{S(z)}{X(z)} \frac{Y(z)}{S(z)} = \frac{Y(z)}{X(z)} = \frac{(1 - e^{-j\omega_0} z^{-1})}{(1 - e^{j\omega_0} z^{-1})(1 - e^{-j\omega_0} z^{-1})} = \frac{1}{1 - e^{j\omega_0} z^{-1}} \quad \text{Eq. 69}$$

The algorithm in Matlab for Goertzel filter is in Appendix.

CHAPTER 4

RESULTS & DISCUSSION

This thesis reports the processes, techniques, analysis methods and results to develop prosthetic systems based on the use of myoelectric signals and results for the development of prosthetic devices based on myoelectric signals patterns and features.

4.1 MUSCULAR ACTIVITY BY MOVEMENT

An intrinsic result was obtained from the muscular intensity mapping in the four channels array per user. The level of the intensity was recorded and compared against the six movements. Three intensity levels were set: High Intensity (In_h), 0.7 V to 1 V; Mean Intensity (In_m), 0.35 V to 0.65 V; and Null Intensity (I_{NULL}), 0 V to 0.3 V. Figure 47 shows the intensity map for user 1. There is a hint that this is a characteristic, but a pattern.

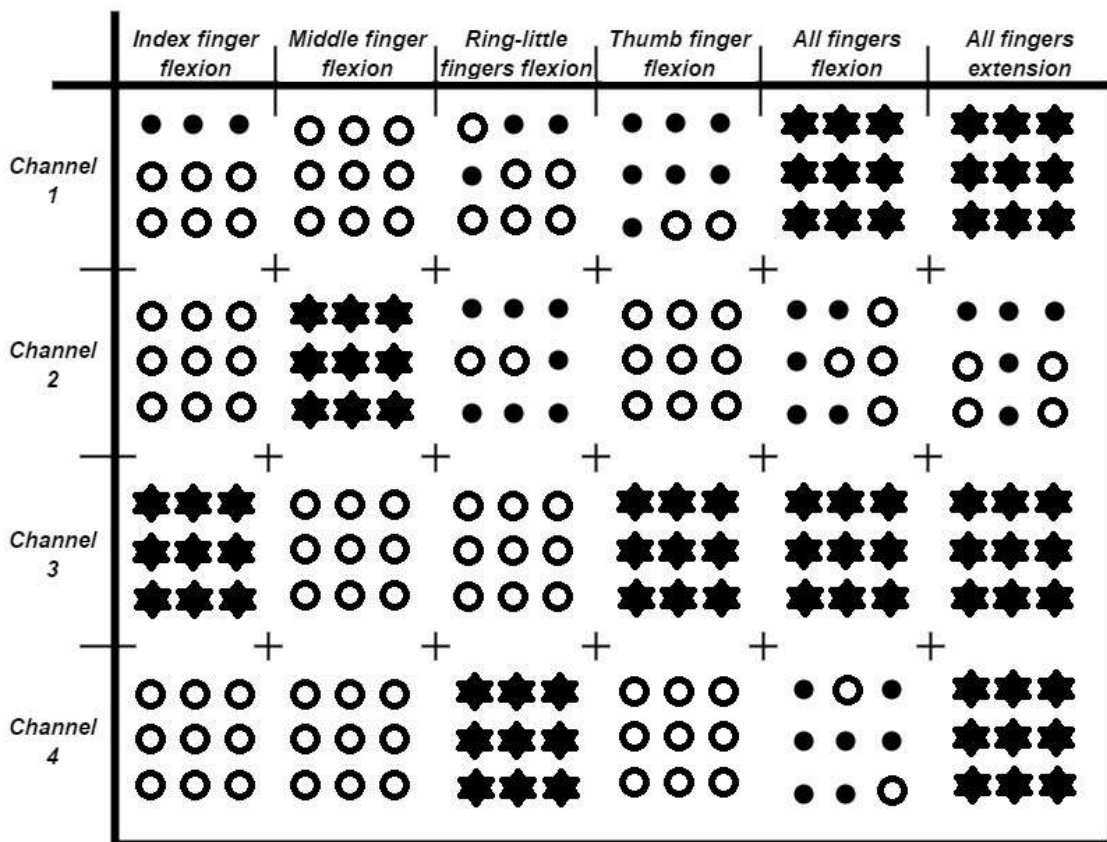


Figure 47. Muscular contraction intensity of subject 1 for four channels versus six movements of the fingers. The map shows the intensity present in the four channels when a movement was performed: star represents 0.7 V to 1 V level, dot represents 0.35 V to 0.65 V level, and circle represents 0 V to 0.3 V. Each icon represents one of nine repetitions.

4.2 WAVELET TRANSFORM ANALYSIS

For EMG signal processing, the wavelet transform is an alternative to other time frequency representations. Wavelet transform has the advantage of being linear and yielding for multiresolution analysis. While discrete wavelet transform provides flexible time-frequency resolution, it suffers from a relative low resolution in the high-frequency region. Its difficulty in differentiating transient components.

A comparison in the scalograms obtained with Meyer wavelet versus the scalograms obtained with Daubechies 44 wavelet, shows that the Meyer wavelet had better definition in time and frequency than Daubechies 44. Daubechies shape form does not fit the MUAP shape as well than Meyer, resolution is better.

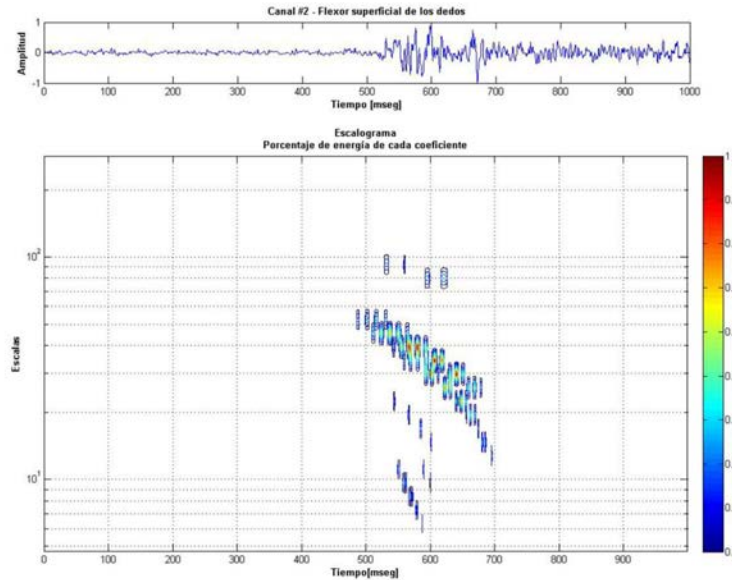


Figure 48. Scalogram of CBA4_234 obtained with Daubechies 44 wavelet

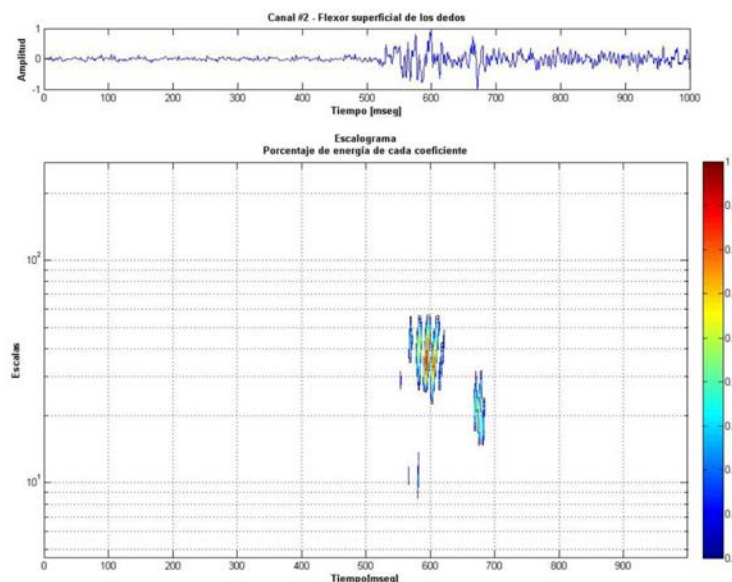


Figure 49. Scalogram of CBA4_234 obtained with Meyer Wavelet

The mean frequencies that resulted are shown in Table 3.

Table 3. Mean \bar{x} and median \tilde{x} frequencies from 4 channels relative to 6 movements obtained by wavelet Meyer base scalogram.

M	CH1	CH2	CH3	CH4	
1	\bar{x} [Hz]	\tilde{x} [Hz]	\bar{x} [Hz]	\tilde{x} [Hz]	\bar{x} [Hz]
1	56.63	53	60.53	57	61.43
2	53.03	49	39.56	42	53.83
3	48.63	45	49.41	45	50.48
4	67.60	67	64.33	62	64.60
5	52.68	49	51.40	59.5	59.20
6	63.70	59.5	60.23	59.5	68.08
					\tilde{x} [Hz]
					65.95
					64.5
					44.79
					445
					50.40
					51
					73.75
					79
					46.49
					45
					69.40
					67

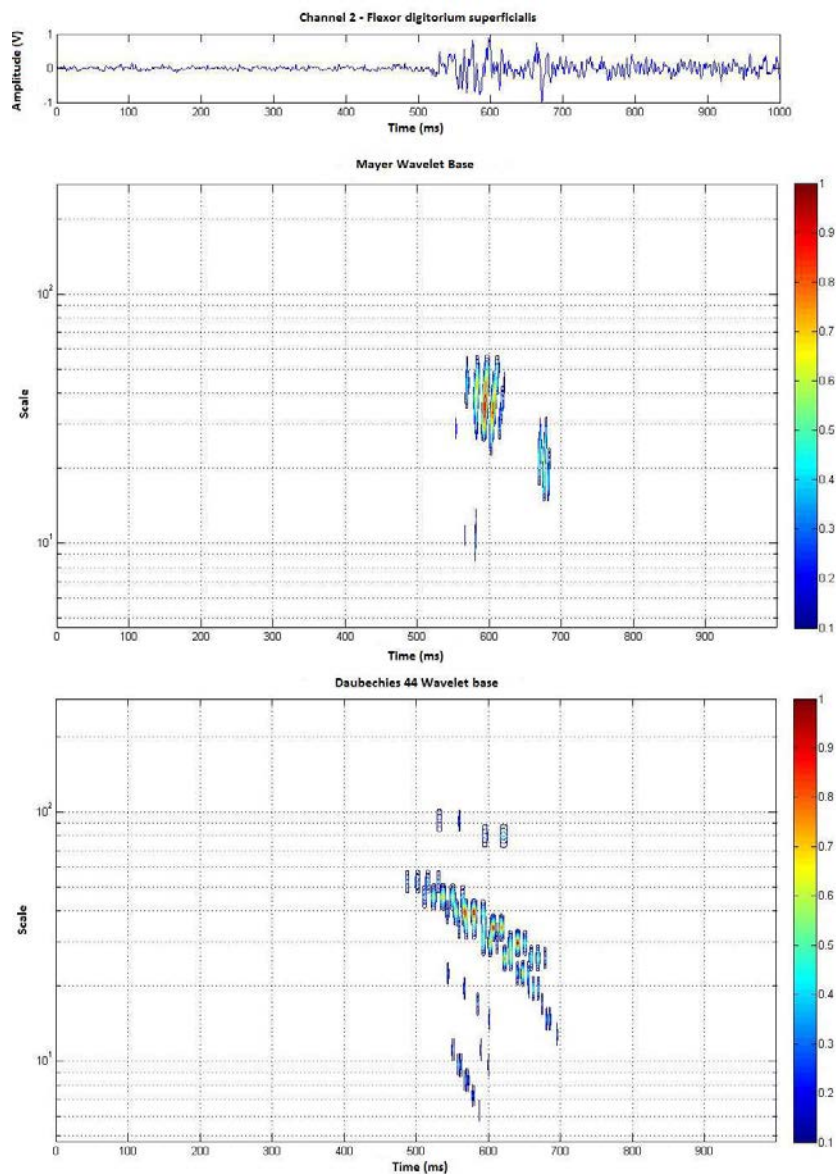


Figure 50. Scalograms for signal from channel 2 (Flexor digitorum superficialis). Meyer base (upper) and Daubechies base (bottom)

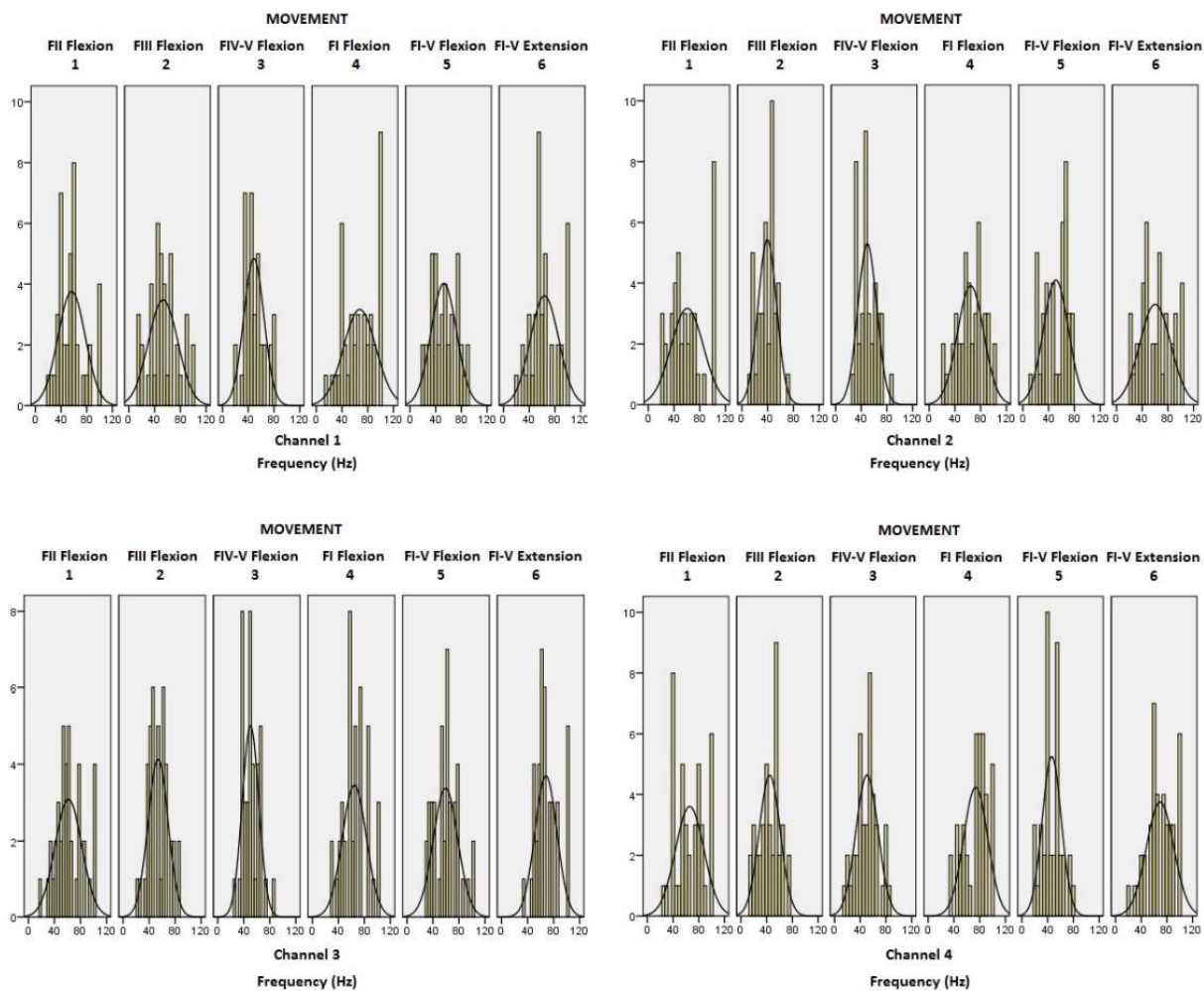


Figure 51. 4-Channel Histogram of mean frequencies obtained from Wavelet Analysis.

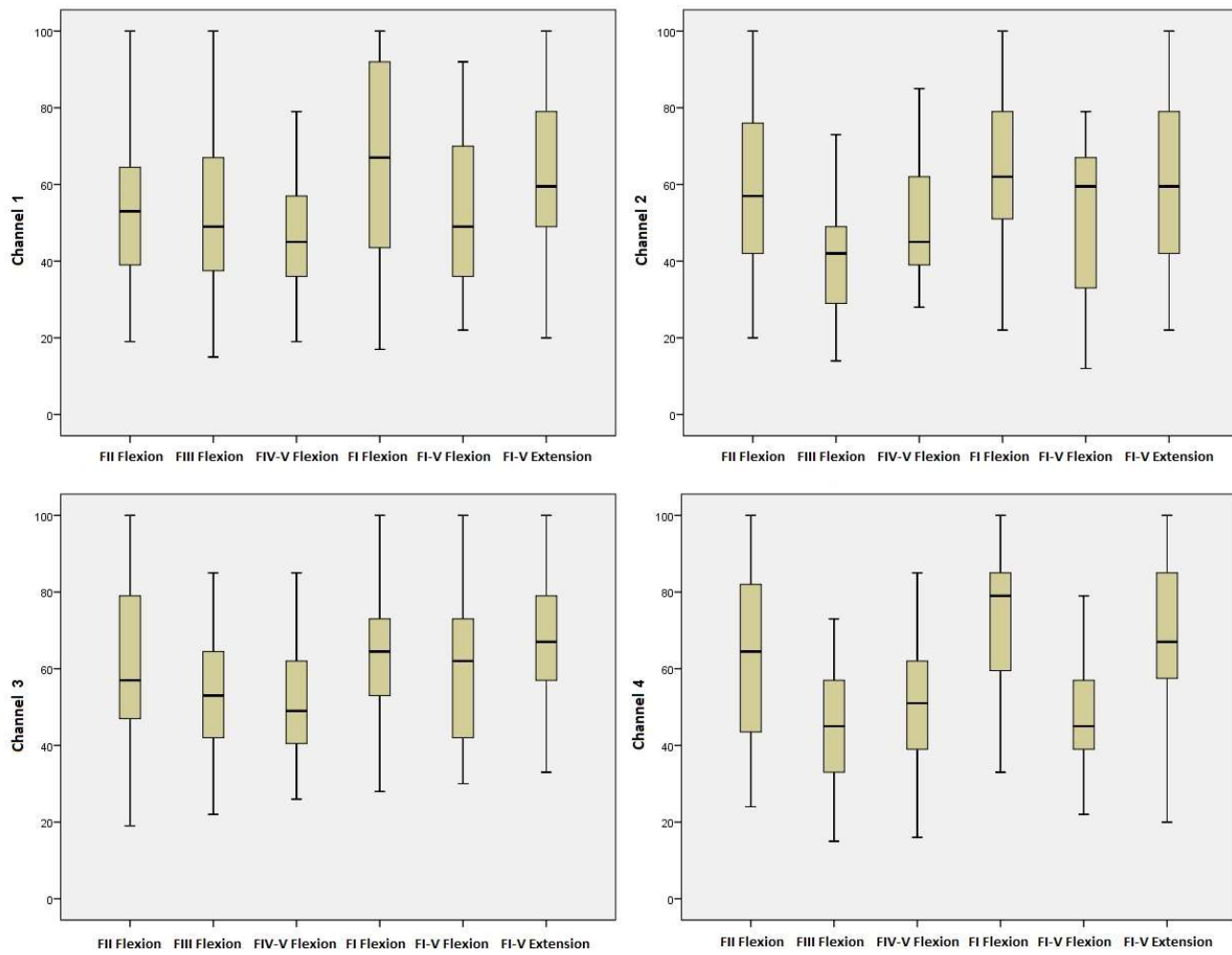


Figure 52. 4-Channel Boxplot for ANOVA results of mean frequencies obtained from Wavelet analysis.

4.3 HILBERT-HUANG ANALYSIS

EMD aims to decompose a multi-component signal, i.e. myoelectric signals, into a few mono-components called IMFs. The EMD signal processing technique is suitable for filtering EMG signals. The major drawback of the EMD method is that it is more sensitive to the presence of noise.

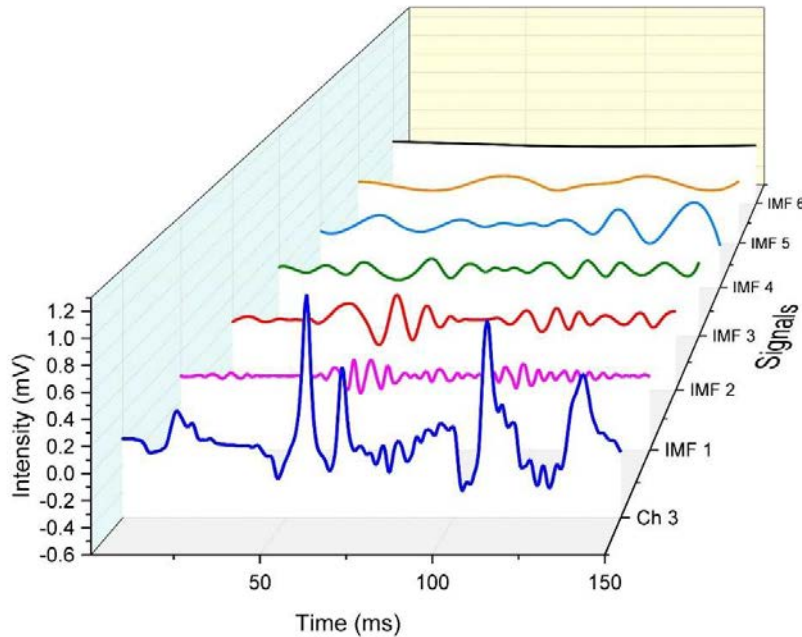


Figure 53. sEMG signals and their IMFs of channel 3 related to the flexion and extension of all fingers. 6 decomposition levels are shown. IMF 2 shows two MUAPs in 50 ms and 100 ms approximately.

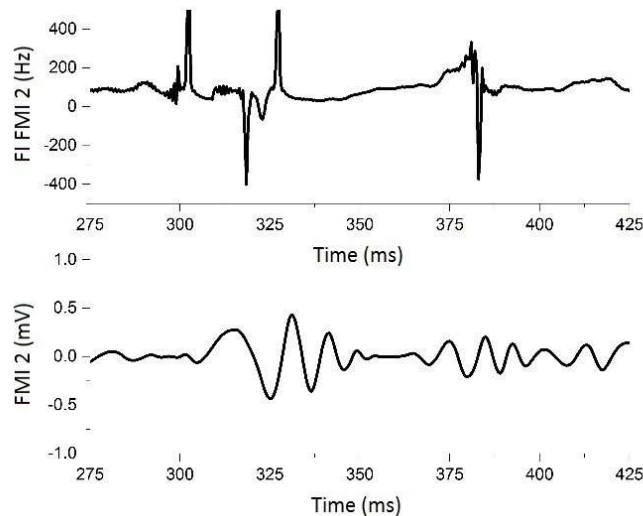


Figure 54. Instantaneous frequency (*upper*) of the Intrinsic Mode Function 2 (*lower*) for signal of channel 3. Drastic frequency changes are present in the Instantaneous frequency related with the start and end of the contraction.

For EMD, using the first normalization, section 3.1.3, the number of IMF obtained were between 8 IMFs and 19 IMFs per channel; Alike, for the second normalization were obtained between 5 IMFs and 11 IMFs.

After decomposition, The Hilbert Transform and the Instantaneous Frequency computation was applied to each IMF from each channel. The resulting data are shown from Figure 56 to Figure 63. Red lines, upper and lower envelopes, are the Instantaneous envelops; they are useful to compute the instantaneous frequencies for each IMF in a short interval. The values of these frequencies were from 105 Hz to 310 Hz, and their plots showed changes in specific regions of the signals, particularly in the beginning and ending of a voluntary contraction, form doss to active and *vice versa*. Instantaneous frequency was useful to locate the significative changes in the energy signal, i.e. voluntary contraction and relaxation. The obtained IMF could reconstruct almost 98% of the original signal. Adding the three first IMFs could reconstruct up to 92% of the original signal.

Main frequencies of the IMFs are in order of 200 Hz +/- 20 Hz, detected into the first IMFs. Low frequencies detected in the last IMFs were 12 Hz, 8 Hz and 6 Hz. High energy detected frequencies are groups of AM/FM signals with average frequencies of 83.3 Hz (73.57 Hz – 85.9 Hz), 96.7 Hz (94.35 Hz – 99.82 Hz), 59 Hz (58.5 Hz – 61.3 Hz) and 113.3 Hz (111 Hz – 117.04 Hz). These frequencies were approximated using Fourier series, 1 term to 8 terms, with R^2 of 0.98 and 0.99.

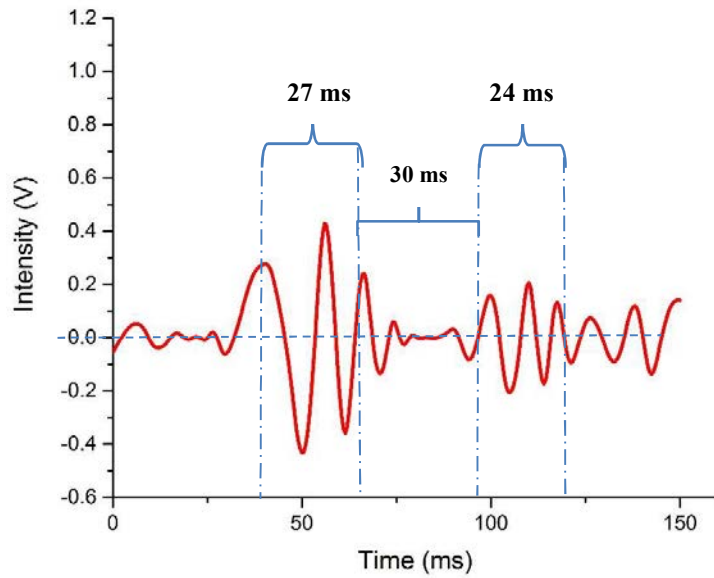


Figure 55. Time patterns associated to MUAP. Period of 24.5 ms average of MUAP.

In the 87% of the IMFs, three patterns were founded: Two MUAPs with the same period and, time slot between the these MUAPs and size ratio. First, two oscillations with frequencies of 83.3 Hz, 96.7 Hz or 113.3 Hz into a period of 24.5 ms in average. Second pattern is a 30 ms average period in the middle of these two oscillations. Finally, the size ratio 2:1 between first MUAP and second MUAP.

For IMFs extracted from Channel 1,

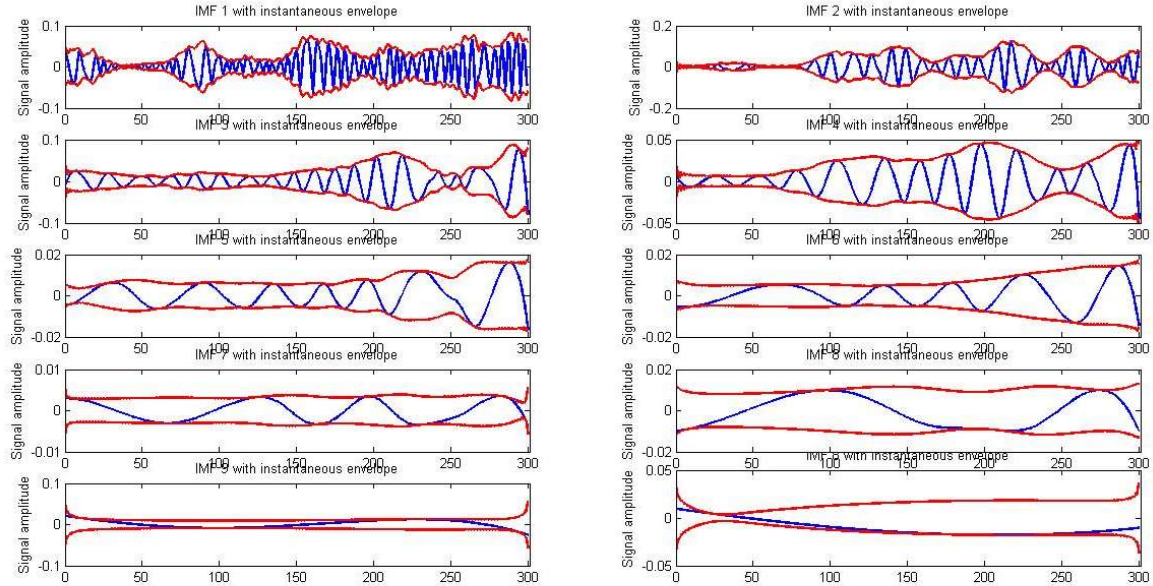


Figure 56. Hilbert transform (red lines envelops) of IMFs for Channel 1 during supination movement in transient segment.

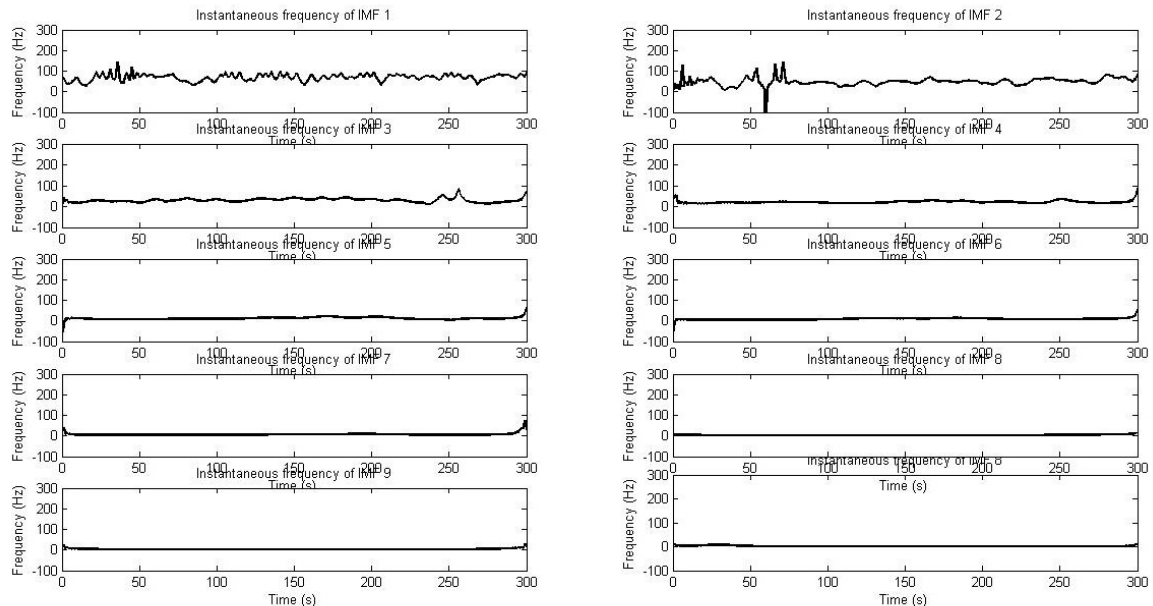


Figure 57. Instantaneous frequencies for Channel 1 during supination movement in transient segment.

Finally, analyzing the resulting instantaneous frequencies, it is possible to identify changes in the first four IMFs, those are related to the activation flexion movement.

For IMFs extracted from Channel 2,

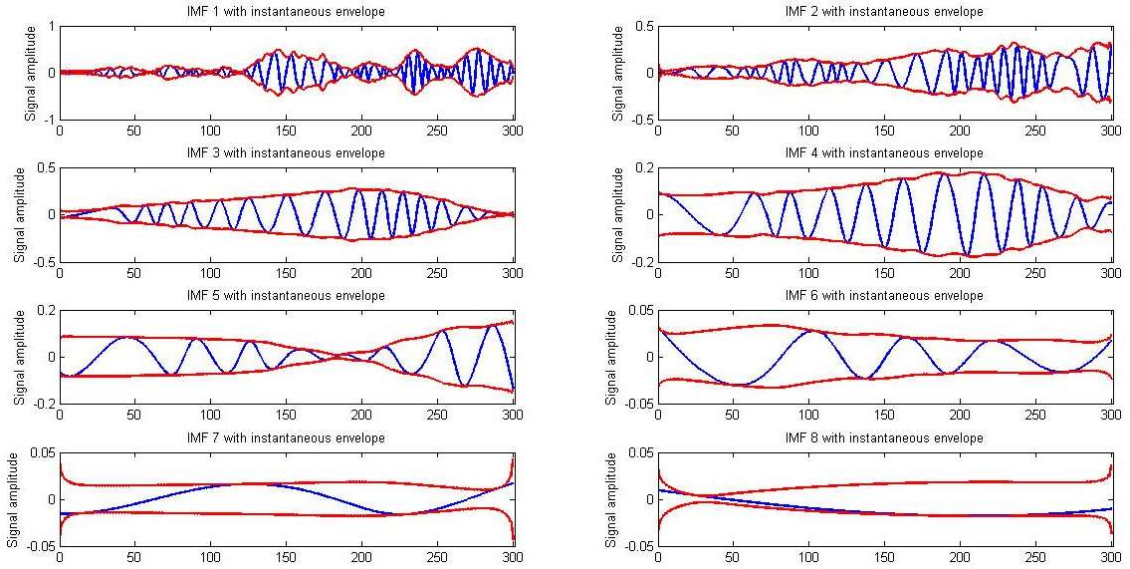


Figure 58. Hilbert transform of IMFs for Channel 2 during supination movement in transient segment.

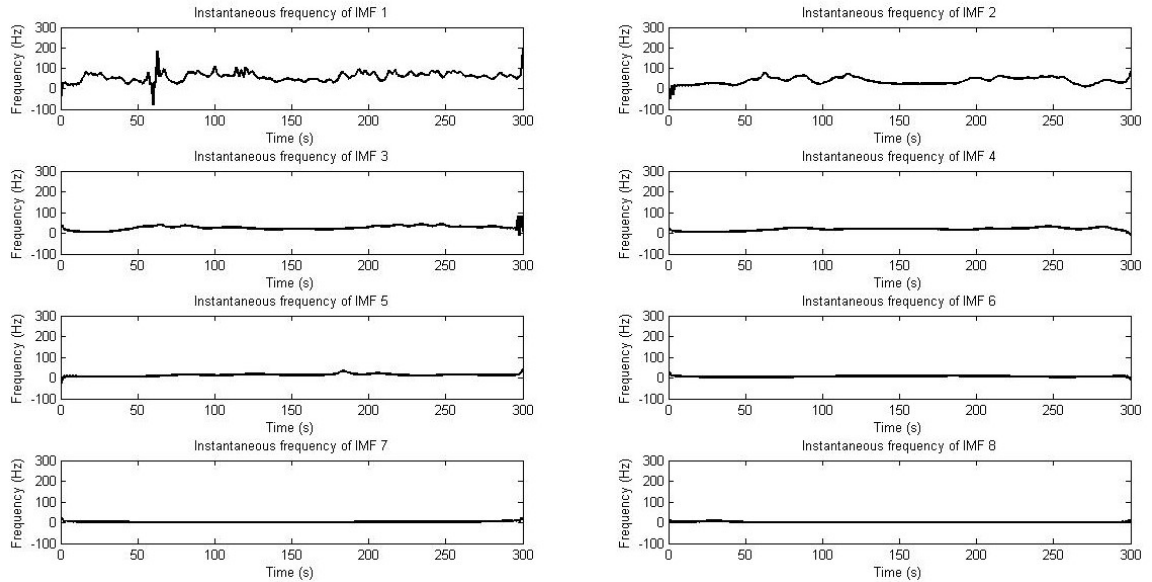


Figure 59. Instantaneous frequencies for Channel 1 during supination movement in transient segment.

For IMFs extracted from Channel 3,

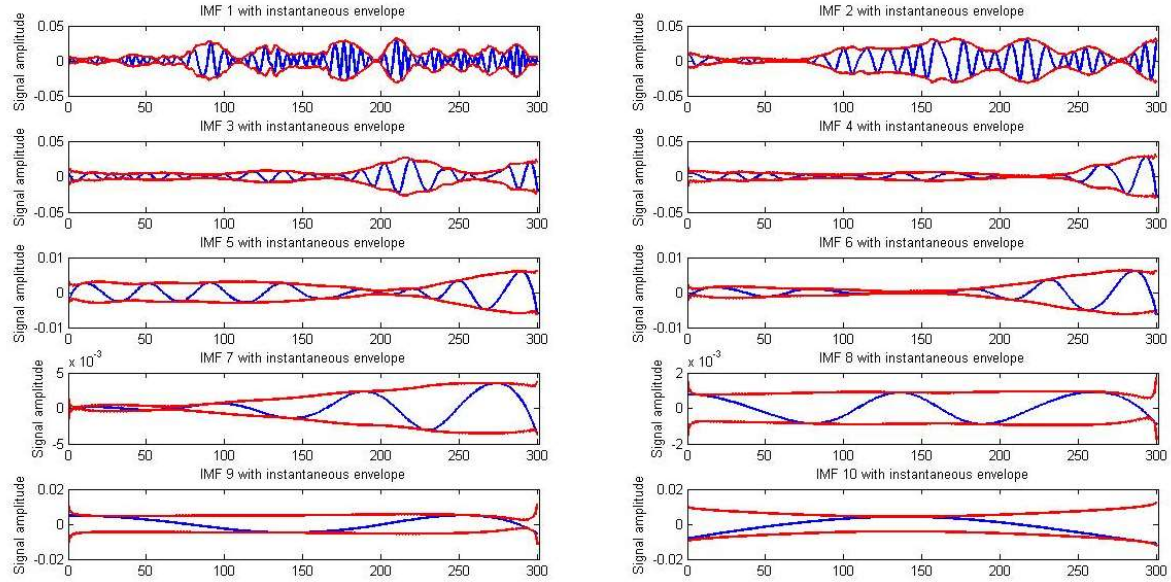


Figure 60. Hilbert transform of IMFs for Channel 3 during supination movement in transient segment.

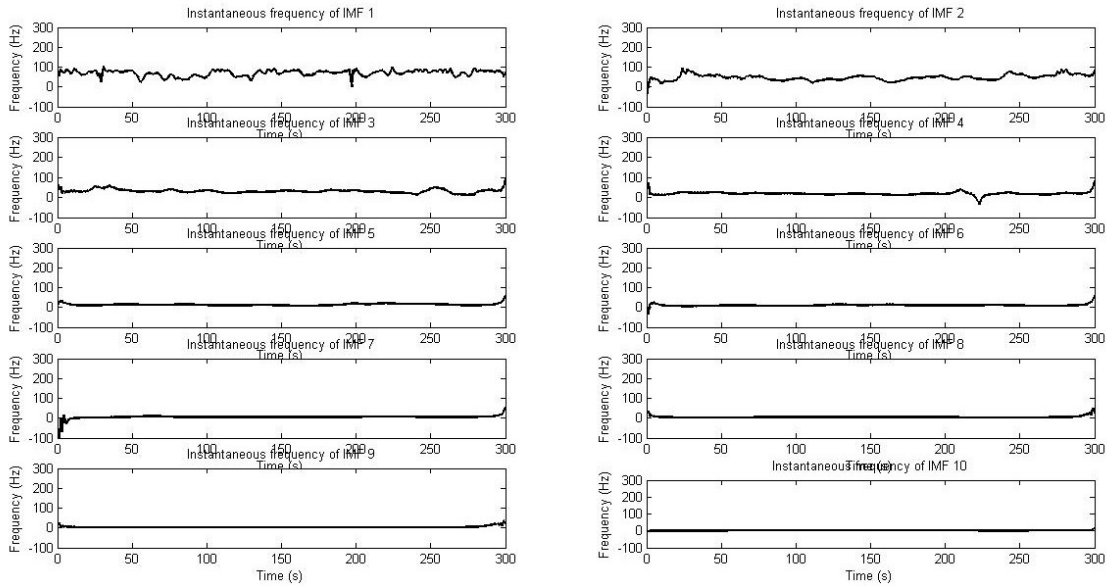


Figure 61. Instantaneous frequencies for Channel 3 during supination movement in transient segment.

For IMFs extracted from Channel 4,

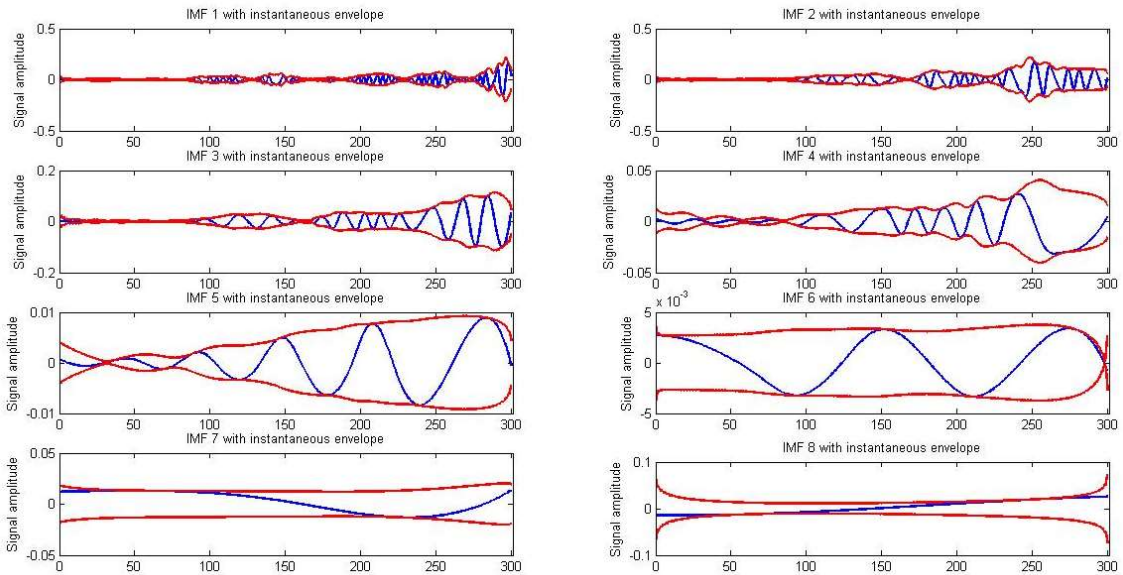


Figure 62. Hilbert transform of IMFs for Channel 3 during supination movement in transient segment.

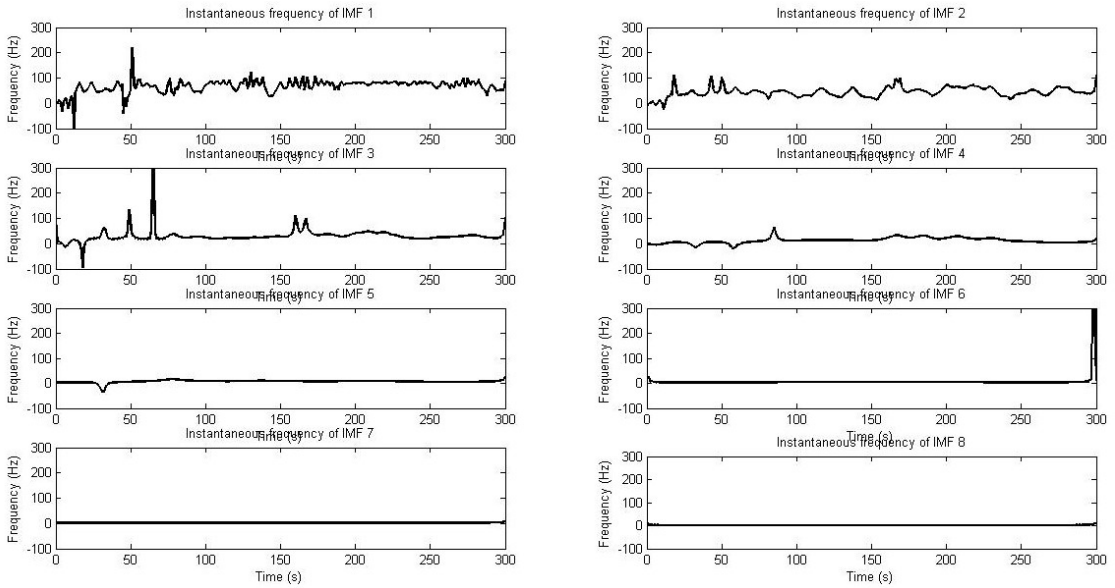


Figure 63. Instantaneous frequencies for Channel 4 during supination movement in transient segment.

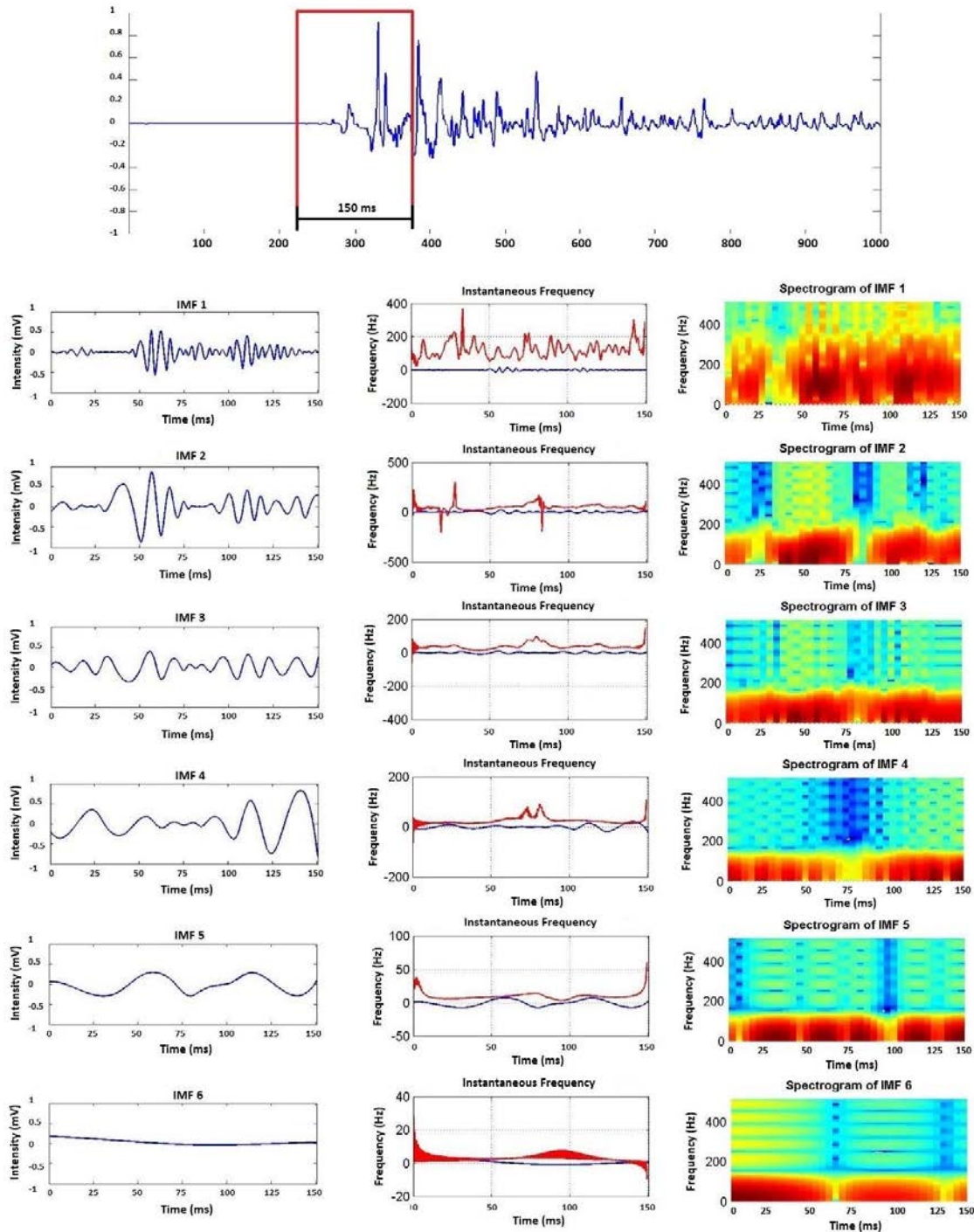


Figure 64. sEMG signal of Extensor Digitorum muscle (Channel 3) for All fingers extension (5th Movement). Upper figure shows 2 seconds of record with a 300 ms window between 450 ms -750 ms section. 3-Column section shows in the first column the IMFs, from 1st to 6th; second column shows the Instantaneous Frequencies (IFs) of the previous IMF; third column shows the spectrogram of the previous IF.

4.4 RECONSTRUCTION

The Intrinsic Mode Functions represent something inside the original signal, *a priori* is impossible to determine in the major cases, but sometimes is easy to do it, especially if the IMFs shown some known shapes like those reported by Luca et al. 2006. To reconstruct most of the original sEMG signal is able with the 1st and 2nd IMFs. To get the MUAP shape is possible with the 2nd and 3rd IMF, average.

From Empirical Mode Decomposition, the IMFs resulted, i.e. CBA4_153_3, showed in Figure 65, were used to reconstruct the original signal.

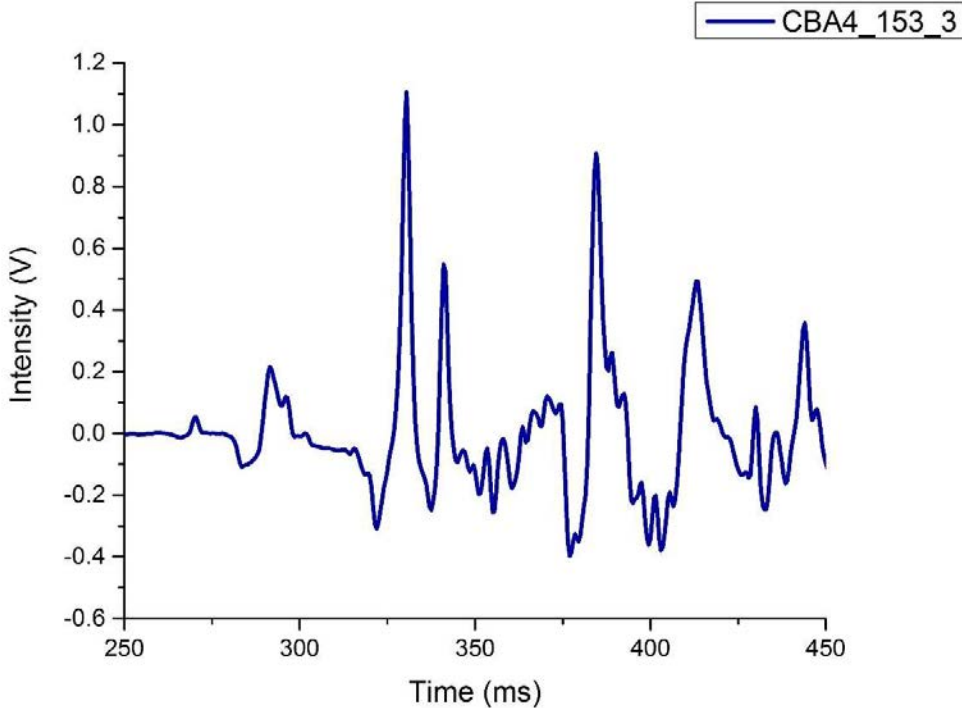


Figure 65. Original signal from the record CBA_153_3 windowed between 250 ms and 450 ms.

Each IMF was sum in combination with the others to reconstruct signals until to get the original signal and the MUAP shape. The equation for this is:

$$x(t) = \sum_{i=1}^n c_i + r_n = \sum_{i=1}^6 c_i \quad \text{Eq. 70}$$

For signal CBA4_153_3, all the obtained functions, 6 IMFs, were used to reconstruct a signal, shown in Figure 66, as follows:

$$x(t) = \sum_{i=1}^6 c_i \quad \text{Eq. 71}$$

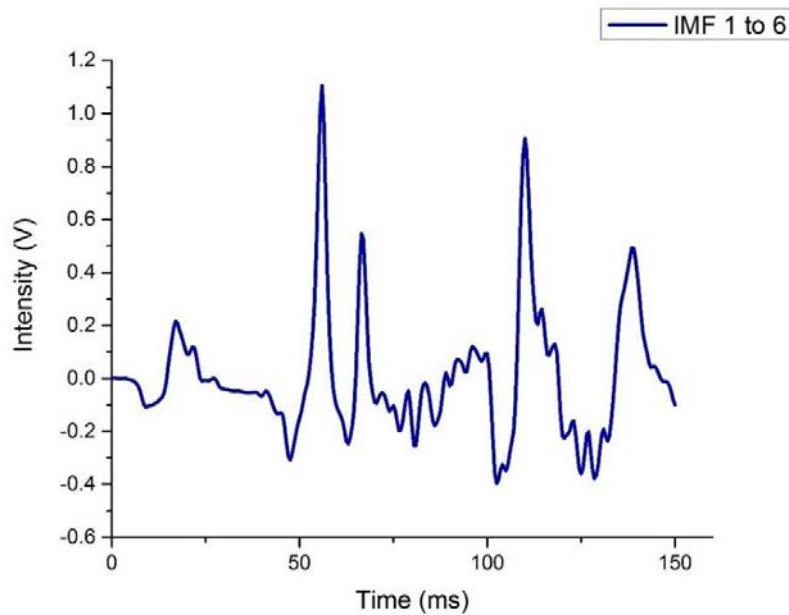


Figure 66. Signal reconstruction using IMFs 1 to 6.

Similarly, for IMFs from 1 to 5, was obtained:

$$x(t) = \sum_{i=1}^5 c_i \quad \text{Eq. 72}$$

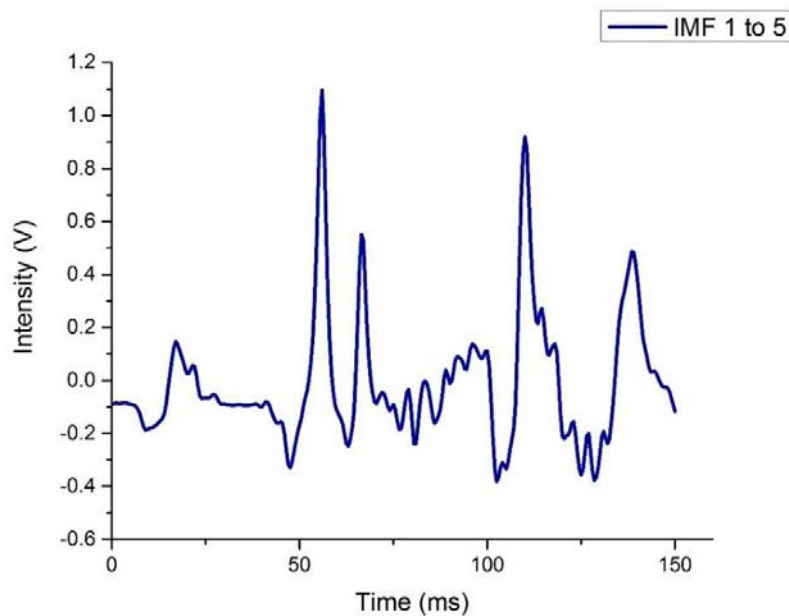


Figure 67. Signal reconstruction using IMFs 1 to 5.

Using IMF 1 to IMF 4, the resulting signal is shown in Figure 68:

$$x(t) = \sum_{i=1}^4 c_i \quad \text{Eq. 73}$$

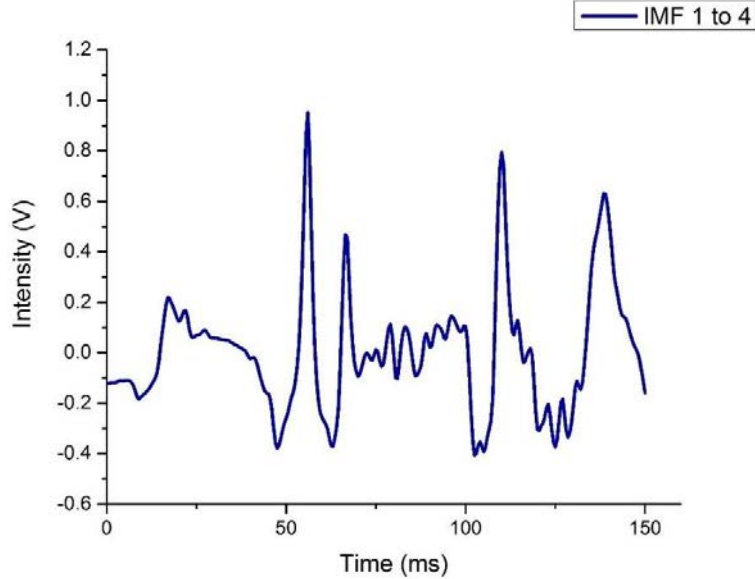


Figure 68. Signal reconstruction using IMFs 1 to 4.

For IMF 1 to IMF 3, result is shown in Figure 69:

$$x(t) = \sum_{i=1}^3 c_i \quad \text{Eq. 74}$$

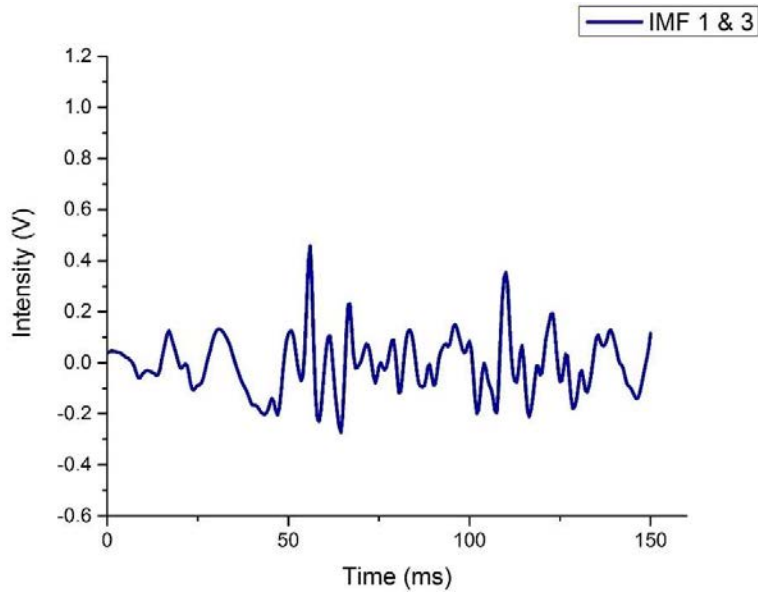


Figure 69. Signal reconstruction using IMFs 1 to 3.

IMFs signal reconstruction shows that the decomposition is almost well done, using IMFs 1 to 6, 1 to 5 and 1 to 4, and all the Intrinsic Mode Functions are part of the original signal.

There is a decrement in the intensity of the reconstructed signals, in order of the decrement of the components of these.

Using the IMF 2 and IMF 3, is possible to construct specific shapes, these forms are shown in Figure 70 and in Figure 71, respectively.

$$x(t) = c_2 \quad \text{Eq. 75}$$

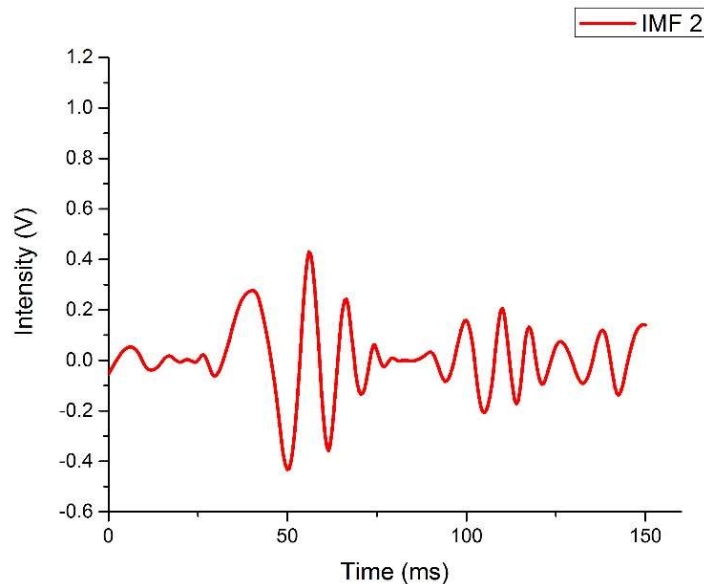


Figure 70. IMF 2 from signal CBA4_153 channel 3 between 275ms to 425 ms.

For signal with IMF 2 & 3, equation is:

$$x(t) = c_2 + c_3 \quad \text{Eq. 76}$$

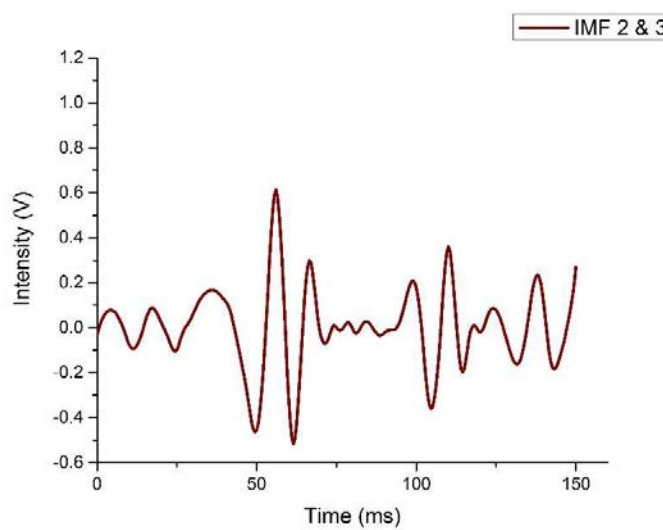


Figure 71. Signal reconstruction using IMFs 2 and 3.

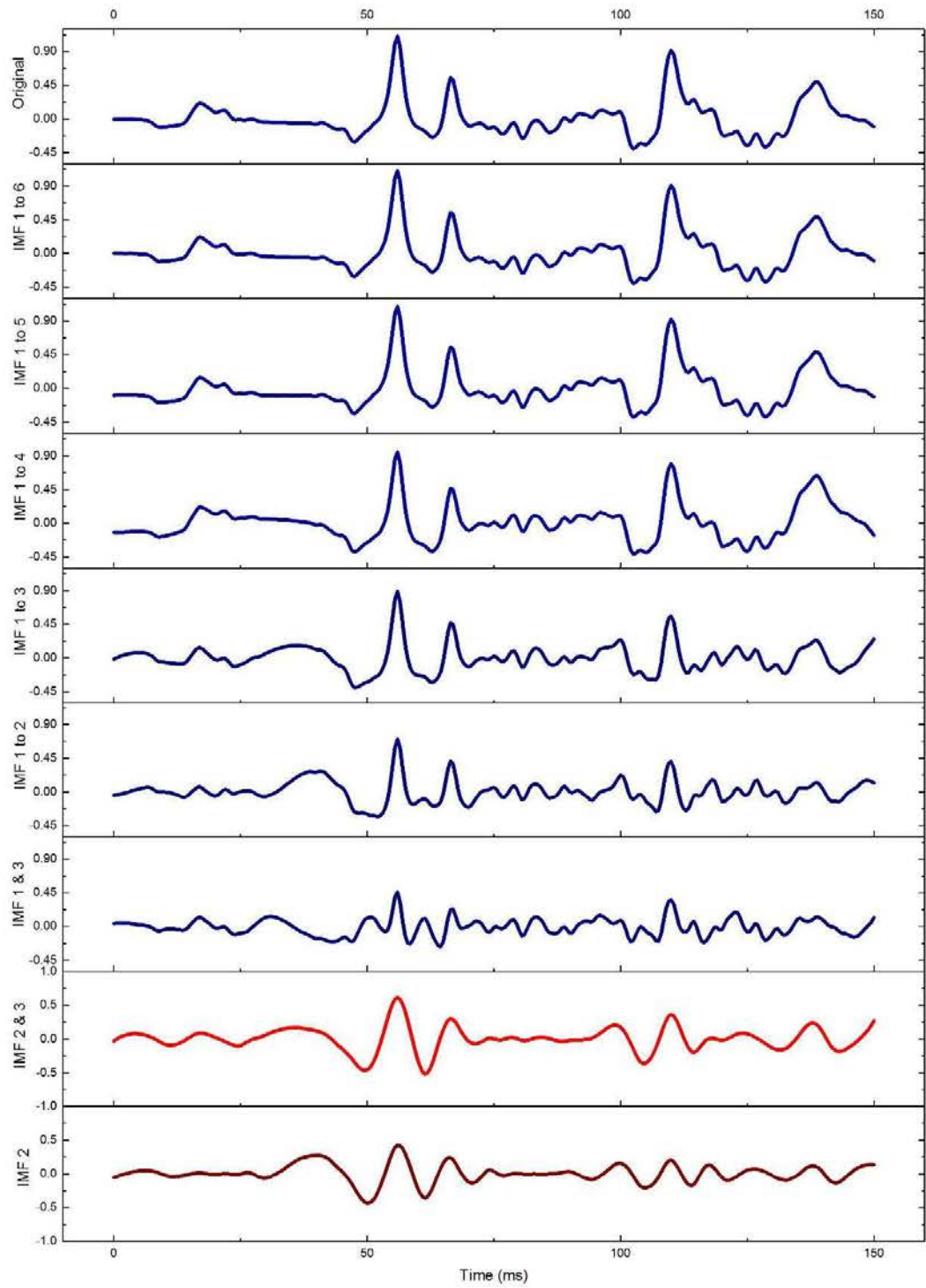


Figure 72. Original signal vs reconstruction in different levels, from up to down: 1. Original signal, reconstruction 2. using IMFs 1 to 6, 3. IMFs 1 to 5, 4. IMFs 1 to 4, 5. IMFs 1 to 3, 6. IMFs 1 and 3, 7. IMFs 2 and 3, and IMF 2. The sequence shows a decrement in intensity directly dependent of the number of IMFs. IMF 2 is the most defined shape into all signals, the IMF 3 represents only a small significance in addition with IMF 2.

4.5 CURVE FITTING

Every time that a data is obtained, you can plot it into 2D or 3D graph, also you can compute many parameters of that result, but sometimes, these results are not useful by their selves, because the data that they represent is a curve that you ignore completely, it means that you don't know what is the equation for that.

It is useful to have an equation that describes the phenomena, then a mathematical model is established. To approximate the obtained curves in the decomposition process Fourier coefficients were used.

The curve, i.e. IMF 2 from signal CBA4_153, there are two MUAPs. The Fourier approximation of these curves are a sum of sines described with the following equation:

$$x(t) = \sum_{i=1}^k a_i \sin(b_i t + c_i) \quad \text{Eq. 77}$$

Using Matlab reconstruction tools, the terms for every founded pattern were approximated. For CBA4_153, the IMF 2 in the interval between 45 ms to 75 ms, a sum of sines between 1 term and 8 terms were computed to find the b_i terms. Also, a_i weights were obtained for each sine term. In the other hand, c_i phase was not considered¹⁰.

Using 8 sine components, we obtained:

Table 4. Frequencies and Intensities relatives to IMF 2 reconstruction using 8 sinusoidal terms.

Sine Component	Angular Frequency $b_i [\text{rad/s}]$	Intensity a_i	Frequency $f_i [\text{Hz}]$
1	599.1	0.09192	95.34
2	415.4	0.07531	66.11
3	472.4	0.07148	75.18
4	745.7	0.04358	118.68
5	309.9	0.04675	49.32
6	534.6	0.08743	85.08
7	367.6	0.05595	58.5
8	693.3	0.05878	110.34

Using 6 sine components:

Table 5. Frequencies and Intensities relatives to IMF 2 reconstruction using 6 sinusoidal terms

Sine Component	Angular Frequency $b_i [\text{rad/s}]$	Intensity a_i	Frequency $f_i [\text{Hz}]$
1	603.4	0.1013	96.03
2	422.6	0.065	67.25
3	479.5	0.05196	76.31
4	697.6	0.055	111.02
5	320.2	0.034	50.96
6	539.6	0.0803	85.88

¹⁰ In future work it is possible to consider this phase changing or phase shifting.

Using 3 terms:

Table 6. Frequencies and Intensities relatives to IMF 2 reconstruction using 3 sinusoidal terms

Sine Component	Angular Frequency $b_i \text{ [rad/s]}$	Intensity a_i	Frequency $f \text{ [Hz]}$
1	530.3	4.398	84.35
2	535.1	4.525	85.16
3	800	0.079	127.32

Using 2 terms:

Table 7. Frequencies and Intensities relatives to IMF 2 reconstruction using 2 sinusoidal terms.

Sine Component	Angular Frequency $b_i \text{ [rad/s]}$	Intensity a_i	Frequency $f_i \text{ [Hz]}$
1	496.2	0.1694	78.97
2	649.7	0.2765	103.4

Using 1 term:

Table 8. Frequencies and Intensities relatives to IMF 2 reconstruction using 1 sinusoidal term.

Sine Component	Angular Frequency $b_i \text{ [rad/s]}$	Intensity a_i	Frequency $f_i \text{ [Hz]}$
1	610.1 (593-627)	0.3447	97 (94.37-99.82)

In Table 4 and Table 5 there are frequencies in the range of 50 Hz y 119 Hz, some of them are apparently harmonic frequencies, i.e. 58.5 Hz and its harmonic 110.34 Hz, also 66.11 Hz & 118.68 Hz.

The frequency pattern is described as a sum of sinusoidal components of the Fourier series. The pattern is described as follows:

$$x(t) = \sum_{i=1}^3 a_i \sin(b_i t) = \sum_{i=1}^k a_i \sin(2\pi f_i t) \quad \text{Eq. 78}$$

where $i = 3$

$$\begin{aligned} f_1 &= 83.3 \text{ Hz} & a_1 &= 0.8 \\ f_2 &= 96.7 \text{ Hz} & a_2 &= 0.9 \\ f_3 &= 113.3 \text{ Hz} & a_3 &= 0.4 \end{aligned}$$

Then, the frequency pattern for all studied subjects for this work is expressed as:

$$\begin{aligned} x_{pattern}(t) &= a_1 * \sin(2\pi f_1 t) + a_2 * \sin(2\pi f_2 t) + a_3 * \sin(2\pi f_3 t) \\ &= 0.8 * \sin(523.389t) + 0.9 * \sin(607.584t) + 0.4 * \sin(711.885t) \end{aligned} \quad \text{Eq. 79}$$

Figure 73 shows the plot of the $x_{pattern}$ signal in a time slot of 512 ms.

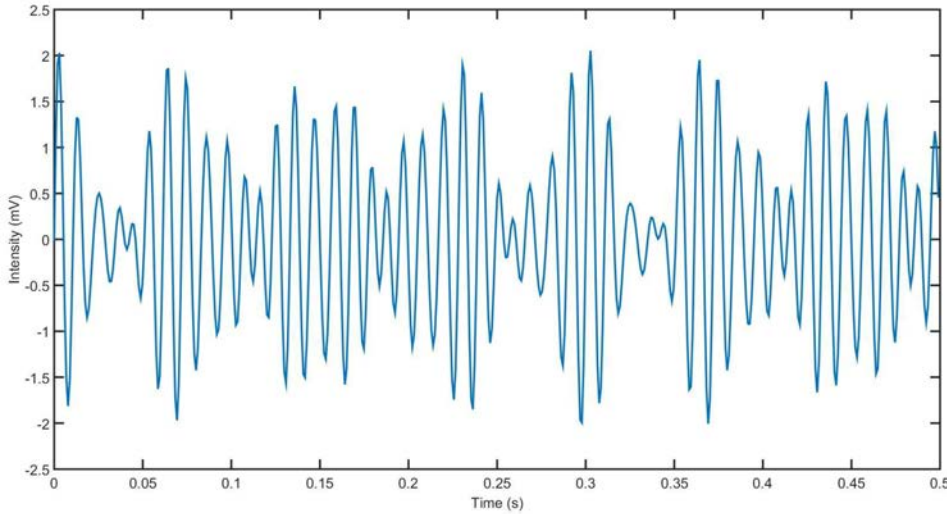


Figure 73. Frequency pattern plot with 83.3 Hz, 96.7 Hz and 113.3 Hz components.

4.6 KALMAN FILTER, ESTIMATION AND PREDICTION

After the acquisition stage of the myoelectric signals, for real-time applications, it is necessary to decode the information present in the sEMG signal. Filtering the signals is the proposed way to do it. Specific filtering algorithms are required to take out the noise and the unwanted information. Also, to decrease the computational costs of the identification process is necessary to involve a prediction state system into these filtering process to take decisions in advance about the muscular activity behavior.

The application of the Kalman filter assisted to approach myoelectric signal reconstruction and prediction. Is possible to obtain an accurate reconstruction of the MUAP shape form present in the raw sEMG acquired. Although the accuracy of reconstruction does not go above 90%, in terms of the coefficient of determination.

4.6.1 State-Space Representation of Nonlinear Model

For the use of Kalman Filter, a model representation in state space form is required. This model consists of a process equation and measurement equation. Generally, for a model (l, m, n) , its state-space model can be written as: process equation and measurement equation.

$$\begin{aligned} \text{Process} \\ \text{equation} \quad x_k &= f(x_{k-1}, u_{k-1}) = Ax_{k-1} + \sum_{i=1}^n B_i(u_{k-1})^i \end{aligned} \quad \text{Eq. 80}$$

$$\begin{aligned} \text{Measurement} \\ \text{equation} \quad y_k &= Cx_k \end{aligned} \quad \text{Eq. 81}$$

In the process equation, u is the model input, $x = [x_1, x_2, \dots, x_q]^T$ is the state vector, $q = \max\{l, m\}$. The $q \times q$ matrix A relates the state at previous time step x_{k-1} , to the state at the current step x_k . The $q \times 1$ matrix B_i relates the model input at the previous time step $(u_{k-1})^i$, $i = 1, 2, \dots, n$, to the state at the current step x_k . They are represented as

$$A = \begin{bmatrix} a_1 & 1 & 0 & \cdots & 0 & 0 \\ a_2 & 0 & 1 & \cdots & 0 & 0 \\ \vdots & \vdots & \vdots & \ddots & \vdots & \vdots \\ a_{q-1} & 0 & 0 & \cdots & 0 & 1 \\ a_q & 0 & 0 & \cdots & 0 & 0 \end{bmatrix}, \quad B_i = \begin{bmatrix} \mu_{1,i} \\ \mu_{2,i} \\ \vdots \\ \mu_{q-1,i} \\ \mu_q \end{bmatrix} \quad \text{Eq. 82}$$

In the system, the matrices A and B_i change with each time step due to the time-varying property of muscle activation.

The y , in measurement equation, is the measurement of the electric intensity of the muscle. The $1 \times q$ matrix C relates the state at the current step x_k , to the measurement at the current step y_k with the following expression:

$$C = [1 \ 0 \ \cdots \ 0 \ 0] \quad \text{Eq. 83}$$

For online estimation and prediction, Kalman Filter is used for the recursive estimation of the model parameters. The Kalman Filter estimates the internal states and parameters of a discrete-time system from a series of noisy measurements. Parameter estimation with Kalman Filter is performed considering the unknown parameters. That is, the meta-state vector w has the expression

$$w = [x^T \ g^T]^T. \quad \text{Eq. 84}$$

The parameters in g are assumed time-invariant comparing to the process, that is:

$$g_k = g_{k-1} \quad \text{Eq. 85}$$

The augmented system is then:

$$w_k = F(w_{k-1}, u_{k-1}) = \begin{bmatrix} f(x_{k-1}, u_{k-1}) \\ g_k \end{bmatrix} \quad \text{Eq. 86}$$

$$y_k = Hw_k = [C \ 0_{1 \times (l+m*n)}]w_k \quad \text{Eq. 87}$$

The recursive estimation of the state-space model using Kalman Filter consists in two stages: prediction and correction. The main equations are given by:

$$\begin{aligned} \widehat{w}_k^- &= F(\widehat{w}_{k-1}, u_{k-1}) \\ P_k^- &= D_k P_{k-1} D_k^T + Q_{k-1} \end{aligned} \quad \text{Eq. 88}$$

$$\begin{aligned} K_k &= P_k^- H_k^T (H_k P_k^- H_k^T + R_k)^{-1} \\ \widehat{w}_k &= \widehat{w}_k^- + K_k (y_k - H \widehat{w}_k^-) \\ P_k &= (I - K_k H_k) P_k^- \end{aligned} \quad \text{Eq. 89}$$

Equations of the prediction stage project the state and error covariance estimate forward from time step $k - 1$ to step k . \hat{w}_{k-1} and P_{k-1}^- are initial estimates for the state and measurement variance, respectively. R_k is the measurement noise covariance, while Q_k is the process of noise covariance. D_k is the Jacobian matrix of the plant transfer functions with respect to the involved variables at step k , with each element $D_{[i,j]}$ computed.

In correction stage, the equations adjust the projected estimates by an actual measurement at step k . K_k is the Kalman gain.

In Figure 74 is shown how the sEMG signal could be estimated using the Kalman filter to adjust the shape of the MUAP shape to the mathematical model of the pattern, $x_{pattern}$, this allows to create a predictable trajectory of the input signal. The output result from the Kalman filter will go directly to the Goertzel algorithm.

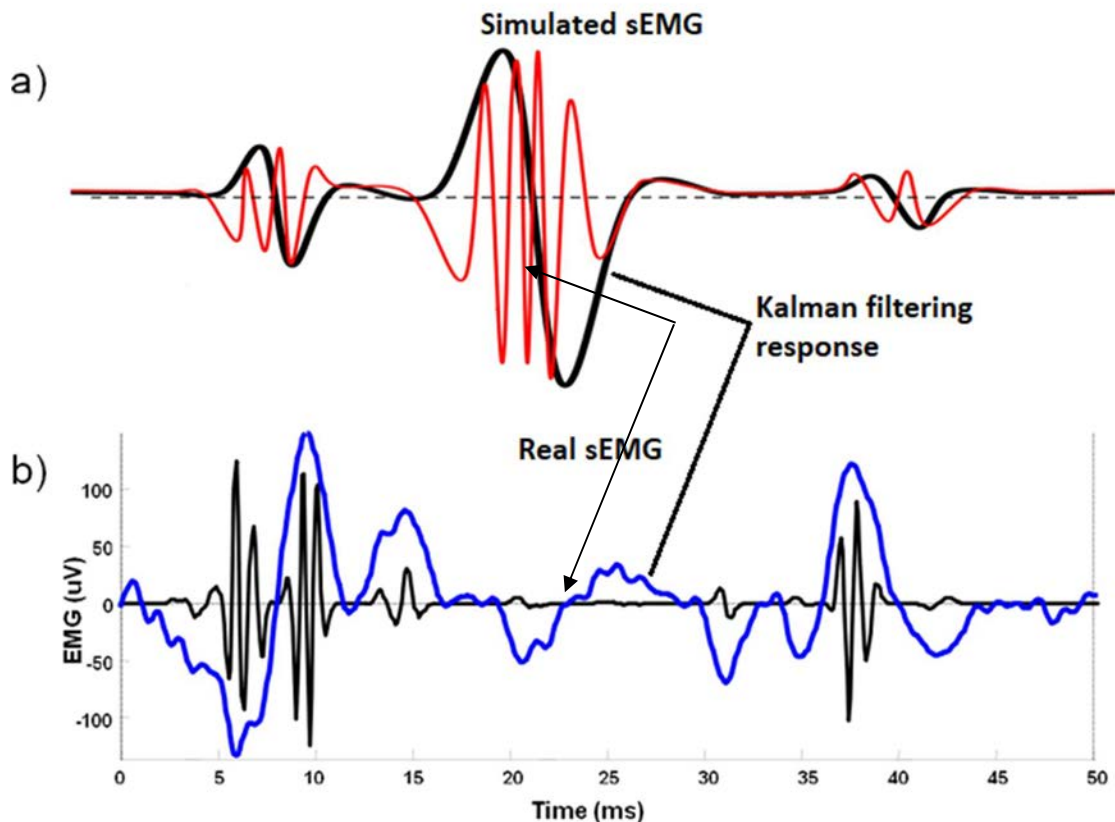


Figure 74. Kalman filter responses in simulated and real sEMG signals. a) Simulated sEMG signal (red line) is fitted with the math sEMG model established in the filtering parameters. **b)** Real sEMG signal (black line) is fitted with the math sEMG model settled in the parameters.

4.7 GOERTZEL FILTER, FREQUENCY DETECTION

If the specific frequencies of the pattern signal are known, then Goertzel filter can recognize these frequencies instantly. Alike, a quick identification of the myoelectric instruction is possible to detect for a specific and desired movement.

Goertzel filters uses the known frequency values of the pattern signal to identify inside of a time window the frequencies present on an input signal. If known frequencies matched with one or more of these, then filter responds. Using f_1, f_2 y f_3 , of $x_{pattern}$, the Goertzel filter was applied to a $x[n]$ input.

To show the behavior of this filter, $x[n] = x_{pattern}[n]$ in two conditions: with noise (white and power line) and without noise.

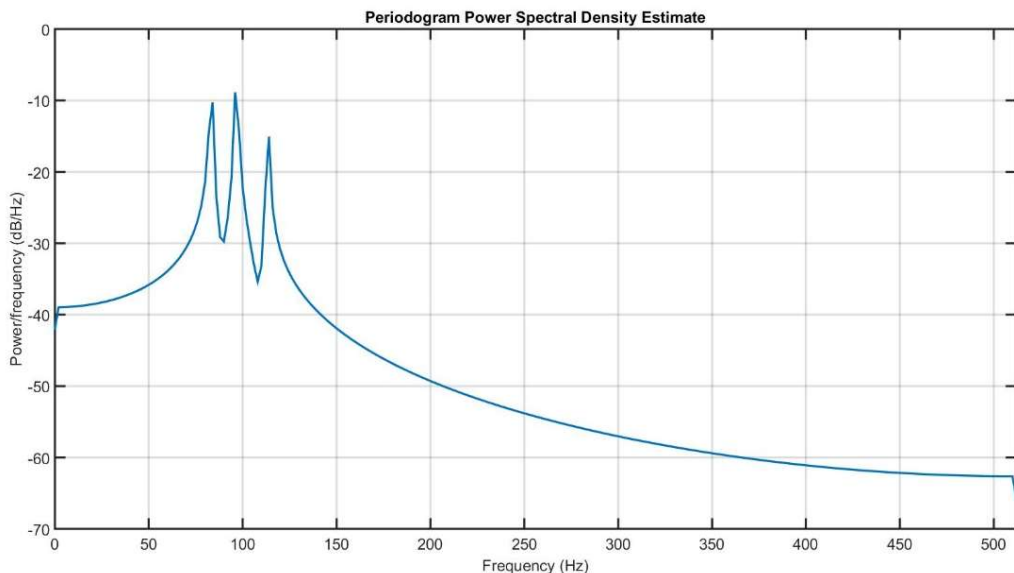


Figure 75. Periodogram of the PSD estimated with FFT for $x_{pattern}$ signal without noise

In Figure 75 is shown the periodogram of the $x_{pattern}[n]$ input signal without noise for the Power Spectral Density (PSD) present into the signal, this periodogram was calculated using the Fast Fourier Transform (FFT). The three frequency components, 83.3 Hz, 96.7 Hz and 113.3 Hz are easily detected.

In Figure 76 is shown the periodogram of the $x_{pattern}[n]$ input signal with white and power line noises for the PSD present into the signal. This periodogram was also calculated with the FFT. Three frequency components are in 83.3 Hz, 96.7 Hz and 113.3 Hz, but also 59 Hz signal referred to power line is present, just with less density. Other signals are resulting of the white noise.

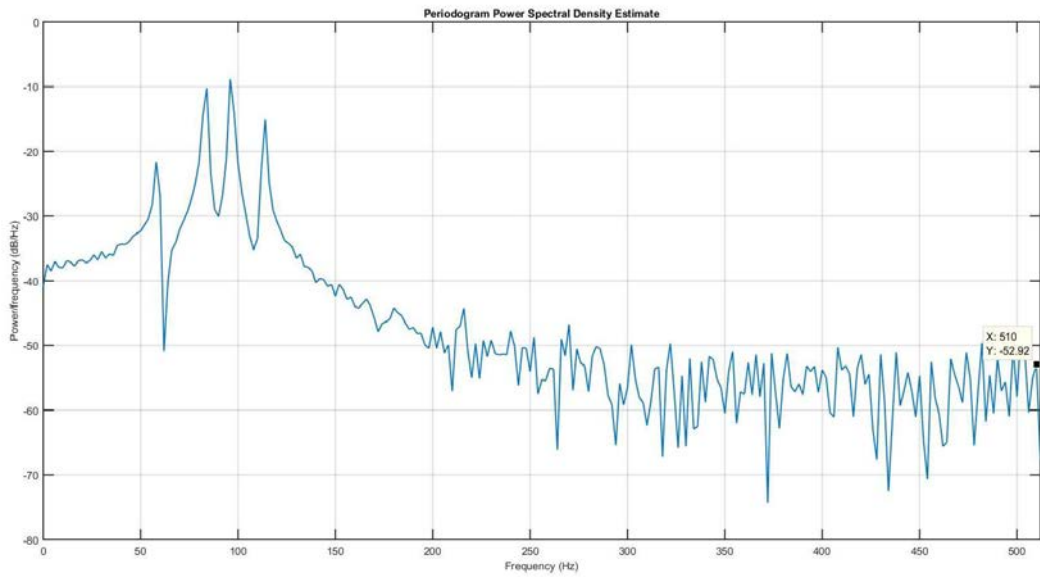


Figure 76. Periodogram of the PSD estimated with FFT for $x_{pattern}$ signal with white noise and power line noise.

If the $x_{pattern}$ signal is filtered with the Goertzel filter, then the PSD will be calculated into a determined time window identifying only the settled frequencies: 83.3 Hz, 96.7 Hz and 113.3 Hz.

Figure 77 shows the Discrete Fourier Transform (DFT) of the $x_{pattern}$ signal without any noise. Density of each frequency component is different, related to the weight of the sinusoidal component.

In Figure 78, is shown the DFT of the $x_{pattern}$ signal with white and power line noises. Density of each frequency component is different, associated to the weight of the sinusoidal component. Also, the 59 Hz DFT is different than previous, those to the fact that power line component was set in the Goertzel filter to prove the algorithm.

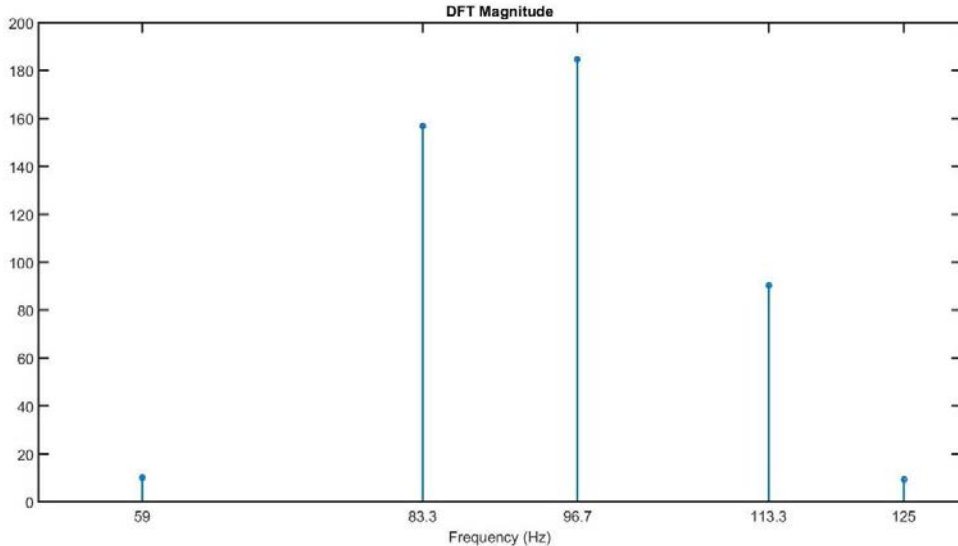


Figure 77. Discrete Fourier Transform of the $x_{pattern}$ signal without noise obtained by Goertzel Algorithm.

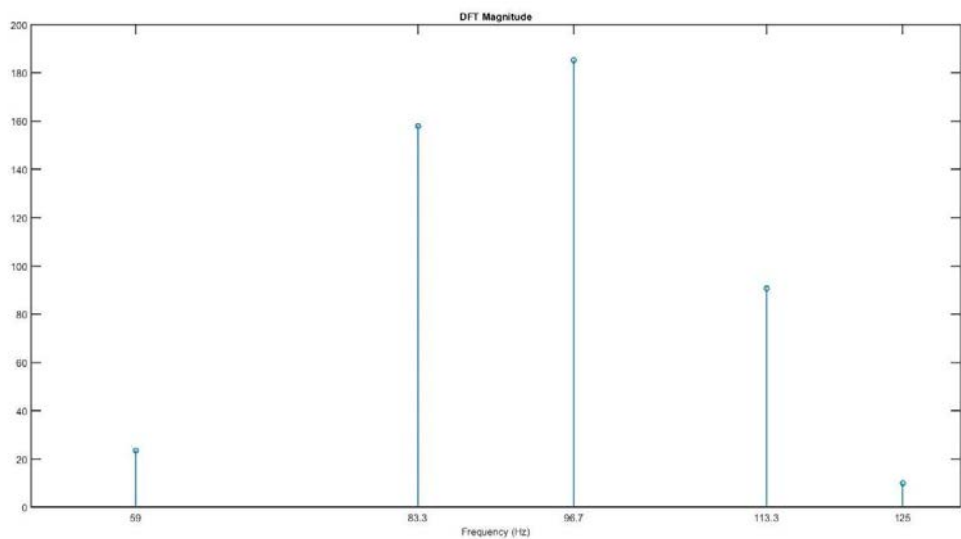


Figure 78. Discrete Fourier Transform of the $x_{pattern}$ signal with white and power line noises obtained by Goertzel Algorithm.

4.8 CONTRIBUTIONS

In this work is reported the methods, techniques, algorithms and conditions under which it is possible to perform the identification, prediction and correction of the characteristics and patterns of the myoelectric signals linked to groups of the movements in the fingers of the hand. Until the conclusion of this work, there was no similar contributions to characterize, modeling, prediction or classification of the characteristics and patterns of the myoelectric signals of the forearm muscles related with the movements of the fingers.

A method to reduce time computing in the analysis of the myoelectric signal to use as control source for prosthetic devices is proposed. This method consists in two stages of analysis: stationary and nonstationary. The stationary analysis aims in establish the conditions for acquisitions of the myoelectric signals for groups of four channels systems, or more, throughout simple normalization, likewise the techniques and necessary parameters for the decomposition, identification, modeling and mapping of the characteristics and patters that the signal have in the performing of specific finger movements. The nonstationary analysis, or dynamic analysis, consists in use the characteristics and patterns as basis of comparison models via dynamic filters, that fit the signals and take out the undesired data and apply these to the input of a prosthetic control.

4.8.1 Scientific contributions

The contributions solve and simplify several challenges in myoelectric signal analysis.

Electrode array to reduce noise from acquisition. An electrode array is proposed with an ellipsoidal configuration that reduce electrodes in a multichannel system, reference electrodes mainly, that improves the quality of the signal respect to other arrangements, also reduce artifacts. Likewise, a simple, suitable and sufficient pre-processing method for myoelectric signals analysis required to the application of any analyzing technique to reduce time computing of the basis features and patterns that compound these signals is described. In section 6.1 the details for these processes are described and works robustly, in stationary and dynamic process, for a four-channel system, also for 8, 16 or more channels.

Hilbert-Huang Transform. The Hilbert-Huang transformation was introduced as a technique for the decomposition of signals, the identification of instantaneous frequencies and the calculations of the energy present within a myoelectric signal, in forearm muscles, associated to specific movements of the fingers. This method is not suitable for use in dynamic applications due to the computation time that it requires, only for identification in stationary processes. Compared with Wavelets, this provides an improvement in the identification of the actual waveforms of the signal.

Time and Frequency patterns. The patterns of the myoelectric signals vary according to the type of movement performed, the type of the muscle used and the function that the muscle performs. For muscles of the forearm linked to the finger movements showed two patterns, in time and frequency. A period of MUAP manifestation of 24.5 ms and a period of 30 ms of reversibility of the contraction signal is the time pattern. A group of three frequencies 83.3 Hz, 96.7 Hz and 113.3 Hz compose the MUAP signal for the voluntary contraction and relaxation. The algorithms proposed in sections 6.2 and 6.3 are suitable for any signal and the obtained results will have to be analyzed in detail to establish the patterns of different muscle groups and different movements. It was shown that the forearm muscles associated with finger movement have similar, statistically tested, time and frequency patterns that are useful in dynamic identification.

Dynamic filtering to identify, predict and correct signal in less than 100 ms. Traditional methods developed by many authors reported that they perform real-time processes to analyze myoelectric using complex methods that consume a lot of time of computing, up than 100 ms, i.e. applying traditional techniques or non-specific filters. Identifying the patterns of the myoelectric signal can determine the mathematical models that improves the filtering of the myoelectric signals using effective algorithms that identify, predict or correct the desired and known patterns of the signals. i.e. Kalman filter predicts and corrects the input signal with the mathematical model of the MUAP, this signal is applied to the Goertzel filter to make sure that the prediction is under the specific terms of the desired and known control signal.

4.8.2 Perspectives

The proposed techniques contribute in many ways to the state-of-the-art for identification, modeling, decomposition and prediction of the myoelectric signal analysis for stationary and nonstationary processes.

The criterion that was least considered in the developing of the analyzing algorithms was computation time. It is mandatory to analyze the myoelectric signal in a stationary way to describe their characteristics and patterns, then nonstationary signal analysis could be performed to reduce time computing. Also, one solution way to decrease computation time is to use parallel processors for multichannel arrays, instead of one processor per channel. This proposed method can easily have modified to adapt other muscles, analyzing techniques, algorithms and prosthetic devices, such as commercial.

High level classifiers could be used to increase the patterns classification to the input signals increases to make a robust system of motion control of a prosthetic device.

CONCLUSIONS

The algorithms and methodologies used to detect, process and quantify myoelectric signal features and some patterns were discussed in their advantages and disadvantages. This comparison helped to propose a method for analyze sEMG signals for prosthetic applications, but other biomedical and physiological applications could be considered.

Filtering is essential in signal processing, but mandatory. If the correct and necessary filters are applied to the signals, then time computing, mathematical framework and electronic resources, and others, should decrease drastically.

A method for treating biological signals is described on this work. Several ways to analyze myoelectric signals were applied to reveal the features contained in a raw EMG; those to filter, de-noise, decompose, time-changing, frequency behavior and intensity.

Most of the noise into myoelectric raw signals came from other muscles and surrounding tissues of the studied muscle. Undesired signals sources can be attenuated by using a better electrode configuration, as proposed in section 3.1, however this technique is not enough for the annihilation of the noise problem. Proper techniques and filters can improve myoelectric signal quality. Using the proposed ellipse-array electrodes configuration, section 3.1.1, is possible to obtain a noise reduction in almost 43.5% in the input data compare with traditional differential configurations. These results were compared with previous records made with the same acquisition system for the same users and conditions and placing the reference electrode over the closest bone terminal.

Normalization process is basic for all signal processing techniques, but generalized procedure. Each technique needs to adapt the best algorithms to obtain the desired results. It is an important signal processing step for any applied technique, good pre-treating data is useful to obtain better results.

The wavelet transform is particularly useful for MUAP detection in the presence of additive white noise. In this situation, the noise is located over the entire segment of the signal, independently of the wavelet used. The disadvantage of the wavelet proposal was that the Meyer and Daubechies 44, even others, wavelets are not perfectly matched to the MUAP shape. Accordingly, the obtained results are likely to be a subject to further improvement is a perfect matching is reached.

The Hilbert-Huang transform method can remain more valuable detail of the signal, because it can make prevention of energy leak and the energy is centralized in the spectrum. Likewise, could help us to find intrinsic features of the EMG signals for real-time applications, but slower. To avoid all the traditional calculations, only identifying the main frequencies components and their features that are involved in the hand movements.

In Hilbert-Huang algorithm it is possible to identify more frequency components of the analyzed signal if the normalization sets the maximum value to 1 V and the minimum value to -1 V. To reduce time computing of the Intrinsic Mode Functions it is not necessary to set the values to 1 V and -1 V, but it is recommendable to reduce the samples in a time slot of almost 50 ms. HHT algorithm is adaptive and do not requires special modifications to adapt the new window of samples.

The Empirical Mode Decomposition is very effective for noise reduction in nonstationary data because is a nonlinear method. This process makes no assumptions about the input data as wavelets. Also, this method provides better results for noise attenuation in EMG when compared with different wavelet prototypes as Meyer or Daubechies. This method is very effective in processes to extract symmetric components which overlap in time and frequency. Empirical Mode Decomposition filters cases of power-line noise, white noise and body artifacts. Is not recommendable to apply a decomposition method in real-time applications due to the number of iterations that are needed to calculate each component, maybe in parallel processors it could be work.

sEMG signal could be filtered or denoise just taking away one or more of the IMFs. With just 2 IMFs is possible to detect the MUAPs. 1st, 2nd and 3rd IMFs presented the most characteristic frequency changes for the signals. Computing the Intrinsic Mode Functions takes a lot of time when compared with wavelets. IMF computing is recommended only to decompose signals to obtain inherent characteristics than the wavelets cannot find by their construction. HHT method could help us to find intrinsic features of the EMG signals for real-time analysis. These to avoid all the traditional calculations, only identifying the main frequencies involved the hand movements.

Using Fourier series, a pattern of three frequencies was obtained: 83.3 Hz, 96.7 Hz and 113.3 Hz associated to voluntary muscular activation and deactivation, these are muscular control signals with an average period of 24.5 ms. Also, these signals have an interval of 30 ms one respect to other. A minimum sample window for myoelectric signals is about 30 ms at least. This time slot could be smaller if and only if a prediction system is used.

Frequency and time patterns were identified in almost 86% of the signals, in the other 14% was not possible to find any pattern or characteristic. Main problems in detection were by the low intensity of the signals or that the algorithm couldn't decompose. A 59 Hz frequency, detected in almost 81% of the signals, is certainly commercial power line noise.

For myoelectric signals, nonstationary and nonlinear, it is important to use adaptive algorithms, i.e. using wavelets, the scale and translation is essential to fit the wave form to the shape of the signals, with Hilbert-Huang the result depends of the input signal. AM-FM features, frequencies and firing rates can be reliable in real-time control of a robotic hand, but classification methods are required. If the number of acquisition channels and features increases, the number of control commands increases too. There are many and different significant types of information into myoelectric signals that could be used as input to classifiers. For increase the classification accuracy, a combinations of processing methods and techniques are strongly recommended.

Proposed prediction method is suitable for real-time applications using only the EMG signals as input. The dynamical nature of the Kalman filter provides for the time varying optimal fusion of the information and allows to consider myoelectric activity, muscular intensity features and statistical of the finger movements. Using Kalman filter is also possible to reduce the noise and provide a quick reconstruction of the desired shape form of the patterns reported. Goertzel filter provides a simple identification method of the pattern frequencies in a time of almost 5 ms or above, just to locate the desired frequencies. The time pattern establishes a period of 24.5 ms for activation signal, a period of 30 ms for reversibility and 24.5 ms of period for deactivation signal. This time slot suggest that the minimum time windowing is 30 ms to apply any of the analyzing method used for this work. With a window of 30 ms, almost 15 ms to performs prediction (Kalman filtering) and 5 ms to perform Goertzel filtering; then time consumption for the identification, detection, prediction and correction of the myoelectric signal could be performed in under 100 ms.

PUBLICATIONS AND STAGES

INTERNATIONAL JOURNAL JCR

Identificación de Patrones en Tiempo y Frecuencia de Señales sEMG Usando la Transformada de Hilbert-Huang (Time and Frequency Patterns Identification of sEMG Signals Using Hilbert-Huang Transform) Alvaro Altamirano, Arturo Vera, Roberto Muñoz, Lorenzo Leija, Didier Wolf. **Revista IEEE América Latina.** Publication Date: Oct. 2017 Volume: 15, Issue: 10, ISSN: 1548-0992. ACCEPTED AND PUBLISHED.

Superficial myoelectric patterns of independent finger movements to control prosthetic devices. A. Altamirano-Altamirano, C. V. Cervantes-Martínez, L. Leija, A. Vera, and D. Wolf. Prosthetics and Orthotics International (ISPO) Journal. UNDER REVIEW.

INTERNATIONAL CONFERENCES

Altamirano-Altamirano, A.; G. A. Valentino Orozco; A. Vera-Hernández; L. Leija-Salas. **Hand Prosthesis with 5 DOF using Embedded Systems.** PAHCE 2013, Medellín, Colombia. pp. 627-632. ACCEPTED AND PUBLISHED.

Altamirano-Altamirano, A.; A. Vera-Hernández; R. Muñoz-Guerrero; L. Leija-Salas; D. Wolf. **Fixing EMG multichannel signals to perform EMD method.** 7th International Conference on Biomedical Electronics and Devices, BIODEVICES 2014. Eseo, Angers, Loire Valley, France. ACCEPTED.

A. Ruvalcaba, A. Altamirano, C. Toledo, R. Muñoz, A. Vera and L. Leija, "**Multichannel EMG acquisition system for arm and forearm signal detection,**" 2014 IEEE International Instrumentation and Measurement Technology Conference (I2MTC) Proceedings, Montevideo, 2014, pp. 1075-1078. doi: 10.1109/I2MTC.2014.6860907

A. Altamirano-Altamirano, A. Vera-Hernández, L. Leija-Salas and D. Wolf, "**Feedback system based on current measurements to improve a hand prosthesis,**" 2014 Pan American Health Care Exchanges (PAHCE), Brasilia, 2014, pp. 1-4.

doi: 10.1109/PAHCE.2014.6849616

A. Ruvalcaba, A. Altamirano, C. Toledo, R. Muñoz, A. Vera and L. Leija, "**Design and Measurement of the Standards of a Miniaturized sEMG Acquisition System with Dry Electrodes Integrated,**" 2015 International Conference on Mechatronics, Electronics and Automotive Engineering (ICMEAE), Prague, 2015, pp. 99-104.

A. Altamirano-Altamirano, A. Vera, L. Leija and D. Wolf, "**Myoelectric signal analysis using Hilbert-Huang Transform to identify muscle activation features,**" 2016 13th International Conference on Electrical Engineering, Computing Science and Automatic Control (CCE), Mexico City, 2016, pp. 1-4. doi: 10.1109/ICEEE.2016.7751246

STAGES

3 stages at Centre de Recherche en Automatique de Nancy, Université de Lorraine CRAN CNRS UMR 7039, Vandoeuvre-les-Nancy, Nancy, France.

April 13th to July 13th, 2013; **May 1st to June 30, 2014;** June 21th, 2015 to January 12th, 2016.

REFERENCES

- Adam, A. & De Luca, C., 2003. Recruitment order of motor units in human vastus lateralis muscle is maintained during fatiguing contractions.. *Journal of Neurophysiology*, Issue 90, pp. 2919-2927.
- Adam, A., De Luca, C. & Erim, Z., 1998. Hand dominance and motor unit firing behavior. *Journal of Neurophysiology*, Issue 80, pp. 1373-1382.
- Altamirano-Altamirano, A., Valentino-Orozco, G. A., Vera, A. & Leija, L., 2013. *Hand Prosthesis with 5 DOF using Embedded Systems*. Medellín, Colombia, IEEE, pp. 627-632.
- Altamirano-Altamirano, A. y otros, 2014. *Multichannel sEMG Signal Analysis Using Hilbert-Huang Transform to Identify Time-Frequency Features*. Chicago, IL, IEEE.
- Amsuss, S. y otros, 2014. Self-correcting pattern recognition system of surface EMG signals for upper limb prosthesis control. *IEEE Transactions on Biomedical Engineering*, 61(4), pp. 1167-1176.
- Basmajian, J. & De Luca, C., 1985. *Muscles Alive - The Functions Revealed by Electromyography*. Baltimore: The Williams & Wilkins Company.
- Beck, T. W. et al., 2005. Comparision of Fourier and Wavelet transform procedures for examining mechanomyographic and electromyographic frequency versus isokinetic torque relationships. *Electromyography and Clinical Neurophysiology*, 2(45), pp. 93-103.
- Boostani, R. & Moradi, M. H., 2003. Evaluation of the forearm EMG signal features for the control of a prosthetic hand. *Physiological Measurement*, 24(2), p. 309.
- Burrus, C. S., Gopinath, R. A. & Guo, H., 1998. *Introduction to Wavelets and Wavelet Transforms*. New Jersey: Prentice Hall, Inc..
- Castellini, C. & van der Smagt, P., 2009. Surface EMG in advanced hand prosthetics. *Biological Cybernetics*, Issue 100, pp. 35-47.
- Chi, C. K. & Chen, G., 2009. *Kalman Filtering with Real-Time Applications*. s.l.:Springer Berlin Heilderberg.
- Chowdhury, R. H. y otros, 2013. Surface Electromyography Signal Processing and Classification Techniques. *Sensors*, 13(9), pp. 12431-12466.
- Chu, J.-U., Moon, I. & Mun, M.-S., 2005. *A Real-Time EMG Pattern Recognition System Based on Linear-Nonlinear Feature Projection for a Multifunction Myoelectric Hand*. Chicago, IL, USA, Proceedings of the 2005 IEEE 9th International Conference on Rehabilitation Robotics.
- Chung, W. & Dong-ling, P., 2004. The Hilbert-Huang Transform and Its Application on Signal De-noising. *China Journal of Scientific Instrument*, 25(4), pp. 42-45.
- Daubechies, I., 1991. *Ten lectures on wavelets..* Philadelphia, PA.: CBMS-NSF series in applied mathematics..
- De Luca, C. J. et al., 2006. Decomposition of Surface EMG Signals. *Journal of Neurophysiology*, 96(3), pp. 1646-1657.
- Engelberg, S., 2008. *Digital Signal Processing*. s.l.:Springer London.
- Englehart, K., Hudgins, B. & Parker, P., 2001. Multifunction control of prostheses using the myoelectric signal. *Intelligent Systems and Technologies in Rehabilitation Engineering*.
- Fang, J., Agarwal, G. & Shanani, B. T., 1997. *Decomposition of EMG signal by wavelet spectrum matching*. s.l., s.n., pp. 1253-1256.

- Flanders, M., 2002. Choosing a wavelet for single-trial EMG. *Journal of Neuroscience Methods*, pp. 165-177.
- Fougner, A. y otros, 2011. Resolving the limb position effect in myoelectric pattern recognition. *IEEE Transactions on Neural Systems and Rehabilitation Engineering*, 19(6), pp. 644-651.
- Gao, R. X. & Yan, R., 2011. *Wavelets: Theory and Applications for Manufacturing*. s.l.:Springer US.
- García-Moreira, C., 1991. Análisis de Señales Electromiográficas. *Revista Mexicana de Ingeniería Biomédica*, 12(1), pp. 101-112.
- Geng, Y., Zhou, P. & Li, G., 2012. Toward attenuating the impact of arm positions on electromyography pattern-recognition based motion classification in transradial amputees. *Journal of Neuroengineering and Rehabilitation*, 9(1), p. 74.
- Guglielminotti, P. & Meletti, R., 1992. Effect of electrode localization on surface myoelectric signal variables: a simulation study. *9th International Congress of ISEK*.
- Hargrove, L., Englehart, K. & Hudgins, B., 2008. A training strategy to reduce classification degradation due to electrode displacements in pattern recognition based myoelectric control. *Biomedical Signal Processing and Control*, 3(2), pp. 175-180.
- Hochberg, Y., 1988. A Sharper Bonferroni Procedure for Multiple Test of Significance. *Biometrika*, 75(4), pp. 800-802.
- Hoffman, A. & Herr, H., 2002. *Predicting Human Biomechanics with EMG*, Boston, Massachusetts, USA.: MIT AI Lab Abstracts.
- Hoozemans, M. J. & van Dieën, J. H., 2005. Prediction of handgrip forces using surface EMG of forearm muscles. *Journal of Electromyography and Kinesiology*, Issue 15, pp. 358-366.
- Hou, Y., Zurada, J. & Karwowski, W., 2004. Prediction of EMG signals of trunk muscles in manual lifting using a neural network model. *Neural Networks, 2004. Proceedings. 2004 IEEE International Joint Conference on*, 25-29 July, Issue 3, pp. 1935-1940.
- Huang, H.-P. & Chen, C.-Y., 1999. *Development of a Myoelectric Discrimination System for a Multi-Degree Prosthetic Hand*. Detroit, Michigan, Proceedings of the IEEE International Conference on Robotics and Automation .
- Huang, N. E., 2005. Introduction to the Hilbert-Huang Transform and Its Related Mathematical Problems. En: N. E. Huang & S. S. P. Shen, edits. *Hilbert-Huang Transform and Its Applications*. Massachusetts, USA: World Scientific Publishing Co. Pte. Ltd., pp. 1-26.
- Huang, N. E., Shen, Z. & Long, S. R., 1999. A new view of nonlinear water waves: The Hilbert Spectrum. *Annu. Rev. Fluid Mech.*, Issue 31, pp. 417-457.
- Huang, N. E. et al., 1998. The empirical mode decomposition and Hilbert spectrum for nonlinear and nonstationary time series analysis. *Proceedings of The Royal Society A: Mathematical, Physical and Engineering Sciences*, 454(1971), pp. 903-995.
- Huang, N. y otros, 1998. The empirical mode decomposition and Hilbert spectrum for nonlinear and non-stationary time series analysis. *Proceedings of the Royal Society of London, A(454)*, pp. 903-995.
- Hudgings, B., Parker, P. & Scott, R., 1993. A New Strategy for Multifunction Myoelectric Control. *IEEE Transactions on Biomedical Engineering*, 40(I), pp. 82-94.
- Hussain, M. & Mamun, M., 2012. Effectiveness of the Wavelet Transform on the Surface EMG to Understand the Muscle Fatigue During Walk. *Measurement Science Review*, 12(1), pp. 28-33.

- Jiang, N., Muceli, S., Graumann, B. & Farina, D., 2013. Effect of arm position on the prediction of kinematics from EMG in amputees. *Medical and Biological Engineering and Computing*, 51(1-2), pp. 143-151.
- Jing-tian, T. et al., 2007. *Hilbert-Huang Transform for ECG De-noising*. Wuhan, China, s.n., pp. 664-667.
- Kushaba, R. N., Takruri, M., Miro, J. V. & Kodagoda, S., 2014. Towards limb position invariant myoelectric pattern recognition using time-dependent spectral features. *Neural Networks*, Issue 55, pp. 42-58.
- León-Ponce, M., 2012. *Clasificación de patrones mioeléctricos para la operación de un dispositivo antropomórfico*. Doctoral Thesis. México, D.F.: CINVESTAV - IPN.
- Lesser, V. R., Nawab, S. H. & Klassner, F. I., 1995. IPUS: an architecture for the integrated processing and understanding of signals. *Artificial Intelligence*, December, 77(1), pp. 129-171.
- Levene, H., 1960. Robust tests for equality of variances. En: *Contributions to Probability and Statistics: Essays in Honor of Harold Hotelling*. s.l.:Stanford University Press, pp. 278-292.
- Loren, F. M. & Wilkins, A. N., 2011. *Functional Electromyography*. Springer New York Dordrecht Heidelberg London: Springer Science+Business Media.
- Maddox, I., 1988. *Elements of Functional Analysis*. Second Edition ed. New York: CUP Archive.
- Mainardi, L. T., Bianchi, A. M. & Cerutti, S., 2000. Digital Biomedical Signal Acquisition and Processing. In: *The Biomedical Engineering HandBook, Second Edition*. Boca Raton, FL, USA.: CRC Press LLC.
- Masuda, T. & De Luca, C., 1991. Recruitment threshold and muscle fiber conduction velocity of single motor units.. *Journal of Electromyography and Kinesiology*, Issue 1, pp. 116-123.
- Meeson, J. R. N., 2005. HHT Sifting and Filtering. In: N. E. Huang & S. S. Shen, eds. *Hilbert-Huang Transform and Its Applications*. Danvers, MA, USA: World Scientific Publishing Co., pp. 75-103.
- Muceli, S., Jiang, N. & Farina, D., 2012. Extracting signals robust to electrode number and shift for online simultaneous and proportional myoelectric control by factorization algorithms. *IEEE Transactions on Neural Systems and Rehabilitation Engineering*, 22(3), pp. 7420-7431.
- Munoz, R. y otros, 1997. *Implantable electrode for chronic recording from skeletal muscle*. Chicago, IL, IEEE, pp. 2445-2447.
- Naït-Ali, A., 2009. *Advanced Biosignal Processing*. Springer-Verlag Berlin Heidelberg: Springer.
- Nawab, S. H., Wotiz, R. P., Hochstein, L. M. & De Luca, C. J., 2002. *Improved decomposition of Intramuscular EMG signals*. Orlando, FL., SCI2002 IEEE, pp. 274-279.
- Pallás-Areny, R. & Webster, J. G., 1999. *Analog Signal Processing*. s.l.:John Wiley & Sons.
- Park, W.-l., Kwon, S., Lee, H.-D. & Kim, J., 2012. Real-time thumb-tip force predictions form noninvasive biosignals and biomechanical models. *International Journal of Precision Engineering and Manufacturing*, September, 13(9), pp. 1679-1688.
- Phinyomark, A., Limsakul, C. & Phukpattaranont, P., 2009. A Comparative Study of Wavelet Denoising for Multifunction Myoelectric Control. *Proceedings of the International Conference on Computer and Automation Engineering (ICCAE '09)*, 8-10 March, pp. 21-25.
- Phinyomark, A., Limsakul, C. & Phukpattaranont, P., 2011. Application of Wavelet Analysis in EMG Feature Extraction for Pattern Classification. *Measurement Science Review*, pp. 45-52.
- Phinyomark, A., Phukpattaranont, P. & Limsakul, C., 2012. Feature reduction and selection for EMG signal classification. *Expert Systems with Applications*, 39(8), pp. 7420-7431.

- Pinzon-Morales, R.-D., Baquero-Duarte, K.-A., Orozco-Gutierrez, A.-A. & Grisales-Palacio, V.-H., 2011. Pattern Recognition of Surface EMG Biological Signals by Means of Hilbert Spectrum and Fuzzy Clustering. In: L. Springer Science+Business Media, ed. *Software Tools and Algorithms for Biological Systems*. New York: Springer New York, pp. 201-209.
- Preston, D. C., 2013. *Electromyography and neuromuscular disorders: clinical-electrophysiological correlations*. Third Edition ed. s.l.:ELSEVIER .
- Rafiee, J., Rafiee, M. A., Prause, N. & Schoen, M. P., 2009. *Biorobotics: Optimized biosignal classification using mother wavelet matrix*. Cambridge, MA, USA, s.n.
- Rafiee, J., Rafiee, M. A., Prause, N. & Schoen, M. P., 2011. Wavelet basis functions in biomedical signal processing. *Expert Systems with Applications*, 38(5), pp. 6190-6201.
- Rafiee, J., Rafiee, M., Yavari, F. & Schoen, M., 2010. Feature extraction of forearm EMG signals for prosthetics. *Experts Systems with Applications*, 38(4), pp. 4058-4067.
- Rato, R., Ortogueira, M. & Batista, A., 2008. On the HHT, its problems, and some solutions. *Mechanical Systems and Signal Processing*, 22(6), pp. 1374-1394.
- Reaz, M., Hussain, M. & Mohd-Yasin, F., 2006. Techniques of EMG signal analysis: detection, processing, classification and applications. *Biological Procedures Online*, Issue 8, pp. 11-35.
- Reaz, M., Hussain, M. S. & Mohd-Yasin, F., 2006. *EMG analysis using wavelet functions to determine muscle contraction*. New Delhi, India, IEEE, pp. 132-134.
- Reddy, D. V. R. K., Kumar, P. R. & Rajesh, V., 2009. sEMG based human machine interface for controlling wheel chair by using ANN. *2009 International Conference on Control, Automation, Communication and Energy Conservation*, pp. 1-6.
- Rettinger, J., Schwarz, S. & Schwarz, W., 2016. *Electrophysiology*. s.l.:Springer Heidelberg Dordrecht London New York.
- Ruvalcaba, A. y otros, 2014. *Multichannel EMG Acquisition System for Arm and Forearm Signal Detection*. Montevideo, UR, IEEE, pp. 1075-1078.
- Ruxton, G. D. & Beauchamp, G., 2008. Time for some a priori thinking about post hoc testing. *Behavioral Ecology*, 19(3), pp. 690-693.
- Sahid, S., 2004. *Higher Order Statistics Techniques Applied to EMG Signal Analysis and Characterization*, PhD Thesis. Limerick, Ireland: University of Limerick.
- Scheme, E., Fougner, A., Stavdahl, C. A. D. C. & Englehart, K., 2010. Examining the adverse effects of limb position on pattern recognition based myoelectric control. *2010 Annual International Conference of the IEEE Engineering in Medicine and Biology Society, EMBC*, pp. 6337-6340.
- Stark, P. D. H.-G., 2005. *Wavelets and Signal Processing*. s.l.:Springer Berlin Heidelberg.
- Subramani, P., Sahu, R. & Verma, S., 2006. Feature selection using Haar wavelet power spectrum. *BMC Bioinformatics*, p. 432.
- Tortora, G. J. & Derrickson, B., 2014. *Principles of Anatomy and Physiology*. 14th Edition ed. s.l.:Wiley.
- Tsolis, G. & Xenos, T. D., 2011. Signal Denoising Using Empirical Mode Decomposition and Higher Order Statistics. *International Journal of Signal Processing, Image Processing and Pattern Recognition*, pp. 91-106.
- Wang, N., Chen, Y. & Zhang, X., 2013. The recognition of multi-finger prehensile postures using LDA. *Biomedical Signal Processing and Control*, Issue 8, pp. 706-712.

Xing, K. y otros, 2014. A real-time ENG pattern recognition method for virtual myoelectric hand control. *Neurocomputing*, Volumen 136, pp. 345-355.

Yamada, R., Ushiba, J., Tomita, Y. & Masako, Y., 2003. *Decomposition of Electromyographic Signal by Principal Component Analysis of Wavelet Coefficient*. Keihanna, Japan, s.n., pp. 118-119.

Yan, J. & Lu, L., 2014. Improved Hilbert-Huang transform based weak signal detection methodology and its application on incipient fault diagnosis and ECG signal analysis. *Signal Processing*, pp. 74-87.

Young, A. J., Hargrove, L. J. & Kuiken, T. A., 2011. The effects of electrode size and orientation on the sensitivity of myoelectric pattern recognition systems to electrode shift. *IEEE Transactions on Biomedical Engineering*, 58(9), pp. 2537-2544.

Zennaro, D. y otros, 2003. A Software Package for the Decomposition of Long-Term Multichannel EMG Signal Using Wavelet Coefficients. *IEEE Transactions on Biomedical Engineering* 2003, 1(50), pp. 58-69.

Zhang, X. & Zhou, P., 2014. Filtering of surface EMG using ensemble empirical mode decomposition. *Medical Engineering and Physics*, 35(4), pp. 537-542.

Zong, C. & Chetouani, M., 2009. *Hilbert-Huang transform based physiological signals analysis for emotion recognition*. Ajman, s.n., pp. 334-339.

APPENDIX: MATLAB CODES OF THE ALGORITHMS

HILBERT-HUANG TRANSFORM

Empirical Mode Decomposition basis

```
%*CENTRO DE INVESTIGACIÓN Y DE ESTUDIOS AVANZADO DEL IPN *
%*INGENIERÍA ELÉCTRICA - SECCIÓN DE BIOELECTRÓNICA *
%*LAREMUS *
%*M. EN C. ALVARO ALTAMIRANO ALTAMIRANO *
%*-----
% Based on the algorithm developed by Rato et al, 2008
% "On the HHT, its problems, and some solutions"
%Mechanical Systems and Signal Processing, vol.22,no.6,pp.1374-1394, %August
2008.
%-----
%
%rParabEmd__L: Emd parabolic decomposition with extrapolated extrema
%
%
%Usage: rParabEmd= rParabEmd__L(x,qResol, qResid, qAlfa);
%      x - input signal - must be a real vector
%      qResol - Resolution (in DBs: 10*log(WSignal/Bias energy))-
%              normally between 40 and 60 dB
%      qResid - Residual energy (in DBs: 10*log(WSignal/WqResidual))-%
%              normally between 40 and 60 dB
%      qAlfa - Gradient step size (normally is set to 1)
%
%
function rParabEmd = rParabEmd__L (x, qResol, qResid, qAlfa)

dbstop if warning
if nargin~=4), error('rParabEmd__L: Use with 4 inputs.'), end
if(nargout>1), error('rParabEmd__L: Use with just one output.'), end
ArgCheck_s(x, qResol, qResid, qAlfa)

% Actual computation -----
kc = x(:); % ket copy of the input signal
Wx= kc'*kc; % Original signal energy
quntN = length(kc); % Signal length
% loop to decompose the input signal into successive IMFs
rParabEmd= []; % Matrix which will contain the successive IMFs, and the
residue
rParabEmdCnt= 0;
qDbResid= 0; %Equal energies at start
quntOscCnt= quntNOsc_s(kc);
while ((qDbResid<qResid) && (quntOscCnt>2) ) % c has some energy and oscilates
    kImf = kc; % at the beginning of the sifting process, kImf is the signal
    rPMOrI= rGetPMaxs_s(kImf); % rPM= [xM(M), yM(M)];
    rPmOrI= rGetPMIns_s(kImf); % rPm= [xm(m), ym(m)];
    rPM= rPMaxExtrapol_s(rPMOrI, rPmOrI, quntN);
    rPm= rPMinExtrapol_s(rPMOrI, rPmOrI, quntN);
    quntLM= length(rPM); quntLm= length(rPm);
    % if (abs(quntLM-quntLm)>2), disp('Debug: Max-Min count
mismatch.'), keyboard,end;
    if (abs(quntLM-quntLm)>2), disp('Debug: Max-Min count mismatch.'),end;
```

```

if(sum(abs(diff(sign(rPM(1:min(quntLM,quntLm),1)-
rPm(1:min(quntLM,quntLm),1))))>0)
%
    disp('Debug: Max-Min sequence mismatch.'),keyboard;
    disp('Debug: Max-Min sequence mismatch.');
end
if(sum(abs(diff(sign(rPm(1:min(quntLM,quntLm),1)-
rPM(1:min(quntLM,quntLm),1))))>0)
%
    disp('Debug: Max-Min reverse sequence mismatch.'),keyboard;
    disp('Debug: Max-Min reverse sequence mismatch.');
end
bTenv= spline(rPM(:,1), rPM(:,2), 1:quntN); % Top envelop:
bTenv[n];
bDenv= spline(rPm(:,1), rPm(:,2), 1:quntN); % Down envelop:
bDenv[n];
bBias= (bTenv+bDenv)/2; % first bias estimate
while true(1) % inner loop to find each IMF
    WImf= kImf'*kImf; %current IMF energy
    WBias= bBias*bBias'; %bias energy
    if WBias*WImf<0 , warning('rParabEmd_L: Ooops, negative energy
detected.'), end
    if WBias> 0, DbqResol= 10*log10(WImf/WBias); else DbqResol= Inf; end
    if (DbqResol>qResol), break, end %Resolution reached
    %Resolution not reached. More work is needed
    kImf = kImf- qAlfa*bBias'; % subtract qAlfa bias from
kImf
rPMOri= rGetPMmaxs_s(kImf); % rPM= [xM(M), yM(M)];
rPmOri= rGetPMmins_s(kImf); % rPm= [xm(m), ym(m)];
rPM= rPMMaxExtrapol_s(rPMOri, rPmOri, quntN);
rPm= rPMinExtrapol_s(rPMOri, rPmOri, quntN);
bTenv= spline(rPM(:,1), rPM(:,2), 1:quntN); % Top envelop:
bTenv[n];
bDenv= spline(rPm(:,1), rPm(:,2), 1:quntN); % Down envelop:
bDenv[n];
bBias= (bTenv+bDenv)/2; % new bias estimate
end % Wend true
%
rParabEmd = [rParabEmd; kImf']; % store the extracted rParabEmd in
the matrix rParabEmd
kc = kc - kImf; % subtract the extracted rParabEmd from the
signal
quntOscCnt= quntNOsc_s(kc);

rParabEmdCnt=rParabEmdCnt+1;
if (kc'*kc)>0
    qDbResid= 10*log10(Wx/(kc'*kc));
else
    qDbResid = Inf
end
%
end % Wend ((DbR... ))
if ((kc'*kc)/Wx)>(10^-12)
    rParabEmd=[rParabEmd; kc'];
    rParabEmdCnt=rParabEmdCnt+1;
    NumOscqResiduais= quntNOsc_s(kc);
end
rParabEmd= rParabEmd';

```

```

end %main function

%SubFunctions -----
function ArgCheck_s(x, qResol, qResid, qAlfa)

[qL, qC] = size(x);
if ((qL*qC) ~= max(qL,qC)), error('rParabEmd_L: Input signal must be a one dim vector.'), end
if ((qL*qC)<= 1), error('rParabEmd_L: Input signal must be a vector.'), end

[qL,qC] = size(qResol);
if (~((qL==1)&(qC==1)) ), error('rParabEmd_L: Input resolution must be a scalar.'), end
if ( qResol<=0 ), error('rParabEmd_L: Input resolution must strictly positive.'), end

[qL,qC] = size(qResid);
if (~((qL==1)&(qC==1)) ), error('rParabEmd_L: Input residual must be a scalar.'), end
if ( qResid<=0 ), error('rParabEmd_L: Input residual must strictly positive.'), end

[qL,qC] = size(qAlfa);
if (~((qL==1)&(qC==1)) ), error('rParabEmd_L: qAlfa step must be a scalar.'), end
if ( qAlfa<=0 ), error('rParabEmd_L: qAlfa step must be strictly positive.'), end

%-----
% Returns the oscilation count, no steps
function quntNOsc = quntNOsc_s (x)
y=0; qisTop= false; qisDown= false;
for i=2:(length(x)-1)
    if( ((x(i-1)) < (x(i))) && ((x(i+1))< (x(i)))) %Max /-\%
        y=y+1;
    end
    if( ((x(i-1)) > (x(i))) && ((x(i+1))> (x(i)))) %min \_/
        y=y+1;
    end
%Top
    if( ((x(i-1)) < (x(i))) && ((x(i+1))== (x(i)))) %StepL /-
        qisTop= true; qisDown= false;
    end
    if( ((x(i-1)) == (x(i))) && ((x(i+1))< (x(i)))) %stepR -/
        if qisTop; y=y+1; end;
        qisTop= false;
    end
%Downs
    if( ((x(i-1)) > (x(i))) && ((x(i+1))== (x(i)))) %stepL \
        qisTop= false; qisDown= true;
    end
    if( ((x(i-1)) == (x(i))) && ((x(i+1))> (x(i)))) %StepR _/
        if qisDown; y=y+1; end
        qisDown=false;

```

```

        end
    end % for i=2:(length(x)-1)
quntNOsc= y;
end % function y = quntNOsc_s (x)
function rPMaxExtrapol= rPMaxExtrapol_s(rPM, rPm, quntL)
rPM= sortrows(rPM); %assumes nothing on rPM sort order
rPm= sortrows(rPm); %assumes nothing on rPm sort order
kTopTim1= rPM(:,1); kTopVal= rPM(:,2);
kDwnTim1= rPm(:,1); kDwnVal= rPm(:,2);
%Start extrapolation -----
if ( (kTopTim1(1)== 1) && (kDwnTim1(1)== 1) )
    disp ('rPMaxExtrapol_s: Poliextrema at signal''s start');
elseif ( (kTopTim1(1)<1) || (kDwnTim1(1)< 1) )
    disp ('rPMaxExtrapol_s: Invalid extrema at signal''s start');
else
    kTopTim1=[2-kDwnTim1(1); kTopTim1]; % New first Top at the (one based)
specular Min
    kTopVal=[kTopVal(1); kTopVal]; % Same Val as old first Top
end
% End extrapolation -----
if ( (kTopTim1(end)== quntL) && (kDwnTim1(end)== quntL) )
    disp ('rPMaxExtrapol_s: Poliextrema at signal''s end');
elseif ( (kTopTim1(end)> quntL) || (kDwnTim1(end)> quntL) )
    disp ('rPMaxExtrapol_s: Invalid extrema at signal''s end');
else
    kTopTim1=[kTopTim1; (2*quntL - kDwnTim1(end))]; % New last Top at the
specular Min
    kTopVal=[ kTopVal; kTopVal(end)]; % Same Val as old last Top
end
% return value -----
rPMaxExtrapol= sortrows([kTopTim1, kTopVal]);
end

function rPMinExtrapol= rPMinExtrapol_s(rPM, rPm, quntL)
%Init -----
rPM= sortrows(rPM); %assumes nothing on rPM sort order
rPm= sortrows(rPm); %assumes nothing on rPm sort order
kTopTim1= rPM(:,1); kTopVal= rPM(:,2);
kDwnTim1= rPm(:,1); kDwnVal= rPm(:,2);
%Start extrapolation -----
if ( (kTopTim1(1)== 1) && (kDwnTim1(1)== 1) )
    disp ('rPMinExtrapol_s: Poliextrema at signal''s start');
elseif ( (kTopTim1(1)<1) || (kDwnTim1(1)< 1) )
    disp ('rPMinExtrapol_s: Invalid extrema at signal''s start');
else
    kDwnTim1=[2-kTopTim1(1); kDwnTim1];% New first Dwn at the (one based)
specular Max
    kDwnVal=[kDwnVal(1); kDwnVal]; % Same Val as old first Dwn
end
% End extrapolation -----
if ( (kTopTim1(end)== quntL) && (kDwnTim1(end)== quntL) )
    disp ('rPMinExtrapol_s: Poliextrema at signal''s end');
elseif ( (kTopTim1(end)> quntL) || (kDwnTim1(end)> quntL) )
    disp ('rPMinExtrapol_s: Invalid extrema at signal''s end');
else
    kDwnTim1=[kDwnTim1; (2*quntL - kTopTim1(end))]; % New last Dwn at the
specular Max

```

```

kDwnVal=[ kDwnVal; kDwnVal(end) ]; % Same Val as old last Dwn
end
% return value -----
rPMinExtrapol= sortrows([kDwnTim1, kDwnVal]);

end
function rPMax= rGetPMaxs_s(aS) %Get Parabolic Maxs, plateaus out
kS= aS(:);
quntLenS=length(kS);
quntMaxCnt=0;
kSMNdx1= []; kSMVal=[]; %signal S Maxima indices and values
kSPMTim1= []; kSPMVal=[]; %signal S Parabolic Maxima times and values

if (quntLenS>2) %if signal has enough length
    for Cnt=2:(quntLenS-1) %search the Maxs
        if ( ((kS(Cnt) > kS(Cnt+1))) && ((kS(Cnt) >= kS(Cnt-1))) || ((kS(Cnt) >= kS(Cnt+1))) && ((kS(Cnt) > kS(Cnt-1))) )
            quntMaxCnt=quntMaxCnt+1;
            kSMNdx1= [kSMNdx1; Cnt]; kSMVal=[kSMVal; kS(Cnt)];
        end
    end
end

% Now we have the Maxs, lets get the Parabolic Maxs
oldxv= -Inf; oldyv= -Inf;
intGapMax= max(kS)-min(kS);
for jj=1:quntMaxCnt %for all Maxs
    %xa= -1; xb= 0; xc= 1;
    ya= kS(kSMNdx1(jj)-1); % Sample point before
    yb= kS(kSMNdx1(jj)); % Sample point, == kSMVal(jj)
    yc= kS(kSMNdx1(jj)+1); % Sample point after
    D= (-4*yb+2*ya+2*yc);
    if (D==0), xv= kSMNdx1(jj);
    else xv= kSMNdx1(jj)+(ya-yc)/D; end; % Vertix abscissa
    D= (-16*yb+8*ya+8*yc);
    if (D==0), yv= yb;
    else yv= yb+ (2*yc*ya- ya*ya- yc*yc)/D; end;
    % Lets check for double maxima
    if ( (xv==oldxv) || (abs(yv-oldyv)/abs(xv-oldxv))> (2*intGapMax) )
        xv= (xv+ oldxv)/2; yv= max(yv,oldyv); %Double found
        kSPMTim1(length(kSPMTim1))= xv; kSPMVal(length(kSPMVal))= yv;
    else
        kSPMTim1= [kSPMTim1; xv]; kSPMVal=[kSPMVal; yv];
    end
    oldxv= xv; oldyv= yv;
end % for jj=1:quntMaxCnt

if quntMaxCnt>0
    if ( kS(1) >= kSPMVal(1) )
        kSPMTim1= [1; kSPMTim1]; kSPMVal=[kS(1); kSPMVal ]; %Start must be
included as a Max
    end
    if ( kS(end) >= kSPMVal(end) )
        kSPMTim1= [kSPMTim1; quntLenS]; kSPMVal=[kSPMVal; kS(end) ]; %End must
be included as a Max
    end

```

```

end

if quntMaxCnt==0
    if ( kS(1) > kS(2) )
        kSPMTim1= [1; kSPMTim1];  kSPMVal=[kS(1); kSPMVal ] ;      %Start must be
included as a Max
    end
    if ( kS(end) > kS(end-1) )
        kSPMTim1= [kSPMTim1; quntLenS];  kSPMVal=[kSPMVal; kS(end) ] ;      %End must
be included as a Max
    end
end
if quntMaxCnt<0
    error('rGetPMaxs_s: Invalid MaxCnt value');
end

rPMax= sortrows([kSPMTim1, kSPMVal]);
end
%----- make at 17-Jul-07 10:16:59.44
function rPMin= rGetPMins_s(aS)           %Get Parabolic Mins, plateaus out
%                                         build 20070612001
kS= aS(:);
quntLenS=length(kS);
quntMinCnt=0;
kSMNdx1= []; kSMVal=[];                  %signal S Minima indices and values
kSPMTim1= []; kSPMVal=[];                  %signal S Parabolic Minima times and values

if (quntLenS>2)      %if signal has enough length
    for Cnt=2:(quntLenS-1) %search the Mins
        if ( ((kS(Cnt) < kS(Cnt+1))) && ((kS(Cnt) <= kS(Cnt-1))) || ((kS(Cnt) <=
kS(Cnt+1))) && ((kS(Cnt) < kS(Cnt-1))) )
            quntMinCnt=quntMinCnt+1;
            kSMNdx1= [kSMNdx1; Cnt];  kSMVal=[kSMVal; kS(Cnt) ];
        end
    end
end

% Now we have the Mins, lets get the Parabolic Mins
oldxv= -Inf; oldyv= -Inf;
intGapMax= max(kS)-min(kS);
for jj=1:quntMinCnt      %for all Mins
    %xa= -1; xb= 0; xc= 1;
    ya= kS(kSMNdx1(jj)-1);  % Sample point before
    yb= kS(kSMNdx1(jj));    % Sample point, == kSMVal(jj)
    yc= kS(kSMNdx1(jj)+1);  % Sample point after
    D= (-4*yb+2*ya+2*yc);
    if (D==0), xv= kSMNdx1(jj);
    else xv= kSMNdx1(jj)+(ya-yc)/D; end; % Vertix abscissa
    D= (-16*yb+ 8*ya+ 8*yc);
    if (D==0), yv= yb;
    else yv= yb+ (2*yc*ya- ya*ya- yc*yc)/D; end;
    % Lets check for double minima
    if ( (xv==oldxv) || (abs(yv-oldyv)/abs(xv-oldxv))> (2*intGapMax) )
        xv= (xv+ oldxv)/2; yv= min(yv,oldyv);   %Double found
        kSPMTim1(length(kSPMTim1))= xv; kSPMVal(length(kSPMVal))= yv;
    else

```

```

        kSPMTim1= [kSPMTim1; xv];  kSPMVal=[kSPMVal; yv];
    end
    oldxv= xv; oldyv= yv;
end % for jj=1:quntMinCnt

if quntMinCnt>0
    if ( kS(1) <= kSPMVal(1) )
        kSPMTim1= [1; kSPMTim1];  kSPMVal=[kS(1); kSPMVal ];      %Start must be
included as a Min
    end
    if ( kS(end) <= kSPMVal(end) )
        kSPMTim1= [kSPMTim1; quntLenS];  kSPMVal=[kSPMVal; kS(end) ];      %End must
be included as a Min
    end
end

if quntMinCnt==0
    if ( kS(1) < kS(2) )
        kSPMTim1= [1; kSPMTim1];  kSPMVal=[kS(1); kSPMVal];      %Start must be
included as a Min
    end
    if ( kS(end) < kS(end-1) )
        kSPMTim1= [kSPMTim1; quntLenS];  kSPMVal=[kSPMVal; kS(end) ];      %End must
be included as a Min
    end
end
if quntMinCnt<0
    error('rGetPMins_s: Invalid MinCnt value');
end

rPMin= sortrows([kSPMTim1, kSPMVal]);

```

Empirical Mode Decomposition for 4 Channels

```

%*CENTRO DE INVESTIGACIÓN Y DE ESTUDIOS AVANZADO DEL IPN *
%*INGENIERÍA ELÉCTRICA - SECCIÓN DE BIOELECTRÓNICA      *
%*LAREMUS          *
%*M. EN C. ALVARO ALTAMIRANO ALTAMIRANO                  *
%*-----*
clc; clear all; close all;
%Select the Recorded data, these are matrix array of 20480 x 4 &
%20480x 8
[FileName, PathName]=uigetfile('*.*','Select the Matrix to
import','D:\Documents\PhD\MATLAB Codes\EMG_DATA');
if isequal(FileName,0)
    disp('User selected Cancel')
else
    disp(['User selected ', fullfile(PathName,FileName)])
end
filefullpath=[PathName, FileName]; %Full path address
recfileoriginal=load(filefullpath); %load the file that contains the matrix
array
%-----*
%           Plot four Channels from the Input Matrix

```

```

for a=1:4
    figure(1);
    subplot(4,1,a)
    plot(recfileoriginal(:,a), 'LineWidth', 1.5);
    %ylim([-5 5]);
    xlim([0 2000]);
    ylabel(['EMG Channel ' num2str(a)], 'FontSize', 13); xlabel('Time
(ms)', 'FontSize', 13);
end
%-----
amp=input('Please, enter the scale factor: ');
recfile=amp*recfileoriginal;
% Ask for the interval to analyze
%longinicial=;
%longfin=1200;
interval=input('Select the window 1:450-750  2:550-850  3:750-1050  4:850-
1150  5:1100-1400 : ');
switch interval
    case 1
        longinicial=450;
        longfin=750;
        disp('450');
    case 2
        longinicial=550;
        longfin=850;
        disp('550');
    case 3
        longinicial=750;
        longfin=1050;
        disp('750');
    case 4
        longinicial=850;
        longfin=1150;
        disp('850');
    case 5
        longinicial=1100;
        longfin=1400;
        disp('1100');
    otherwise
        disp('That window is incorrect, please select another one')
end
%----- Plot selected window
for b=1:4
    figure(2);
    subplot(4,1,b)
    plot(recfile(:,b), 'LineWidth', 1.5);
    ylim([-1 1]); xlim([longinicial longfin]); ylabel(['EMG Channel '
num2str(b)], 'FontSize', 13); xlabel('Time (ms)', 'FontSize', 13);
end
%-----
pause;

qResol=45;
qResid=45;
qAlfa=1;

```

```

x1=recfile(longinicial:longfin,1);
x2=recfile(longinicial:longfin,2);
x3=recfile(longinicial:longfin,3);
x4=recfile(longinicial:longfin,4);

rParabEmd1= rParabEmd_L(x1,qResol, qResid, qAlfa);
rParabEmd2= rParabEmd_L(x2,qResol, qResid, qAlfa);
rParabEmd3= rParabEmd_L(x3,qResol, qResid, qAlfa);
rParabEmd4= rParabEmd_L(x4,qResol, qResid, qAlfa);

[c1,d1]=size(rParabEmd1);
[c2,d2]=size(rParabEmd2);
[c3,d3]=size(rParabEmd3);
[c4,d4]=size(rParabEmd4);

e1=round(d1/2);
e2=round(d2/2);
e3=round(d3/2);
e4=round(d4/2);

for i=1:d1
    figure(3);
    subplot(e1,2,i)
    plot(rParabEmd1(1:c1,i), 'LineWidth',1.7);
    xlim([0 300]); ylabel(['IMF ' num2str(i)], 'FontSize', 14); xlabel('Time
(ms)', 'FontSize', 12);
end
for i=1:d2
    figure(4);
    subplot(e2,2,i)
    plot(rParabEmd2(1:c2,i), 'LineWidth',1.7);
    xlim([0 300]); ylabel(['IMF ' num2str(i)], 'FontSize', 14); xlabel('Time
(ms)', 'FontSize', 12);
end
for i=1:d3
    figure(5);
    subplot(e3,2,i)
    plot(rParabEmd3(1:c3,i), 'LineWidth',1.7);
    xlim([0 300]); ylabel(['IMF ' num2str(i)], 'FontSize', 14); xlabel('Time
(ms)', 'FontSize', 12);
end
for i=1:d4
    figure(6);
    subplot(e4,2,i)
    plot(rParabEmd4(1:c4,i), 'LineWidth',1.7);
    xlim([0 300]); ylabel(['IMF ' num2str(i)], 'FontSize', 14); xlabel('Time
(ms)', 'FontSize', 12);
end
%-----%HILBERT TRANSFORM-----
t=linspace(0,300/Fs,301)'; %separation between points.
channeltocalculate=input('Enter a channel's number, between 1-4, to calculate HT
& IF: ');
switch channeltocalculate
    case 1
        x=rParabEmd1;
        disp('Channel 1');

```

```

case 2
x=rParabEmd2;
disp('Channel 2');
case 3
x=rParabEmd3;
disp('Channel 3');
case 4
x=rParabEmd4;
disp('Channel 4');
otherwise
    disp('That channel doesn't exist, please select one or type '0' to
exit')
end

Fs=2000; %sampling frequency
[vectors, columns]=size(x);
for i=1:columns
    [env(:,i), freq(:,i)]=hilbert2(x(:,i),Fs);
end
p=round(columns/2);
for j=1:columns
    figure(7);
    subplot(p,2,j)
    plot(t,x(1:vectors,j), 'LineWidth',1.5);hold on;
    plot(t,[env(:,j) -env(:,j)], 'LineWidth',1.5, 'Color',[1 0 0]);
    xlim([0 301]); ylabel('Signal amplitude', 'FontSize', 10);
    title(['IMF ' num2str(j), ' with instantaneous envelope'], 'FontSize',10);
end
for k=1:columns
    figure(8)
    subplot(p,2,k)
    plot(t,freq(1:vectors,k), 'k', 'LineWidth',1.5);
    xlabel('Time (s)', 'FontSize',10); ylabel('Frequency (Hz)', 'FontSize',10);
    ylim([-100 300]);
    title(['Instantaneous frequency of IMF ' num2str(k)], 'FontSize',10);
end

for l=1:columns
    figure(9)
    subplot(p,2,l)
    xcenters=0:300;
    %hist(freq(1:vectors,l),xcenters);
    hist(freq(1:vectors,l));
    [vecfreq(l,:), vecpos(l,:)] = hist(freq(1:vectors,l),300);
    xlim([0 300]);
    xlabel('Frequency (Hz)'); ylabel('Elements');
    title('Histogram of frequencies');
end
for m=1:columns
    fmaxima(m)=max(vecfreq(m,20:280));
    for n=1:300
        if vecpos(m,n) == fmaxima(m)
            freqfundamental(m)=vecfreq(m,n);
        else
        end
    end
end

```

Hilbert Transform and Instantaneous frequency

```
%*CENTRO DE INVESTIGACIÓN Y DE ESTUDIOS AVANZADO DEL IPN *
%*INGENIERÍA ELÉCTRICA - SECCIÓN DE BIOELECTRÓNICA      *
%*LAREMUS          *
%*M. EN C. ALVARO ALTAMIRANO ALTAMIRANO           *
%*-----*
clc; clear all; close all;
%Get the file to compute
[FileName,PathName]=uigetfile('.*','Select the data to import','C:\Users\Dr.
ALTAMIRANO\OneDrive\PhD\MATLAB Codes\HHT Matlab\Registros EMG\USER 1');
if isequal(FileName,0)
    disp('User selected Cancel')
else
    disp(['User selected', fullfile(PathName,FileName)])
end
filefullpath=[PathName, FileName];
%Define the numbers to save the images, record is more easy to define, even
%to prevent errors.
user=1; movement=5;record=input('Number of record:');channel=1;
%-----
%----Import the file----Convert .mat to vars-----
recfileoriginalmat=load('-mat',filefullpath);
%create new variables in the base workspace from those fields.
vars=fieldnames(recfileoriginalmat);
for i=1:length(vars)
    assignin('base', vars{i}, recfileoriginalmat.(vars{i}));
end
%-----
recfileoriginal=100*rParabEmd1;
[elementos, imf]=size(recfileoriginal);
z=zeros(elementos,imf);
instfreq=zeros(elementos-1,imf);
Fs=2000; % Sample frequency determined by the BIOPAC system
t = 0:1/Fs:0.15; % Time of the signal into the segment of 1 second.
%-----
%SPECTROGRAM
for s=1:imf
    figure(1);
    subplot(round(imf/2),2,s)
    spectrogram(recfileoriginal(:,s),32,16,4096,Fs,'yaxis');
    % spectrogram=(x, window, noverlap,nfft,fs,'yaxis')
    % To avoid the issues to how code attempts to analyze and visualize the
    signal using the spectrogram function is
    % Fs=2000 samples per second, while the number of samples in each FFT
    % is 4096 samples, as a result, the frequency resolution of the
    % spectrogram is nearly 0.5 Hertz,
    % dF= Fs/NFFT = 2000/4096 = 0.4882
    view(-40,60)
    title(['Spectrogram of IMF ', num2str(s)],'FontWeight','bold')
    hold on;
end
print('-f1',['CBA4_',num2str(user),
num2str(movement),num2str(record),'_',num2str(channel),'_',num2str(imf),'_Spectr
e'], '-djpeg')
%---Plot the original signal-----
```

```

for a=1:imf
    figure(2);
    subplot(round(imf/2),2,a)
    plot(t,recfileoriginal(:,a),'LineWidth',1.5,'color','blue');
    hold on;
    xlim ([0 0.15]);
    ylabel(['IMFs ' num2str(a)],'FontSize', 14); xlabel('Time (ms)', 'FontSize',
14);
    hold on;
    title('IMFs','FontWeight','bold')
end
print('-'
f2,['CBA4_',num2str(user),num2str(movement),num2str(record),'_',num2str(channel
),'_',num2str(imf),'_IMF'],'-djpeg')
%-----*
%.... INSTANTANEOUS FREQUENCY....
for b=1:imf
    z(:,b) = hilbert(recfileoriginal(:,b));
    instfreq(:,b)= Fs/(2*pi)*diff(unwrap(angle(z(:,b)))); 
    figure(3);
    subplot(round(imf/2),2,b)
    plot(t(2:end),instfreq(:,b));
    xlim([0 0.15]);
    xlabel('Time')
    ylabel('Hz')
    grid on
    title('Instantaneous Frequency')
end
print('-'
f3,['CBA4_',num2str(user),num2str(movement),num2str(record),'_',num2str(channel
),'_',num2str(imf),'_IF'],'-djpeg')

```

WAVELET TRANSFORM ALGORITHM

```

%*CENTRO DE INVESTIGACIÓN Y DE ESTUDIOS AVANZADO DEL IPN *
%*INGENIERÍA ELÉCTRICA - SECCIÓN DE BIOELECTRÓNICA      *
%*LAREMUS                                                 *
%*M. EN C. ALVARO ALTAMIRANO ALTAMIRANO                 *
%*ING. ALAN BELTRAN                                     *
%*-----*
function [ ] = escalograma( archivo,canal )

close all;
%% EMG signal parameters
fs = 2000; % Sample frequency
Ts = 1/fs; % Period
t = 0:Ts:1-Ts; % time slot
tm = t*1000; % time (ms)
%Channel selection
m = load(archivo);
ch1 = m(:,1)';
ch2 = m(:,2)';
ch3 = m(:,3)';
ch4 = m(:,4)';
% Normalization
max1 = max([abs(max(ch1)) abs(min(ch1))]);
max2 = max([abs(max(ch2)) abs(min(ch2))]);

```

```

max3 = max([abs(max(ch3)) abs(min(ch3))]);
max4 = max([abs(max(ch4)) abs(min(ch4))]);

ch1 = ch1/max1;
ch2 = ch2/max2;
ch3 = ch3/max3;
ch4 = ch4/max4;

figure('OuterPosition',[10,500,1100,580]);
subplot(4,1,1);
plot(tm,ch1);
title('Canal #1 - Extensor breve del pulgar');
subplot(4,1,2);
plot(tm,ch2);
title('Canal #2 - Flexor superficial de los dedos');
subplot(4,1,3);
plot(tm,ch3);
title('Canal #3 - Extensor de los dedos');
subplot(4,1,4);
plot(tm,ch4);
title('Canal #4 -Flexor cubital del carpo');

switch canal
    case 1
        ch = 'Canal #1 - Extensor breve del pulgar';
        disp(ch)
        y = ch1;
    case 2
        ch = 'Canal #2 - Flexor superficial de los dedos';
        disp(ch)
        y = ch2;
    case 3
        ch = 'Canal #3 - Extensor de los dedos';
        disp(ch)
        y = ch3;
    case 4
        ch = 'Canal #4 -Flexor cubital del carpo';
        disp(ch)
        y = ch4;
end
%% Scalogram
% Bandwidth
freqrange = [5 300];
% Scale-frequency ratio
fc          = centfrq('meyr');
scalerange = fc./(freqrange*Ts);

% Logarithmic scale vector
scalerange = log10(scalerange);
scales     = logspace(scalerange(end),scalerange(1),30);

% Frequency vector
freqs = scal2frq(scales,'meyr',Ts);

% CWT function
coefs = cwt(y,scales,'meyr');

```

```

% Scalogram
S = abs(coefs.*coefs);
SC = 100*S./sum(S(:));

% Umbral
V = SC'; V = V(:)';
V = V/max(V);
for i = 1:length(V)
    if V(i) <= 0.3
        V(i) = 0;
    end
end
c = size(SC,2);
SC = vec2mat(V,c);
SC = mat2gray(SC);

%% Scalogram Plot
positionVector1 = [0.09, 0.85, 0.835, 0.1];
positionVector2 = [0.09, 0.08, 0.9, 0.65];

figure('OuterPosition',[10,50,1100,900]);

% Analyzed signal
subplot('Position',positionVector1);
plot(tm,y);
xlabel('Tiempo [mseg]', 'fontweight', 'bold');
ylabel('Amplitud', 'fontweight', 'bold');
title(ch, 'fontweight', 'bold');
subplot('Position',positionVector2);
[C,h] = contour(tm,scales,SC);
set(gca, 'YScale','log');
colorbar;
grid on;
title({'Escalograma'; 'Porcentaje de energía de cada coeficiente'}, ...
    'fontweight', 'bold');
xlabel('Tiempo[mseg]', 'fontweight', 'bold');
ylabel('Escalas', 'fontweight', 'bold');

%% Scale vs frequency plot
figure('OuterPosition',[1150,50,570,510]);
semilogy(freqs,scales);
axis([freqs(end) freqs(1) scales(1) scales(end)]);
title('Escalas Vs Frecuencias', 'fontweight', 'bold');
xlabel('Frecuencias', 'fontweight', 'bold');
ylabel('Escalas', 'fontweight', 'bold');
end

```

KALMAN FILTER ALGORITHM

```
function [k,s] = kfilter(A,C,V1,V2,V12)
%*CENTRO DE INVESTIGACIÓN Y DE ESTUDIOS AVANZADO DEL IPN *
%*INGENIERÍA ELÉCTRICA - SECCIÓN DE BIOELECTRÓNICA      *
%*LAREMUS          *
%*M. EN C. ALVARO ALTAMIRANO ALTAMIRANO          *
%Kalman Filter can have arguments: (A,C,V1,V2)
%    KFILTER calculates the kalman gain, k, and the stationary
%    covariance matrix, s, using the Kalman filter for:
%
%        x[t+1] = Ax[t] + Bu[t] + w1[t+1]
%        y[t]   = Cx[t] + Du[t] + w2[t]
%
%        E [w1(t+1)] [w1(t+1)]' = [V1   V12;
%        [ w2(t) ] [ w2(t) ]       V12' V2 ]
%
% where x is the mx1 vector of states, u is the nx1 vector of controls, y is
% the px1 vector of observables, A is mxm, B is mxn, C is pxm, V1 is mxm,
% V2 is pxp, V12 is mxp.
%
%*-----*
```

```
m=max(size(A));
[rc,cc]=size(C);
if nargin==4; V12=zeros(m,rc); end;
if (rank(V2)==rc);
A=A-(V12/V2)*C;
V1=V1-V12*(V2\V12');
[k,s]=doubleo(A,C,V1,V2);
k=k+(V12/V2);
else;
s0=.01*myo(m);

dd=1;
it=1;
maxit=1000;

while (dd>1e-8 & it<=maxit);
k0= (A*s0*C'+V12)/(V2+C*s0*C');
s1= A*s0*A' + V1 -(A*s0*C'+V12)*k0';
k1= (A*s1*C'+V12)/(V2+C*s1*C');
dd=max(max(abs(k1-k0)));
it=it+1;
s0=s1;
end;

k=k1;s=s0;
if it>=maxit;
disp('WARNING: Limit iteration');
end;
end;
```

GOERTZEL ALGORITHM

```
%*CENTRO DE INVESTIGACIÓN Y DE ESTUDIOS AVANZADO DEL IPN *
%*INGENIERÍA ELÉCTRICA - SECCIÓN DE BIOELECTRÓNICA      *
%*LAREMUS                                                 *
%*M. EN C. ALVARO ALTAMIRANO ALTAMIRANO                 *
%*-----*
Fs = 1024; %Sampling Frequency
Ts = 1/Fs; %Period
f1 = 83.3; % 1st Pattern
f2 = 96.7; % 2nd Pattern
f3 = 113.3; % 3th Pattern
f4 = 59; % Line signal
f5 = 125; % Extra signal
f = [59 83.3 96.7 113.3 125]; % Patterns and Signals
N = 512;
t = Ts*(0:N-1)';
x =
0.8*sin(2*pi*f1*t)+0.9*sin(2*pi*f2*t)+0.4*sin(2*pi*f3*t)+0.2*sin(2*pi*f4*t)+0.1*
wgn(N,1,-10); %Signal
figure(1);
plot(t,x);
%title('');
xlabel('Time (ms)');
ylabel('Intensity (mV)');
figure(2);
periodogram(x,[],[],Fs); % PSD with FFT
% (computed with all N points of signal)
% PSD with Goertzel Algorithm only in the
region of interest
figure(3);
stem(f,abs(X));
ax=gca;
ax.XTick=f;
title('DFT Magnitude')
xlabel('Frequency (Hz)');
```

RÉSUMÉ

PRÉDICTION DE MOUVEMENTS DES MEMBRES SUPÉRIEURS PAR ANALYSE DES SIGNAUX EMG À L'AIDE DES TRANSFORMÉES EN ONDELETTES ET DE HILBERT-HUANG

Cette thèse porte sur l'analyse des signaux sEMG multicanaux à l'aide de la transformée en ondelettes, de la transformation de Hilbert-Huang et d'autres méthodes d'analyse ou de traitement des signaux, telles que le filtrage de Kalman et de Goertzel, pour détecter, mesurer, filtrer et décomposer les signaux sEMG afin d'identifier des tendances dans le temps et en fréquence des mouvements de flexion-extension des doigts de la main en observant les signaux myoélectriques des muscles superficiels. Le but est de prédire le mouvement des doigts de la main et de minimiser le temps de calcul pour permettre de contrôler des prothèses à l'aide de capteurs superficiels. L'hypothèse est fondée sur l'idée que tous les mouvements de la main sont une réponse active de l'activité myoélectrique des muscles spécifiques et que l'activité électrique peut être mesurée comme un signal associé à une séquence de mouvement des éléments de la main (doigts). Chaque doigt peut effectuer une trajectoire de la position de repos à la position finale, cette trajectoire qui n'est évidemment pas instantanée, engendre un signal myoélectrique lui-même non instantané. L'activité électrique du muscle est présente sur les signaux enregistrés. Cette activité électrique peut être reconnue par un algorithme à partir d'une base de données de modèles de mouvement. Comparer l'activité électrique des muscles en temps réel par rapport à ces données peut permettre de détecter une tendance du comportement de la main et donc de prévoir le mouvement spécifique avant ou en même temps. Cette prédiction doit autoriser une baisse du temps de réponse de la prothèse.

Signal EMG, prédiction, ondelettes, Hilbert-Huang, kalman, Göertzel, filtrent

EMG PATTERN PREDICTION OF UPPER LIMB MOVEMENTS BASED ON WAVELETS AND HILBERT-HUANG TRANSFORM

This thesis deals with the analysis of multichannel sEMG signals using wavelet transform, Hilbert-Huang transformation and other signal analysis or processing methods such as Kalman and Goertzel filtering, for detecting, measuring, filtering and decomposing sEMG signals to identify patterns in the time and frequency of flexion-extension movements of the fingers of the hand by analyzing the myoelectric signals of the superficial muscles. The aim is to predict the movement of the fingers of the hand and to minimize the computation time to allow the control of prostheses by means of superficial sensors. The hypothesis is based on the idea that all hand movements are an active response of the myoelectric activity of specific muscles and that electrical activity can be measured as a signal associated with a sequence of motion of the elements of the hand (fingers). Each finger can make a trajectory from the rest position to the final position, this trajectory which is obviously not instantaneous, generates a non-instantaneous myoelectric signal itself. The electrical activity of the muscle is present on the recorded signals. This electrical activity can be recognized by an algorithm from a database of the motion models. Comparing the electrical activity of the muscles in real time with respect to these data can make it possible to detect a tendency in the behavior of the hand and therefore to predict the specific movement before or at the same time. This prediction must allow a reduction in the response time of the prosthesis.

EMG signal, prediction, wavelets, Hilbert-Huang, kalman, Göertzel, filtering